Stem cell bioprocessing strategies for cardiac regeneration

Unveiling CCBE1 role as a modulator of cardiomyocyte differentiation

Marta Sofia Marques Silva

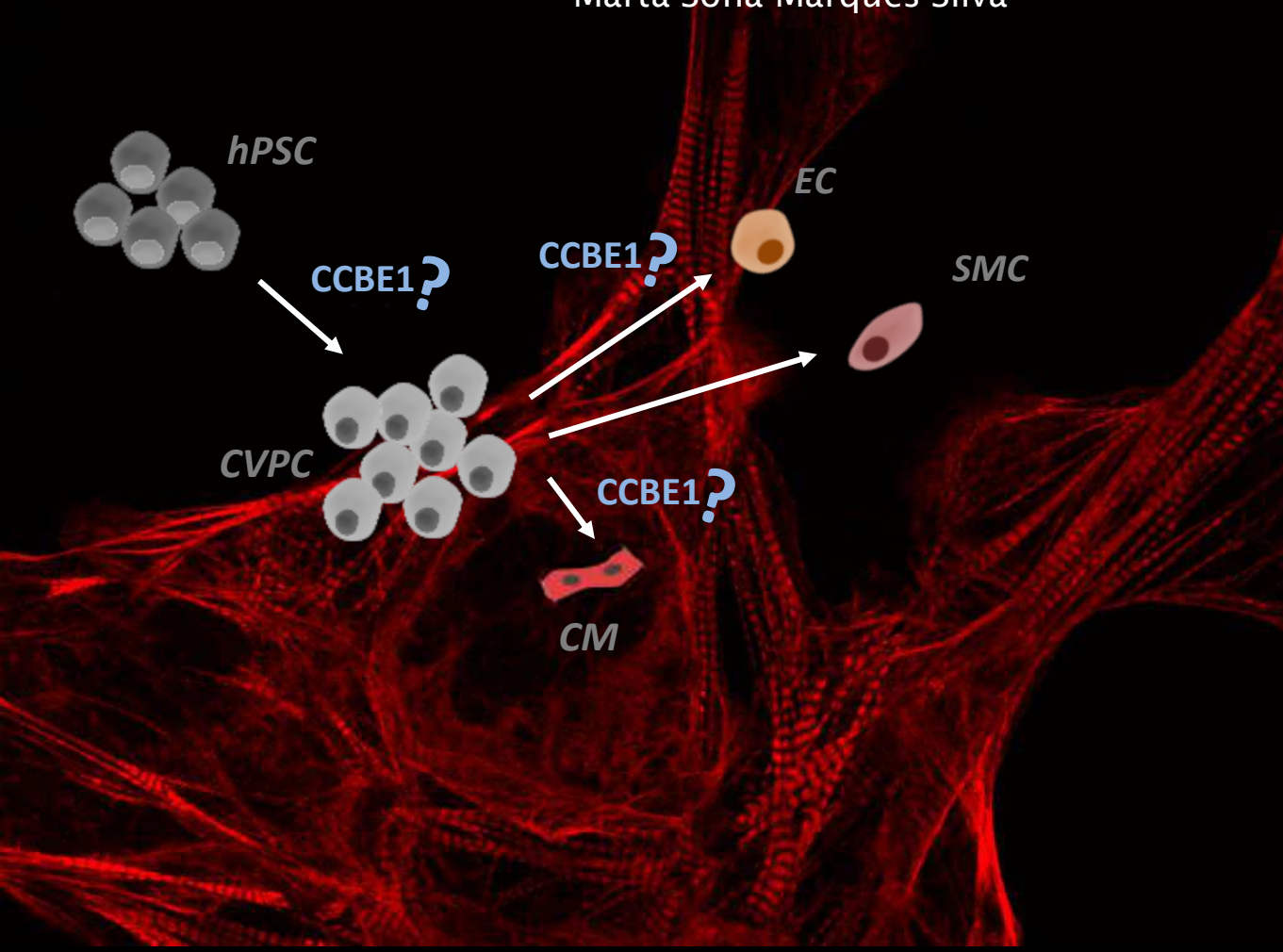

Dissertation presented to obtain the Ph.D degree in Engineering and Technology Sciences, Biomedical Engineering

Instituto de Tecnologia Química e Biológica António Xavier | Universidade Nova de Lisboa

Oeiras,
September, 2018

UNIVERSIDADE NOVA DE LISBOA

Stem cell bioprocessing strategies for cardiac regeneration

Unveiling CCBE1 role as a modulator of cardiomyocyte differentiation

Marta Sofia Marques Silva

Dissertation presented to obtain the Ph.D degree in Engineering and Technology Sciences, Biomedical Engineering

Instituto de Tecnologia Química e Biológica | Universidade Nova de Lisboa

Oeiras, September 2018

Stem cell bioprocessing strategies for cardiac regeneration

Unveiling CCBE1 role as a modulator of cardiomyocyte differentiation

Marta Sofia Marques Silva

The work developed in this thesis was supervised by:

- **Doctor Paula Marques Alves**, Instituto de Tecnologia Química e Biológica António Xavier, Universidade Nova de Lisboa (ITQB NOVA) e Instituto de Biologia Experimental e Tecnológica (iBET)

- **Doctor José António Belo**, CEDOC - Chronic Diseases Research Center, NOVA Medical School, Universidade Nova de Lisboa

Stem cell bioprocessing strategies for cardiac regeneration: Unveiling CCBE1 role as a modulator of cardiomyocyte differentiation

Instituto de Tecnologia Química e Biológica António Xavier

Universidade Nova de Lisboa

Financial support from:

Fundação para a Ciência e Tecnologia (FCT)

Ph.D grant PD/BD/52481/2014

iNOVA4Health (UID/Multi/04462/2013) financially supported by FCT/MEC, through national funds and co-funded by FEDER under PT2020

CardioRegen (HMSP-ICT/0039/2013)

European Commission

HYPERLAB: High-Yield and Performance Stem Cell Lab, 223011

À minha família

Acknowledgements

I would like to express my gratitude to all the people who, directly or indirectly, have helped me during these years and contribute to this thesis.

To my supervisor, Dr Paula M Alves, for the scientific support and excellent conditions provided throughout these years. For all the professional advices and opportunities, including courses and conferences, that contributed for my development as a scientist. For challenging me and giving me the opportunity to explore new technologies to fulfill my research aims. For the strong example of leadership, for pushing and challenging me towards my goals in this inspiring and excellent scientific environment.

To my supervisor, Dr José A Belo, for giving me the opportunity to work in a challenging scientific project. For all the fruitful discussions and suggestions on the CCBE1 project. Also, for your rough skepticism, which taught me to always have a second look on the obvious and the non-obvious.

To Dr Margarida Serra, for all the scientific discussions, support, guidance and motivation provided since I arrived at the lab. Thank you for the opportunity to work with stem cells, when it just started with a small project that ended up as part of this thesis. For pushing me towards my goals and helping me to grow as a scientist.

To Dr Patrícia Gomes-Alves, for all the scientific support, guidance, motivation and friendship along this journey. For sharing your enthusiasm and confidence in this project and for being there for all the good and bad moments that I had. For always pushing me to pursue my project and career goals and helping me with the mass spectrometry tools.

To Prof. Manuel Carrondo, for your example of leadership and for transmitting us that excellence, rigor and hard work are essential for our scientific success.

To all my colleagues of the Animal Cell Technology Unit, for all the help provided and for creating such a great working environment. To Filipa, for all the scientific support and discussion in microarray analysis and for contributing to strength my knowledge in this field. To Marcos, for sharing your enthusiasm and knowledge in working with stirred-tank bioreactors, I will never forget our “PBS” partnership, thank you! To downstream team Bárbara, Sara, Cristina e Ricardo, for all the scientific discussions and support on CCBE1 bioprocessing task. A special thanks to the former “4.18 team”, Ana Paula, Catarina, Daniel

S, Francisca, João S, Marta E, Sofia R, for the strong team spirit and for sharing this journey with me. Thanks for the Stem Cell team members for the scientific discussions, critical suggestions and good working environment in the lab, especially to Marta Paiva for your critical opinion on the last part of this thesis. To Bernardo, for sharing the hopes and disappointments in finishing a PhD Thesis on time! Finally, thanks Pedro V. for confidence, for working with a great spirit and enthusiasm, and for sharing your thoughts and doubts during the last year, that contributed to our results presented in Chapter 4 of this thesis.

To the Stem Cells and Development Lab former and present members, especially to José Inácio and Paulo Pereira, for all the discussions, suggestions and for sharing your enthusiasm and frustrations in working with such a difficult protein.

Pessoalmente gostaria de agradecer:

Aos meus amigos do lab, Ana Paula, Ana O, Catarina, Daniel S, Francisca, João S, João V, Mafalda, Marta E, Rita, Sofia R, que fizeram e fazem com que tudo seja mais fácil! Pela partilha dos sabores e dissabores de trabalhar em ciência, pela amizade ao longo destes anos e que vai continuar por muitos mais! Que não acabem os bons momentos juntos!

À Beatriz, pela amizade e partilha ao longo destes anos, por sabermos sempre que contamos uma com a outra e por nada mudar!

Aos meus amigos de sempre, que nem a distância nos afasta, obrigada por compreenderem a ausência que nem sempre pode ser evitada!

Ao Daniel, por teres partilhado esta viagem comigo da melhor forma! Por veres sempre o lado bom, por nunca deixares que o foco me fuja, por seres o meu maior crítico. Complementamo-nos e só assim faz sentido, obrigada!

Aos meus pais e irmãos, por todo o apoio e confiança em tudo o que faço. Por compreenderem as ausências mais que muitas durante estes anos, mas acima de tudo pelo exemplo de coragem e perseverança e por me terem ajudado a atingir mais um patamar na minha vida! Em especial à Ana, por estar sempre comigo, pelo carinho e por nunca ser preciso dizer uma palavra para ter o teu abraço, isto nunca se vai perder!

Abstract

Cardiovascular diseases (CVD) are the leading cause of morbidity and mortality worldwide. Within CVD, myocardial infarction (MI) is associated with a massive and permanent loss of cardiomyocytes (CM). Advanced therapies based on stem cells' potential to promote cardiac regeneration have been explored in numerous preclinical studies. Nonetheless, their clinical efficacy to improve the heart function remains elusive and controversial. The lack of validated and standardized cell culture protocols and characterization tools are among the contributing factors for this translational failure. Moreover, understanding the key cellular mechanisms underlying cardiac regeneration may also expose a multiplicity of therapeutic targets, paving the way for improved therapies by controlling cardiac tissue remodeling and/or to impose a pro-regenerative state.

This thesis aimed at the implementation of novel strategies that could contribute for improved cardiac regenerative therapies. This work was divided into two main sections covering (A) the implementation of robust and scalable protocols for the expansion of human stem cells and (B) the interrogation of the functional role of a putative therapeutic molecule, CCBE1 (collagen and calcium-EGF binding domain 1), on cardiac commitment.

For translating the stem cell manufacturing protocols towards industrial and clinical settings, it is essential to develop strategies to produce therapeutic cells at high quantity, quality and low cost of goods. Therefore, in the first part of the work (A), we evaluated the impact of different bioprocess parameters, such as culture matrix composition and bioreactor design and hydrodynamics, on stem cell expansion yields and phenotype. Given the clinical potential of human Embryonic Stem Cells (hESC) and human Mesenchymal Stem Cells (hMSC), both cell sources were selected to conduct these studies. In **Chapter 2**, two phenotypically different hESC lines, one feeder-dependent and other feeder-free,

were efficiently expanded on xeno-free microcarriers in stirred culture conditions. We were able to demonstrate the robustness of this strategy to expand different lines of hESC, showing a phenotypic convergence along their expansion, as depicted in their transcriptome. Noteworthy, at low-oxygen levels using environmentally controlled stirred-tank bioreactors, a metabolic rearrangement with upregulation of the glycolytic machinery favoring an anaerobic glycolysis, a stemness feature, was clearly observed in contrast to 2D culture system. Overall, this study provided relevant findings on the physiological and metabolic hallmarks of hPSC expansion. Furthermore, in **Chapter 3**, we aimed at scaling up the hMSC expansion process using disposable bioreactors amenable for translation into clinical-grade bioprocesses. We took advantage of a 2 L-scale single-use low shear stress bioreactor (Vertical-Wheel^{TM} PBS-3 Air) to implement a scalable protocol for improved hMSC expansion. Using this single-use bioreactor, we were able to achieve high hMSC expansion yields (3×10^5 cell/mL), comparable with those obtained in ST bioreactors. Notably, in PBS-3 Air a significantly lower percentage of apoptotic cells as well as reduced levels of HLA-DR positive cells were detected, when compared to ST bioreactors. Ultimately, these data demonstrated that process transfer from ST bioreactor to PBS-3 Air, and scale-up were successfully carried out, proving its potential as a new scalable biomanufacturing platform for microcarrier-based cell therapy products.

In the second part of this thesis (B), we aimed at interrogating CCBE1 role on cardiac commitment that could be used to identify novel CCBE1-modulated pathways as targets for translation into CCBE1-based cardiac therapies.

The putative role of CCBE1 in lymphatic/cardiac vascular development, prompted its study as a therapeutic molecule to restore cardiac tissue upon heart injury, through CCBE1-mediated cardiac commitment and/or augmentation of lymphangiogenesis. Therefore, in **Chapter 4**, we conducted an *in vitro* study to interrogate CCBE1 role on cardiac commitment, combining human induced

pluripotent stem cells and gene editing tools (CRISPR interference technology), to modulate the CCBE1 expression along CM and endothelial cells (EC) differentiation. *CCBE1* knockdown (KD) led to a significant reduction on the expression of cardiac troponin marker *TNNT2* and other cardiac myosin genes. Ultrastructural changes, namely sarcomere length and alignment, were also observed in CM derived from CCBE1 KD cell line at day 15 of differentiation, indicating a more immature state relative to control cell line. *CCBE1* KD along EC differentiation, on the other hand, showed no impact at morphological and gene expression levels. Together, these data suggested a modulatory role of this protein particularly on CM phenotype. Gain-of-function assays would be critical to rescue the normal phenotype. Nonetheless, the lack of efficient protocols for the production of full-length CCBE1 has hindered its use as a soluble and therapeutic molecule. Thus, in **Chapter 5**, we took advantage of different bioprocess strategies to improve the production of full-length CCBE1 protein. Exploring a high cell density transfection protocol, higher volumetric production yield of CCBE1 was observed when compared to standard transfection condition, without compromising rCCBE1 attributes, namely the glycosylation pattern. Following a purification step with higher recovery yields (>95% of full-length rCCBE1), the application of proteomic-based tools allowed the identification of process contaminants after production and purification steps, namely host-cell proteins. Lastly, the angiogenic potential of rCCBE1, as a functional attribute, was confirmed by promoting vessel formation (HUVECs assay).

Finally, we envision that the implemented strategies and knowledge gained during this thesis can contribute for the development of novel and more efficacious cardiac therapies, opening new avenues for the implementation of knowledge-driven approaches and to the identification of CCBE1-modulated proteins/pathways as targets for cardiac commitment.

Resumo

As doenças cardiovasculares são atualmente uma das principais causas de morte a nível mundial, sendo o enfarte do miocárdio (EM) o que apresenta maior incidência. Esta doença está associada a uma perda excessiva e permanente de cardiomiócitos (CM), um dos principais constituintes celulares do coração. As terapias mais inovadoras baseadas em células estaminais, têm demonstrado resultados promissores quanto à sua capacidade regenerativa em estudos pré-clínicos. Contudo, o mesmo não se verifica em ensaios clínicos. Este facto pode estar relacionado com i) a falta de protocolos *standardizados* para a cultura de células estaminais e de métodos analíticos para a caracterização destas células, e ii) o reduzido conhecimento sobre os mecanismos celulares associados à regeneração cardíaca. Assim, este conhecimento permitirá o desenvolvimento de novas terapias através do controlo da remodelação do tecido cardíaco e/ou ativando a sua capacidade regenerativa.

O principal objetivo desta tese foi a implementação de novas estratégias que irão contribuir para o desenvolvimento de terapias mais eficazes na regeneração cardíaca. O trabalho desenvolvido focou-se em 2 grandes blocos: (A) na implementação de protocolos estalonáveis para a cultura de células estaminais humanas e (B) na investigação da funcionalidade da CCBE1 (collagen and calcium-EGF binding domain 1) durante a diferenciação cardíaca, como uma molécula terapêutica.

Atendendo ao objetivo da primeira parte do trabalho (A), a implementação de protocolos de cultura de células estaminais num contexto industrial e clínico deve assegurar que as estratégias alcancem elevados rendimentos celulares, mantendo a identidade das mesmas e a baixo custo. Neste sentido, avaliou-se o impacto de diferentes parâmetros do bioprocesso (ex.: composição da matriz de cultura e o formato e hidrodinâmica dos reatores) no rendimento celular e na sua

identidade. Nestes estudos foram utilizados dois tipos de células estaminais humanas, tento em conta o seu potencial em terapias celulares: células estaminais embrionárias (hESC) e células estaminais mesenquimais (hMSC). No **Capítulo 2** descreve-se a estratégia implementada para a expansão de duas linhas de hESC, com modos de cultura diferentes, utilizando microsuportes sintéticos em sistemas de cultura agitados. A caracterização do transcriptoma destas células, após o processo de expansão, revelou a robustez do sistema implementado. Adicionalmente, e após análise do transcriptoma e metaboloma das hESC quando expostas a baixos níveis de oxigénio, verificou-se um rearranjo metabólico que favoreceu um fenótipo glicolítico. Este estudo permitiu identificar características fisiológicas e metabólicas de hESC durante a sua expansão.

No **Capítulo 3** procedeu-se à implementação de um processo escalonável em reatores descartáveis para a expansão de hMSC, passível de ser transferido para contexto industrial e clínico. Neste processo utilizou-se um bioreator descartável de 2 L com baixa tensão de cisalhamento e agitação vertical (Vertical-Wheel^{TM} PBS-3 Air), permitindo a eficiente expansão de hMSC (3×10^5 cell/mL), cujos valores de hMSC são comparáveis aos obtidos quando cultivadas em bioreatores de tanque agitado (ST). Além do mais, este bioreator descartável permitiu uma redução significativa da morte celular por apoptose e uma diminuição do número de células a expressar o marcador HLA-DR. Estes dados comprovam que foi possível transferir de forma eficiente a expansão de hMSC de bioreatores ST para bioreatores descartáveis, como o PBS-3 Air, potenciando o seu uso em plataformas para cultura de produtos celulares dependentes de microsuportes.

A segunda parte do trabalho (B) teve como objetivo investigar a função da CCBE1 durante a diferenciação cardíaca, permitindo a identificação de novos alvos terapêuticos que sejam modulados pela CCBE1 para terapias cardíacas.

Diversos estudos têm se sugerido uma possível função da CCBE1 na regeneração do tecido cardíaco, através da diferenciação cardíaca ou da

linfangiogenese. Neste sentido, no **Capítulo 4** explorámos o papel desta proteína, utilizando células estaminais pluripotentes induzidas (hiPSC) e métodos de modificação génica (tecnologia de interferência CRISPR) para induzir a perda de função do gene em causa durante a diferenciação em CM e células endoteliais (CE). A inibição da expressão da CCBE1 levou a um decréscimo na expressão de marcadores cardíacos, tais como o gene *TNNT2* entre outros. Após 15 dias de diferenciação, os CM apresentavam alterações ulta estruturais, nomeadamente no tamanho e alinhamento dos sarcómeros, indicativo de um fenótipo imaturo, comparativamente com a cultura sem modificação génica. Por outro lado, esta inibição da expressão da CCBE1 não teve qualquer impacto na diferenciação em CE, tanto a nível morfológico como na expressão génica. Estes dados sugerem que esta proteína pode ter uma função moduladora no fenótipo dos CM. A falta de processos eficientes para a produção desta proteína tem impedido o seu uso como factor terapêutico. Desta forma, no **Capítulo 5** foram implementadas estratégias para melhorar a produtividade da CCBE1, tendo sido o protocolo de transfeção a elevadas densidades celulares (20 milhões de células por mL) aquele que apresentou resultados mais promissores. Pois, através desta estratégia foi possível obter-se um efeito positivo na produtividade da CCBE1 sem comprometer as qualidades da mesma, como o seu padrão de glicosilação. Após a purificação da CCBE1 com elevada percentagem de recuperação da proteína (95 % da proteína de 49 kDa), foram utilizados métodos de espectrometria de massa para identificar as proteínas no produto final, como por exemplo proteínas celulares. O potencial angiogénico da CCBE1 foi também confirmado, tendo em conta a sua capacidade em potenciar a formação de estruturas celulares semelhantes a vasos endoteliais.

Por fim, esperamos que as estratégias implementadas e todo o conhecimento adquirido ao longo deste trabalho possam contribuir para o desenvolvimento de novas terapias cardíacas mais eficazes na regeneração cardíaca, e que possam criar novas oportunidades para a implementação de

metodologias baseadas no conhecimento, bem como na identificação de proteínas que sejam reguladas pela CCBE1 durante a diferenciação cardíaca.

Thesis Publications

Silva MM*, Rodrigues AF*, Correia C, Sousa MF, Brito C, Coroadinha AS, Serra M, Alves PM. (2015) Robust expansion of human pluripotent stem cells: integration of bioprocess design with transcriptomic and metabolomic characterization. *Stem Cells Transl Med*. 4(7):731-42;

Sousa MF*, **Silva MM***, Giroux D, Hashimura Y, Wesselschmidt R, Lee B, Roldão A, Carrondo JM, Alves PM, Serra M. (2015) Production of oncolytic adenovirus and human mesenchymal stem cells in a single-use, Vertical-Wheel bioreactor system: Impact of bioreactor design on performance of microcarrier-based cell culture processes. *Biotechnology Progress,* 31(6):1600-12;

Silva MM, Gomes-Alves P, Rosa S, Simão D, Inácio JM, Peixoto, C, Serra M, Belo JA, Alves PM (2018) Full-length human CCBE1 production and purification: leveraging bioprocess development for high quality glycosylation attributes and functionality. *J Biotechnol.* 10;285:6-14.

Silva MM, Vicente P, Terrasso AP, Inácio JM, Gomes-Alves P, Serra M, Belo JA, Alves PM (2018) Unveiling CCBE1 role as a modulator of human pluripotent stem cells cardiomyocyte differentiation. *Submitted.*

* Authors contributed equally

Additional Publications

Cunha B, Serra M, Peixoto C, **Silva MM**, Carrondo MJT, Alves PM. (2013) Designing clinical grade integrated strategies for the downstream processing of human mesenchymal stem cells. *BMC Proceedings*, 7(Suppl 6):P103.

Cunha B, Peixoto C, **Silva MM**, Carrondo MJT, Serra M, Alves PM. (2015) Filtration methodologies for the clarification and concentration of human mesenchymal stem cells. *J Memb Sci*, 478, 117-129.

Cunha B, Aguiar T, **Silva MM**, Silva RJ, Sousa MF, Pineda E, Peixoto C, Carrondo MJ, Serra M, Alves PM. (2015) Exploring continuous and integrated strategies for the up- and downstream processing of human mesenchymal stem cells. *J Biotechnol*. 213, 97-108;

Rebelo SP, Costa R, **Silva MM**, Marcelino P, Brito C, Alves PM. (2015) Three-dimensional co-culture of human hepatocytes and mesenchymal stem cells: improved functionality in long-term bioreactor cultures. *J Tissue Eng Regen Med* 11(7):2034-2045;

Cunha B, Aguiar T, Carvalho SB, **Silva MM**, Gomes RA, Carrondo MJT, Gomes-Alves P, Peixoto P, Serra M, Alves PM. (2017) Bioprocess integration for human mesenchymal stem cells: From up to downstream processing scale-up to cell proteome characterization. *J Biotechnol*. 248, 87-98.

Simão D, **Silva MM**, Terrasso AP, Arez, F, Sousa MFQ, Mehrjardi NZ, Šarić T, Gomes-Alves P, Raimundo N, Alves PM, Brito C. (2018) Human neural microenvironment specific features are promoted by 3D differentiation of iPSC-derived NPC. *Stem Cell Reports,* 11,1-13.

Table of Contents

List of Abbreviations

2D	two-dimensional
3D	three-dimensional
ALA	Alanine
ANOVA	Analysis of variance
BCAA	Branched-chain aminoacids
bFGF	Basic fibroblast growth factor
BMP	Bone morphogenic protein
BSA	Bovine serum albumin
CCBE1	Collagen and calcium-binding EGF domain-1
CMs	Cardiomyocytes
CPC	Cardiac Progenitor Cells
cTnI	Cardiac muscle troponin I
cTnT	Cardiac muscle troponin T
CVD	Cardiovascular diseases
DMEM	Dulbecco's modified Eagle medium
DMSO	Dimythyl sulfoxide
dpt	days post-transduction
ECM	Extracellular matrix
EdU	5-ethynyl-2´-deoxyuridine
FBS	Fetal bovine serum
FDA	Fluorescein diacetate
FDR	False discovery rate
FSG	Fish skin gelatin
GAPDH	Glyceraldehyde-3-Phosphate Dehydrogenase
GATA4	Transcription factor GATA-4
GLN	Glutamine
GLU	Glutamate
GO	Gene ontology
HEK293-EBNA1-6E	Human embryonic kidney 293 cell line expressing a truncated Epstein-Barr virus nuclear antigen-1 protein
hESC	Human embryonic stem cells
hFF	Human foreskin fibroblasts
HIF	Hypoxia-inducible factor
hiPSC	Human induced pluripotent stem cells
hMSC	Human mesenchymal stem cells

HPLC	High Performance Liquid Chromatography
hPSC	Human pluripotent stem cells
IPA	Ingenuity Pathway Analysis
KDR	Kinase insert domain receptor
LAC	Lactate
MESP1	Mesoderm Posterior BHLH Transcription Factor 1
MS	Mass spectrometry
MYH6	myosin heavy chain 6, α isoform protein
MYH7	myosin heavy chain 7, β isoform protein
MYL2	myosin light chain 2, ventricular/cardiac muscle isoform (MLC2v)
MYL7	myosin light chain 7, atrial isoform (MLC2a)
Nanog	Homeobox Transcription Factor Nanog
Nkx2-5	NK2 Homeobox 5
Oct4	transcription factor octamer 4
PBS	Phosphate-buffered saline
PBS-3 Air	Vertical-Wheel AirDrive PBS bioreactor 3 L
PDGFRα	Platelet-derived growth factor receptor α
PFA	Paraformaldehyde
PI	Propidium iodide
RPL22	Ribossomal protein L22
RT-qPCR	Reverse transcriptase quantitative polymerase chain reaction
SIRPα/β	Signal-regulatory protein alpha/betta
SSEA-1	Stage-specific embryonic antigen-1
SSEA-4	Stage-specific embryonic antigen-4
SSEA-5	Stage-specific embryonic antigen-5
ST	Stirred-tank bioreactors
TNNI1	Troponin I1, Slow Skeletal Type
TNNI3	Troponin I3, Cardiac Type
TNNT2	Cardiac muscle troponin T
TRA-1-60	Human embryonal carcinoma marker antigen 60
TRA-1-81	Human embryonal carcinoma marker antigen 81
VCAM1	Vascular cell adhesion molecule 1
VE-cadherin	Vascular endothelial cadherin, CD144
VEGF	Vascular endothelial growth factor

Introduction

Table of Contents

1. Cardiovascular Diseases: Motivation for Biomedical & Clinical Research

Cardiovascular diseases (CVD) remain the leading cause of morbidity and mortality worldwide (World Health Organization, 2017). Coronary heart disease (myocardial infarction, MI) is included in this group of disorders, occurring when blood supply to the heart is blocked, which leads to massive and permanent loss of cardiomyocytes (CMs). With a limited regenerative capacity driven by CMs turn-over and enhanced by endogenous cardiac progenitor/stem cells (CPC/CSC), the infarcted myocardium is not fully restored. Instead the myocardial tissue is then replaced by non-contractile scar tissue (fibrosis), leading to cardiac dysfunction (Beltrami et al., 2003; Bergmann et al., 2009; Chien & Olson, 2002). Currently, no curative treatment for heart failure is available apart from heart transplantation that is restricted in response to organ donor shortage. Pharmacotherapy targeting the regulatory mechanisms activated by left ventricular dysfunction has also been applied, namely inhibitors of the renin–angiotensin system, β-blockers and mineralocorticoid-receptor antagonists. Still, these approaches are intrinsically non-curative, failing on cardiac regeneration and repair.

2. Stem Cell-based Therapies for Myocardial Regeneration

The limited capacity of human adult heart to renew cardiac tissue after injury in addition to limited therapeutic options have led to the global burden of CVD. In this context, readily available cell sources able to increase heart performance are highly desirable. Therapies relying on stem cell-based approaches have been evaluated in several preclinical and clinical trials (Faiella & Atoui, 2016).

Stem cells hold a great promise in biomedical research, namely in cell therapy, tissue engineering and drug discovery applications. The use of stem cells

in research allows the understanding of basic mechanisms of human development and the identification of key regulators/molecules for their differentiation, potentiating the development of new treatments. Different cell types are under evaluation for cell-based cardiac therapies and its selection relies on their features, accessibility and potential risk. Ideal stem cell source must have the ability to differentiate into CMs and vascular endothelial cells and/or must act via paracrine mechanisms, with the secretion of chemokines or growth factors for improved resident cell survival and heart function (Figure 1.1). Nevertheless, the transplantation of multiple cell sources might stimulate the myocardium regeneration at different levels.

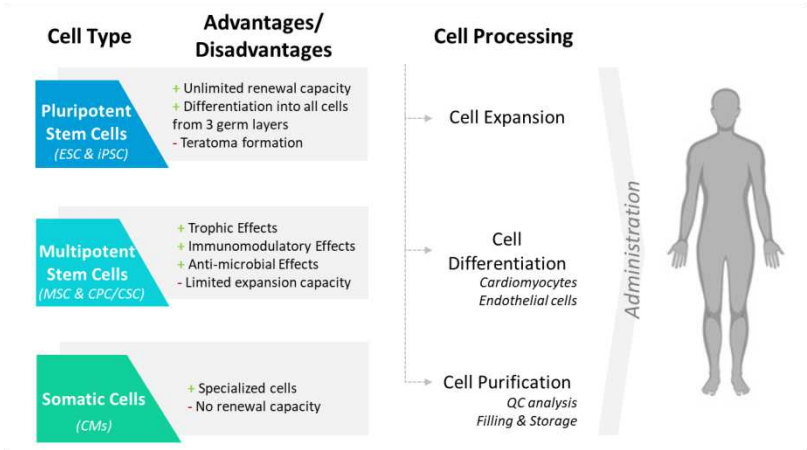

Figure 1.1. Cell sources for cardiac cell -based therapies. Cell manipulation might be needed after cell isolation, namely cell expansion, differentiation and purification to be administrated into the patient. Adapted from (Murphy et al., 2013).

Stem cell-based products are considered an Advanced Therapy Medicinal Product (ATMP) that can be either somatic cell therapy medical product or tissue engineered product. For marketing authorization of cell-based products, regulatory authorities in the USA (Food and Drug Administration) and EU (European Medicines Agency) have published guidance documents for its application and the European Commission adopted Guidelines on Good

Manufacturing Practice (GMP) specific for ATMPs in last year ("Eudralex The Rules Governing Medicinal Products in the European Union, Volume 4, Good Manufacturing Practice").

Such therapies can be either allogeneic or autologous based on their origin. In allogeneic stem cell therapy there is a single healthy donor whose human leukocyte antigens (HLA) are acceptable matches to the patient's and a large cell bank is available. For autologous cell therapy, stem cells are harvested from a patient, expanded or differentiated *ex vivo* if needed and then returned to the same patient (Malik, 2012) (Figure 1.2). Selecting the best therapy to use depends on several factors, namely disease type, stage and/or status as well as availability of a suitable and compatible donor (Richard, 2003). The manufacturing costs and logistics differed between allogeneic and autologous therapies. Such factors are also critical to determine which therapeutic type to pursue to produce a commercially attractive product. In allogeneic stem cell therapies, a larger facility for the manufacturing of each production batch (scale-up processing) is required and its "off-the-shelf" availability as well as the reduction in cost of goods makes this therapy more attractive than autologous therapies. Nowadays, new platforms are being implemented to address the manufacturing challenges for different cell-based products, maintaining its quality (Abraham et al., 2017).

2.1 Stem Cell Sources

2.1.1 Mesenchymal Stem Cells

The first generation of cell-based therapies for cardiac repair and regeneration was based on bone marrow-derived mononuclear cells, mesenchymal stem cells (MSC), among others. MSC unique features make them a very attractive cell source for allogeneic or autologous therapies for inflammatory and fibrotic conditions, due to their immunomodulatory and anti-inflammatory properties, as well as their non-immunogenicity. MSC were originally isolated

from bone marrow (Pittenger et al., 1999), presenting an inherent capacity to self-renew and differentiate into osteoblasts, adipocytes, and chondroblasts. Since then, cells with MSC-like characteristics have been isolated from other adult and fetal tissues, including cord and peripheral blood, fat, placental and umbilical tissues (Anker et al., 2004; O. K. Lee, 2004; Murphy et al., 2013; Zuk et al., 2002). Despite the phenotypic similarities between all MSC populations, there is an inherent heterogeneity at transcriptional and proteomic levels reflecting some disparities on the activity of MSC from different tissues of origin (Klopp et al., 2012).

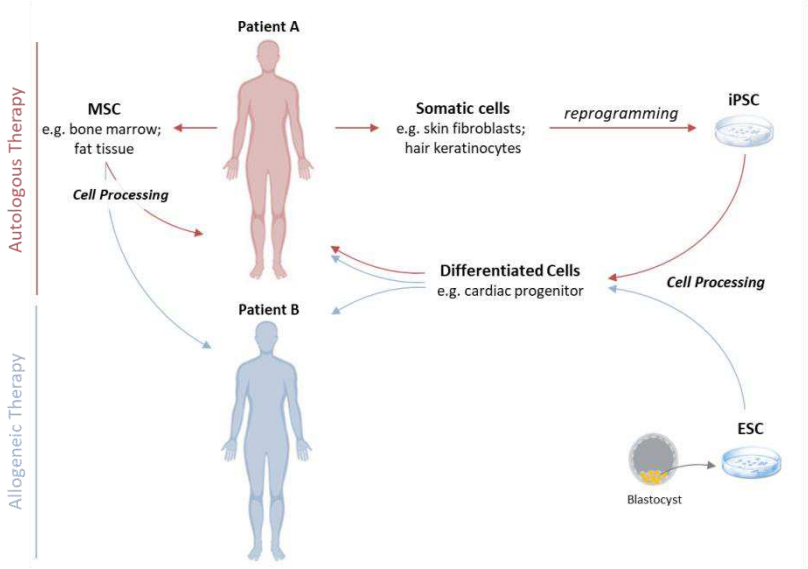

Figure 1.2. Autologous & Allogeneic cell-based therapies for heart repair using MSC isolated from bone marrow, fat tissue, etc., and PSC derivatives. Somatic cells from patient A can be isolated, reprogramed into iPSC and after manipulation (expansion and differentiation into cardiac progenitor cells or cardiomyocytes) those cells can be transplantation into the same patient (autologous) or in a matched donor (allogeneic). ESC derivatives can also be used as stem -based products for allogeneic therapies.

In an attempt to standardize the MSC' definition, the International Society for Cellular Therapy (ISCT) established criteria to characterize these cells in culture, as follow: i) to be plastic-adherent cell population; ii) to exhibit a defined

immunophenotype, more than 95% of cells must express CD73, CD90, CD105 and lack of hematopoietic/endothelial markers expression (e.g. CD45, CD34, CD14/CD11b, CD79/CD19 and HLA-DRI); and iii) to be capable of differentiating toward mesenchymal lineages (e.g., adipogenic, osteogenic and chondrogenic lineages) (Dominici et al., 2006). The intrinsic capability of MSC to migrate towards injured tissues (cellular homing) along with the immunomodulatory effects, emphasizes their suitability for clinical applications, such as anti-cancer agents delivery or tissue repairing capacity (Caplan & Correa, 2011).

Beneficial effects of transplanted adult stem cells (MSC) into infarcted myocardium is likely due to multiple mechanisms such as neovascularization and remodeling of the scar tissue rather than the formation of new CMs (Le & Chong, 2016). Ongoing clinical trials of ischaemic heart diseases employing autologous or allogeneic MSC-based therapy are presented in Table 1.1. MSC-based therapies have shown promising results for cardiac injury, promoting functional recovery (Gaebel et al., 2011). The safety of MSC infusion on infarcted heart was demonstrated in a large randomized phase II-III trial (NCT01392105), whereas the left ventricular ejection fraction (LVEF) was modestly improved at a 6-month follow-up visit (Lee et al., 2014). Nonetheless, the optimal cell dose is a critical parameter that depends on the selected cell type. In the POSEIDON trial (NCT01087996), the high dose of MSC (200×10^6 cells) was less effective in increasing LVEF than a low dose of MSC (20×10^6 cells) after MI (Hare et al., 2012). A randomized and controlled phase II-III trial is under evaluation to compare the effects of single versus repeated application of autologous bone marrow-derived mononuclear cells to treat patients following MI (REPEAT trial; NCT01693042).

Meta-analysis of the first generation of cell-based therapies in patients with MI have shown contradictory clinical outcomes from several single and multicenter studies and multiple publication (Gyöngyösi et al., 2016). This led to a switch towards a second-generation therapy in cardiac regeneration field,

comprising cardiac progenitor/stem cells (CPC/CSC) and pluripotent stem cells (hPSC).

2.1.2 Cardiac Progenitor/Stem Cells

CPC/CSC were identified as resident cell populations within myocardium expressing multiple markers, such as c-Kit, Sca-1, Isl-1, SSEA-1 and Abcg2. Importantly, these cells are able to differentiate into cardiomyocytes, vascular smooth muscle and endothelial cells (Beltrami et al., 2003; Oh et al., 2003). These cells can offer distinct advantages over other adult stem cells for cardiovascular regeneration, being tissue-specific and committed to cardiovascular lineages. CPC/CSC are also characterized by the secretion of growth factors, involved in signaling pathways stimulating the endogenous cardiac cells and/or paracrine mechanisms. The direct contribution of CSC to give rise to new CMs, after cell loss upon injury remains an open question, as well as their origin, *in vivo* activation and their role in tissue homeostasis and repair (Bollini et al., 2011). Still, increased recovery of LV systolic function and decreased infarct size after MI was demonstrated in the first clinical trial using autologous c-kit^{+} CSC (SCIPIO; NCT00474461) (Bolli et al., 2011). Further advances in this field have contributed to the development of novel therapies exploring the combination of different autologous cell sources (MSC and CPC/CSC), which is currently under clinical evaluation and showing a positive synergistic effect (CONCERT-HF; NCT02501811). Repeated cell therapy trials are emerging as alternative approach for cardiac treatment (Bolli & Ghafghazi, 2017). Promising outcomes have been shown in MI rodent models (mice and rats) where 3 repeated doses (12×10^6 cell/dose) of CPC are much more effective than a single administration (36×10^6 cell/dose), resulting in a cumulative improvement in left ventricular function and structure (Tang et al., 2016; X. Tang et al., 2018). Nonetheless, the fundamental aspects of

this administration as well as the optimal dose frequency need to be explored and validated in new clinical trials to test its truly safety and efficacy.

2.1.3 Pluripotent Stem Cells

The intrinsic characteristics of hPSC, such as their ability to proliferate indefinitely and to differentiate into all cell types of the three germ layers (ectoderm, endoderm and mesoderm), makes them also a powerful cell source for the establishment of production platforms of specific human cell types, which can be used in cell therapy and *in vitro* disease modeling (Robinton & Daley, 2012). hPSC include human embryonic stem cells (hESC), derived from the inner cell mass of the blastocyst, and human induced pluripotent stem cells (hiPSC), reprogrammed somatic cells using a cocktail of pluripotency genes. Although the ethical and political controversial in hESC research, these cells have been widely exploited as a tool for early human developmental studies and to understand several human diseases for therapeutic breakthroughs. However, most of the derived and registered hESC lines worldwide are not suitable for clinical applications due to the source of embryonic material and manufacturing processes (Fraga et al., 2011). Given this, new clinical-grade hESC lines were recently derived and characterized under a stringent Good Manufacturing Practice Quality Management System amenable for clinical therapeutic use (Ye et al., 2017). The development and implementation of more efficient protocols to direct differentiation of hESC into a desired cell type has strongly contributed to advances in this field. hESC clinical application is limited by histocompatibility and immunological tolerance of the host (ABO blood group antigens and HLAs). To reduce the likelihood of graft rejection, a study was conducted to estimate the number of hESC lines needed to achieve varying degrees of HLA match, raising practical, political, and ethical implications for the establishment of these cell banks (Taylor et al., 2005).

The emergence of iPSC revolutionized the field of stem cell research, with the ability of a somatic cell to “de-differentiate” into a pluripotent stem cell by introducing only four factors (Takahashi et al., 2007; Takahashi & Yamanaka, 2006). Since then, significant progresses have been made from improved manipulation and culture techniques towards more robust and reproducible disease cell models and drug screening platforms (Takahashi & Yamanaka, 2016). iPSC technology allows well-informed decisions in drug development pipeline, as better predictive tool (Sayed et al., 2016). iPSC research will be the fastest growing market throughout the forecast period 2017-2025, as it possesses application in regenerative medicines, drug screening, disease modelling, and organoid generation. hiPSC are remarkably like hESC in many key aspects critical for their application in regenerative medicine. However, comparative genomic analysis revealed differences between them (Chin et al., 2009), which could be expected due to differences in genetic background; also observed among different hESC lines. Such phenomena was also demonstrated for their differentiation potential into neurons, with a significant reduced efficiency and increased variability of hiPSC compared to hESC (Hu et al., 2010). Still, iPSC offer the unprecedented opportunity to recapitulate and study many other diseases, including Gaucher disease type III, muscular dystrophy, Parkinson disease, Huntington disease, diabetes mellitus (Marchetto et al., 2010; Park et al., 2008). The EBiSC – European Bank for induced pluripotent Stem Cells project aims to address the increasing demands by iPSC researchers for high-quality, disease-relevant and genetically diverse iPSC lines. This large repertoire would enable to predict the clinical outcome of a drug therapy with high accuracy, as well as to be the cell source of the therapy itself.

Menasché and colleagues reported the first clinical trial using hESC-derived cardiac progenitor cells in a patient with severe heart failure as presented in Table 1.1 (Menasché et al., 2015, 2018). A preclinical study using mouse models

demonstrated the functional benefits of hESC-derived cardiac progenitors resulting in sustained improvement in contractility and attenuation of remodeling, probably acting through paracrine mechanisms (Bellamy et al., 2015). Still, their ability to form teratomas *in vivo* and the uncertainty in selecting the most suitable cell source - progenitors *versus* fully differentiated cell type - to provide the best clinical outcome are the major concerns on their effectiveness to be translated into clinics (Trounson & DeWitt, 2016). Actual clinical trials are very costly due to the number of trial sites, training for the transplant procedure and cell manufacturing. A paradigm shift in the field of cell-based therapies for cardiac regeneration/repair was recently proposed by the international consortium TACTICS (Translational Alliance for Regenerative Therapies in Cardiovascular Syndromes) to improve the quality and translatability of preclinical studies (Chamuleau et al., 2018). The identification of truly effective and reproducible therapies at a preclinical level is crucial to avoid costly and inappropriate clinical trials with no therapeutic effect. For that, standardized, robust, reproducible and multicenter preclinical work must be conducted exploring *in vitro* and *in vivo* studies, showing high quality results registered in independent and open database.

2.2 Stem Cell Manufacturing Strategies

For the effective translation of stem cells and/or their derivatives into clinical applications, the manufacturing process is a critical bottleneck. There is a high need to develop safer and cost-effective manufacturing solutions, namely by changing media formulations or bioreactor design towards scalable production platforms compliant with good manufacturing practices (Kropp et al., 2017). Increased efficiency of bioprocess with lower variability could be attained by combining process automation, monitoring and control with physicochemical

culture parameters, e.g. hydrodynamics, oxygen tensions or media composition (King & Miller, 2007; Kropp et al., 2017).

A fundamental part of the manufacturing process is product identity characterization that should be analyzed by multiparametric assays, which allow the evaluation of cellular identity and function with a high level of sensitivity. Both MSC and hPSC are routinely expanded in static conditions as cell monolayers in flat surfaces (two-dimensional (2D) conditions). Still, the lack of culture process control (e.g. oxygen and pH), heterogeneity and low production yields limits its application in the systematic development of cell mass production, since for MI cell-based therapy it would be needed 10^9 cells/patient (Serra et al., 2012; Simaria et al., 2014). The combination of stirred culture systems and microcarrier technology offers great advantages in process scale-up over the standard 2D static culture (i.e., planar technologies), providing a high surface-to-volume ratio in a more controlled and homogeneous microenvironment. Accordingly, manufacturing costs related to the large expansion of adherent cells using microcarrier-based bioreactors are lower compared to planar technologies (Simaria et al., 2014).

2.2.1 Extracellular Matrix Composition

Microenvironmental cues, such as soluble factors, adhesive contexts and physical forces, strongly influence cellular functions and behaviors, as cell proliferation or differentiation into a specific cell lineage (Serra et al., 2012). Cellular events such as adhesion, migration, proliferation, differentiation, and survival can be directly modulated by the mechanical properties of the extracellular matrix (ECM), depending on its biochemical and biophysical nature. The reported expansion protocols for MSC using microcarriers (Cytodex^{TM}3 or Plastic P-102L) do not required the use of coating matrices (Table 1.2).

Table 1.1. Stem cell-based therapies for ischemic heart diseases using adult and pluripotent stem cells. The technologies developed, clinical trial, cell dose and major outcome are presented. Adapted from (Higuchi et al., 2017; Wu et al., 2018) and www.clinicaltrials.gov.

Cell Type	Cell Processing	Technology	Clinical Trial	Cell dose	Myocardial effects	Finish date	Ref.
MSC	*Expansion*	Allogeneic hMSC	Phase II study TRIDENT (NCT02013674)	20-100 × 10^6 cells	Increase % of LVEF in 100 × 10^6 cell dose condition	Jun-2019	(Florea et al., 2017)
MSC	*Expansion*	Autologous bone marrow-derived MSC	Phase II study MESAMI2 (NCT02462330)	61 × 10^6 cells	Still follow-up	Dec-2019	(Guijarro et al., 2016)[1]
MSC	n.m.	Umbilical cord-derived MSC	Phase I/II study UCMSC-Heart (NCT02439541)	10 × 10^6 cells	Still follow-up	Dec 2018	
MSC	n.m.	Allogeneic umbilical cord-derived MSC	Phase I/II study HUC-HEART (NCT02323477)	n.m.	Still follow-up	Feb-2018	
MSC	*Expansion*	Allogeneic human umbilical cord-derived MSC (hUC-MSC)	Phase I/II study (NCT02635464)	100 × 10^6 cells	Still follow-up	Mar-2019	
MSC+ CSC	*Expansion*	Autologous MSC and c-kit$^+$ Cardiac Stem Cells	Phase II study CONCERT-HF (NCT02501811)	150 × 10^6 MSC 5 × 10^6 CSC	Still follow-up	May-2020	
CDC	*Expansion (speroids)*	Allogeneic cardiosphere-derived cells (CAP-1002)	Phase I-II study ALLSTAR (NCT01458405)	25 × 10^6 cells	Still follow-up	Sep-2021	
CDC	*Expansion (speroids)*	Allogeneic cardiosphere-derived cells (CAP-1002)	Phase I study DYNAMIC (NCT02293603)	n.m.	Still follow-up	Apr-2020	
hESC	*Differentiation*	CD15$^+$ Isl-1$^+$ progenitors embedded into a fibrin patch	Phase I study ESCORT (NCT02057900)	4 × 10^6 cells	Increase % of LVEF	Jun-2018	(Menasché et al., 2015)

n.m. indicates not mentioned. [1] Published results from MESAMI pilot study.

Still, some reports showed an efficient expansion of these cells using xeno-free matrix to coat Plastic P-102L microcarriers or synthetic microcarriers (Dos Santos et al., 2014; Hervy et al., 2014). Over the last years, the gold standard for hPSC culture requires the use of Matrigel™ or feeder cells. In stirred culture systems, most of the reported expansion protocols for hPSC use Matrigel™-coated microcarriers (Table 1.2).

However, this matrix is complex, not defined and contains animal components. To meet regulatory safety concerns, efforts have been made to develop fully-defined and xeno-free matrices for hPSC propagation. In particular, Fan and colleagues engineered xeno-free microcarriers for hPSC expansion in stirred vessels, making the hPSC more suitable for clinical applications (Fan et al., 2014). Currently, at least three well-defined and xeno-free components are commercially available: CELLstart™ (Invitrogen), StemAdhere™ (Stem Cell Technologies) and Synthemax® (Corning), amenable for the implementation of standardized, reproducible and scalable cell culture platforms for the production of clinically relevant hPSC.

2.2.2 Physicochemical and Hydrodynamic Environment

In addition to the molecular composition and mechanical properties of the cellular microenvironment, physicochemical parameters as dissolved oxygen, pH and temperature, as well the bioreactor hydrodynamics can greatly influence cell's behavior. The use of environmentally controlled bioreactors should guarantee the i) cell maintenance (expansion or differentiation) in a scale-up process, ii) efficient local exchange of gases (e.g. oxygen), nutrients, metabolites and growth factors, and iii) provide physiological stimuli.

Different bioreactor's configurations have been exploited to cultivate stem cells: (i) microfluidic devices, (ii) rotating wall systems, (iii) stirred culture systems, and (iv) wave bioreactors (Kropp et al., 2017). Nonetheless, to accelerate the

clinical translation of allogeneic cell-based products, scalable disposable bioreactors are required. Today, there are several options of disposable and single-use bioreactors commercially available (e.g. Mobius CellReady, Millipore, Univessel, Sartorius Stedim Biotech or Vertical-Wheel™ from PBS Biotech, Inc.), bypassing high capital expenses, long installation lead times, and avoiding extra-manipulation related to *in situ* sterilization and cleaning between batches (MSC expansion report on Table 1.2). In an attempt to use the "ideal bioreactor" to cultivate the cell source of interest, there are several issues to take into consideration, such as their ability to mix the liquid in a faster and homogeneous way to minimize spatial gradients across the vessel (temperature, pH, dissolved oxygen and nutrient levels) at high mass-transfer and low-shear stress, while maintaining the cells/microcarriers in suspension (Hashimura et al., 2012).

Dissolved oxygen (DO), as a critical process parameter, must be tightly regulated, since low oxygen tensions have a beneficial impact on the maintenance of the undifferentiated state of embryonic and mesenchymal stem cells, among others (revised in Mohyeldin et al., 2010; Serra et al., 2010). Still, more studies using DO-control based are needed to clarify the DO optimal conditions for stem cell expansion.

2.2.3 "Omics" Tools in preclinical and clinical research

The identification of key regulatory mechanisms and pathways associated with stem cell self-renewal or maintenance and along their differentiation is mandatory to be translated into robust and effective stem cell manufacturing platforms or to develop reliable cell-based disease models. In biopharmaceutical and biomedical settings, efforts have been made towards knowledge-driven approaches for the implementation of improved manufacturing processes. Accordingly, characterization of the fundamental cellular mechanisms in such processes, namely mammalian cells lines for therapeutics production or stem cells

for allogeneic or autologous therapies, by exploring multi-omics tools including transcriptomic, proteomic and metabolomics techniques would be crucial (Farrell et al., 2014).

The investigation of the transcriptome, proteome and/or metabolome can provide novel insights on cellular phenotype as to facilitate bioprocess optimization, ensuring product quality and potency. Moreover, these tools allowing the measurement of near-totality of genes, transcripts, proteins and metabolites have prominently facilitated the discovery of molecules that serve as biomarkers (McShane et al., 2013). Over the past 20 years, the FDA´s Office of Women's Health has funded 34 research projects to FDA-regulated products involving omics-related technology, which has contributing to different areas, namely FDA-regulated product safety assessment, drug-induced toxicity and personalized medicine in the diagnosis and treatment for diseases prevalent in women.

Whole-gene expression analyses have been performed to characterize the cell phenotype during expansion and differentiation processes (Huang et al., 2017) or to identify transcriptomic signatures from each cell source (Gao et al., 2017). Proteomic tools can also aid these analyses in stem cell phenotype, such as in MSC studies to identify potential hazards associated with senescence and tumoral transformation, to identify MSC' proteomic signatures along its expansion and differentiation, as well as in disease setting (Mateos et al., 2014).

The similarities and differences between hESC and hiPSC have been extensively studied at several levels, namely global gene expression, epigenetic status and metabolic regulation. Interestingly, DNA methylation analysis demonstrated that the methylome of hiPSC differs from hESC and their counterparts, retaining an "epigenetic memory" from the somatic cells (Doi et al., 2009).

Table 1.2. Studies reporting the expansion of hPSC and hMSC on microcarriers in different culture systems. (MC: microcarriers; N/A: not available; ULA: Ultralow attachment plates; SV: Spinner vessels; STB: Stirred-tank bioreactors).

MC	Coating	Cell Type	Culture System	Cell Yield	Fold Increase	Ref.
Hillex II	N/A	hESC	ULA plates	0.7×10^6 cell/mL	3 fold in 5 days	(Phillips et al., 2008)
DE-53	Matrigel™	hESC	SV (0.025 L)	3.5×10^6 cell/mL	9 fold in 7 days	(Chen, Chen, Choo, Reuveny, & Oh, 2011)
		hiPSC	SV (0.1 L)	6.1×10^6 cell/mL	20 fold in 7 days	(Bardy et al., 2013)
Cytodex™3	N/A	hESC	SV (0.066 L)	1.5×10^6 cell/mL	6.8 fold in 14 days	(Fernandes et al., 2009)
	Conditioning with media	BM-hMSC	STB (1.5 L)	2.6×10^6 cell/mL	10 fold in 5 days	(Zhou et al., 2013)
	Matrigel™	hESC	ULA plates	N/A	3.4 fold in 2.5 days	(Nie, Bergendahl, Hei, Jones, & Palecek, 2009)
		hESC	SV (0.3 L) – 5% pO2 SV (0.3 L) – 30% pO2	2.2×10^6 cell/mL 0.8×10^6 cell/mL	15 in 11 days 7 in 12 days	(Serra et al., 2010)
Cytodex™3 Cytodex™1	Collagen	BM-hMSC	STB (3 L-CellReady)	2×10^5 cell/ml	N/A	(Niss et al., 2013)
Cytodex™1	Matrigel™	hESC hiPSC	SV (0.025 L)	3.7×10^6 cell/ml 3.5×10^6 cell/ml	19 fold in 7 days 18 fold in 7 days	(Ting, Chen, Reuveny, & Oh, 2014)
Plastic P-102L	*Conditioning with media*	BM-hMSC	STB (2.5 L)	1.7×10^5 cell/ml	6 fold in 12 days	(Rafiq, Brosnan, Coopman, Nienow, & Hewitt, 2013)
	CELLstart CTS solution	BM-hMSC AT-hMSC	SV (0.1 L)/STB (0.8 L)	1.3×10^5 cell/ml 0.6×10^5 cell/ml	N/A	(Dos Santos et al., 2014)
ProNectinR®F-coated MC		BM-hMSC	STB (0.1-35L)	$2.8\text{-}3 \times 10^5$ cell/ml	N/A	(Schirmaier et al., 2014)
Polystyrene	Matrigel™	hESC	SV (0.05 L)	1×10^6 cell/ml	34-45 fold in 8 days	(Lock & Tzanakakis, 2009)
		hiPSC	SV (N/A)	3.5×10^6 cell/ml	5.6 fold in 7 days	(Kehoe, Jing, Lock, Tzanakakis, & Ph, 2010)
	Laminin Vitronectin	hESC	ULA plates	1.5×10^6 cell/ml 1.4×10^6 cell/ml	8.5 fold in 7 days	(Heng et al., 2012)
		hESC	SV (0.025 L)	3×10^6 cell/ml	15 fold in 7 days	(Lam et al., 2014)
	pLL solution	hiPSC	SV (0.05 L)	1.6×10^6 cell/ml	19 fold in 6 days	(Fan et al., 2014)

To understand the inherent variability among hPSC cell lines, the Human Induced Pluripotent Stem Cells Initiative (http://www.hipsci.org/), a comprehensively characterized open access iPSC resource from healthy individuals and rare diseased volunteers, recently described the systematic generation, genotyping and phenotyping of 711 iPSC lines derived from 301 healthy individuals using high-throughput and high resolution transcriptomic and proteomic tools (Kilpinen et al., 2017). Indeed, these differences might have an impact on their differentiation potential and further applications. Such differences have also been investigated at metabolic level, mostly in terms of glucose-related genes expression, where hiPSC showed slightly lower levels of expression/activity and differences in mitochondria morphology in comparison to hESC and differentiated cells (Varum et al., 2011). Several studies have reported that highly proliferative cells (e.g. hPSC) have a unique energetic metabolism compared with their counterparts, presenting high glycolytic flux that can be controlled by transcription factors and signaling network molecules, including the phosphatidylinositol 3-kinase/Akt/mammalian target of rapamycin system (Agathocleous & Harris, 2013).

Comparison studies can also be performed using publicly available data sets, providing an extra validation level of the published results (e.g. Genotype-Tissue Expression portal, Human Brain Atlas or Human Protein Atlas). Advances in omics-technologies and bioinformatics is prompting a shift towards integrative pipelines in pre-clinical and clinical research (Manzoni et al., 2018; McShane et al., 2013). Since the transcriptome, proteome and metabolome are not isolated biological entities, (multi)omics data should be concomitantly analyzed and integrated contributing to the understanding of human health and/or disease (Figure 1.3) (Yugi, Kubota, Hatano, & Kuroda, 2016). However, such entities are still mainly analyzed as separate areas that generate a monothematic type of knowledge. Cancer biology field is at the forefront for data integration to be translated into clinics. The ColoRectal Cancer (CRC) Subtyping Consortium applied data integration to categorize molecular

colorectal cancer subtypes for knowledge-driven decisions and predict patient outcomes. Recently, such molecular subtypes were faithfully recapitulated in CRC cell cultures and patient-derived xenografts, enabling researchers to study CRC intrinsic and stable features (Linnekamp et al., 2018).

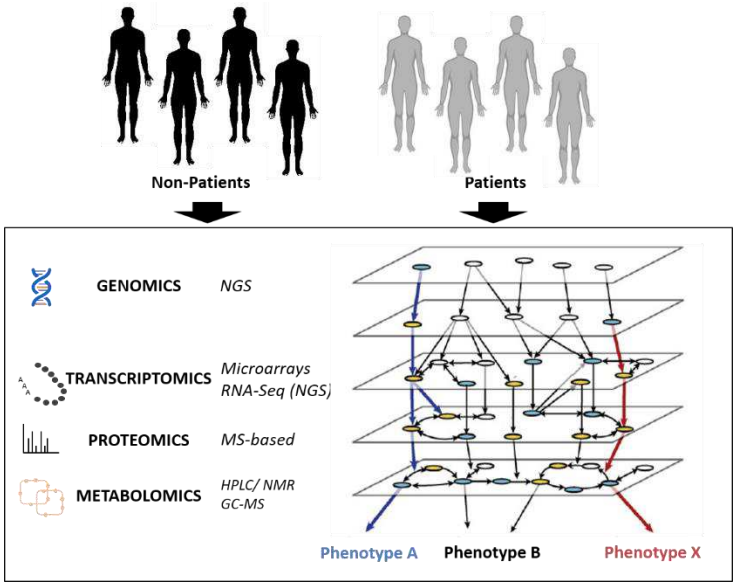

Figure 1.3. Trans-omics analysis. This technology includes the phenotypic relation to multiple-omic layers, reflecting both genetic and environmental factors. Adapted from (Yugi et al., 2016)

Regardless these advances in data integration and sharing, there are still several biological limitations and challenges. Perhaps in near future, with the advances in cell-based modeling, image analysis and machine learning, more complex cell-based assays would emerge leading to a fundamental shift in phenotypic screening towards more global definitions of cell health/disease (Finkbeiner et al., 2015). Nonetheless, the effective translation of this knowledge and advances into complex disorders remains a challenge.

3. Noncellular Therapies for Myocardial Regeneration

Although promising preclinical cell-based studies, small or negligible cardiac function improvements have been observed in most of the clinical trials (phase II-III) mainly due to poor engraftment and rapid cell clearance (Bolli & Ghafghazi, 2017). Fortunately, no adverse effect has been documented so far, evidencing the safety of such therapies. Nonetheless, these results have prompted the search and development of novel therapies implying endogenous heart regeneration (Cahill et al., 2017). Animal models have been widely exploited to study a variety of biological aspects of human development. Particularly, heart regeneration-underlying biological mechanisms have been exploited in several studies using zebrafish and neonatal mouse models (Vivien et al., 2016). The lack of reliable techniques to distinguish newly muscle tissue from the preexisting one is limiting the assessment of adult mammalian heart regeneration (Karra & Poss, 2017). Next-generation therapies for heart regeneration/repair are directed toward cell enhancement or early retention (using 3D cell constructs, cytokines and miRNAs or biomaterials) and cell- free approaches (administration of growth factors, non-coding RNAs and extracellular vesicles or by direct reprograming of fibroblasts into CMs) (Cambria et al., 2017; Menasché, 2018). Cardiac engineering approaches by combining hPSC-derived CMs and cardiac fibroblasts with or without scaffolds have shown cardio-therapeutic potential after MI (Iseoka et al., 2018; Tiburcy et al., 2017). Nonetheless, poor mechanistic insights into the biology of heart regeneration, namely on CMs proliferation, endogenous cell niches, neovascularization, etc., has hampered the effective clinical translation of such therapies targeting heart repair following MI.

3.1 Coronary vasculature formation & revascularization upon injury

Proper coronary vascular development is essential for late embryonic and adult cardiac tissue physiology. Upon MI, even after reperfusion, microvasculature

obstruction persists in up to 50 % of patients, leading to endothelial cell death, inflammation and overall remodeling (Cahill et al., 2017). Regeneration of the coronary microcirculation would be crucial for the effective heart repair. For that, there is a need to better understanding of how coronary vessels are built during development.

In the last years, several groups have identified three major progenitor populations of the embryonic origin of coronary endothelial: proepicardium (PE), sinus venosus (SV), and endocardium (Endo). PE is a transient extracardiac mesothelial cell population that migrates to the developing heart to give rise to the epicardium (Ep). Once the Ep covers the heart tube, a subpopulation of epicardium-derived progenitor cells (EPDCs) undergo epithelial-to-mesenchymal transition, migrate into the myocardium and give rise to vascular smooth muscle cells, fibroblasts and cardiomyocytes (Simões & Riley, 2018; Smart et al., 2009; Smits et al., 2018; Tian et al., 2015). In the adult heart, most epicardial cells remain quiescent, but upon MI these cells differentiate only into SMC and fibroblasts, leading to myocardium remodeling (Figure 1.4).

The crosstalk between epicardium (Ep) and myocardium is essential for coronary vessel formation during heart development, namely through fibroblast growth factor (FGF) and vascular endothelial growth factor (VEGF) signaling pathways, myocardial factor thymosin β4 (Tβ4) or GATA4-FOG2 interaction (Tian et al., 2015). Several preclinical studies have demonstrated the key role of Tβ4 in neovascularization, by promoting the inward migration of EPDCs and differentiation into endothelial and smooth muscle cells to form the coronary vasculature through paracrine stimulus (Smart et al., 2007). These studies also confirmed that the cardiac neovascularization through Tβ4 was mediated by CPC activation. RegeneRx company is developing an injectable Tβ4 formulation (RGN-352) for the treatment of MI and chronic heart failure, which successfully completed the clinical phase I assuring the product safety.

A compensatory mechanism to rebuild the coronary vasculature was recently reported, demonstrating the regulation of distinct coronary progenitor pools by both genetic timing (ELABELA-APJ signaling) and the microenvironment (hypoxia) to ensure the establishment of the proper vasculature needed for heart physiology (Sharma et al., 2017). Still, the precise mechanisms of coronary revascularization upon injury are unclear. Nonetheless, the understanding of how the epicardial response is modulated along regeneration compared to scar formation would guide towards optimal therapeutic approaches.

There are several promising alternative therapeutic strategies that could be considered for heart regeneration, namely (i) the activation of epicardial cells, (ii) the activation of angiogenesis and lymphangiogenesis, (iii) immunomodulation, and (iv) fibrosis inhibition. The delivery of specific recombinant factors (e.g. VEGF-A) to support angiogenesis, cardiomyocyte proliferation and survival, would greatly improve healing and functional outcome of the heart upon injury. However, the use of VEGF-A in clinical trials (EUROINJECT-ONE and NORTHERN) aiming at neovascularization has failed to show beneficial effects (Taimeh et al., 2013). The poor outcomes of these growth factor-based approaches might be due to inappropriate dosages and/or the lack of organ selectivity. Nonetheless, improved heart function was achieved by the intramyocardial injection of synthetic modified RNA encoding human VEGF-A in a mouse and swine myocardial infarction models (Carlsson et al., 2018).

This technology was firstly applied for cell reprogramming to generate hiPSC and has been under investigation as a new way to trigger heart regeneration (Chien, et al., 2015; Warren et al., 2010). An epicardial follistatin-related protein 1 (FSTL1) was identified as an alternative growth factor that promotes myocardial regeneration after injury, showing a 10 % improvement in LVEF at large-animal preclinical studies (Wei et al., 2015).

Cardiac lymphatic vessels emerged at E12.5, from extra-cardiac regions proximal to the outflow tract, on the ventral side (Figure 1.4). Coronary lymphatic endothelial cells (LECs) within the expanding plexus on the developing heart co-expressed VEGFR-3, Prox1 and LYVE-1 (Klotz et al., 2015). Recently, Klotz L. and colleagues showed that the adult cardiac lymphatics underwent a significant angiogenic response initiating the lymphatic developmental program followed by MI (Klotz et al., 2015). Augmentation of lymphangiogenesis is an emerging strategy for clearance of edema and reduce inflammation, promoting cardiac repair through the ectopic VEGF-C stimulation following injury (Henri et al., 2016; Klotz et al., 2015).

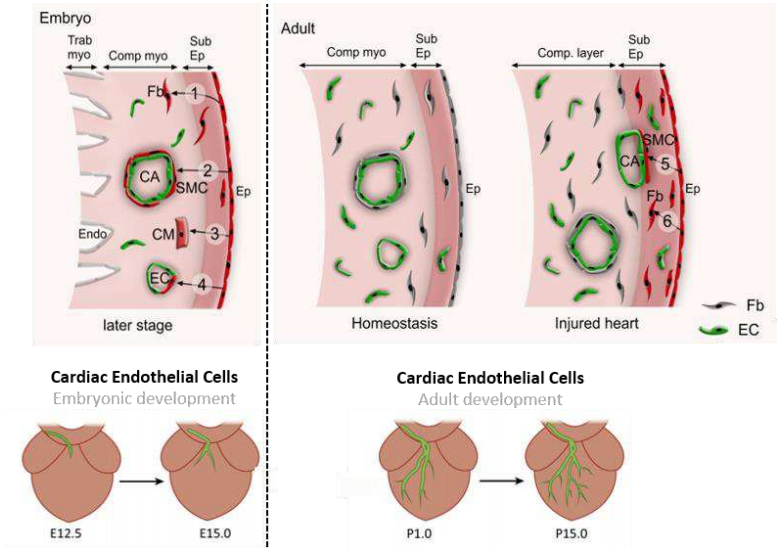

Figure 1.4. Heart Vasculature Formation. In late embryonic stages, epicardial cells (Ep) form mesenchymal epicardium-derived cells (EPDCs) by epithelial-to-mesenchymal transition in subepicardial layer (Sub Ep) and also migrate into myocardium (myo), where they differentiate into fibroblasts (Fb), smooth muscle cells (SMC), cardiomyocytes (CM), and endothelial cells (EC). By embryonic day E12.5, cardiac lymphatic endothelial cells (LEC) enter the heart to form the first lymphatic capillaries. After birth, the lymphatic network expands towards the apex following the coronary veins and by day P15 the cardiac lymphatic network is fully developed. In normal conditions (homeostasis), Ep cells remain quiescent (homeostasis), while after myocardium infarction, Ep cells become activated in Sub Ep differentiating into Fb and SMC. MI also affect coronary lymphatic vasculature. Adapted from (Aspelund et al., 2016; Vuorio et al., 2017).

VEGF-C is the key mediator of lymphangiogenesis during development and is required for proper development of SV-derived coronary vessels through its binding to VEGF receptor 3 (VEGFR3) following maturation process (Chen et al., 2014a, 2014b). Genetic studies in zebrafish and mice models displaying lymphatic vessels defects, as well as in rare individuals with Hennekam syndrome, have contributed to the identification of a secreted protein collagen and calcium-binding EGF domain 1 (CCBE1) that is required for proper lymphatic vascular development (Alders et al., 2009; Hogan et al., 2009). Recent studies have reported the requirement of CCBE1 and a metalloproteinase (ADAMTS3) for the proteolytic processing of VEGF-C but not VEGF-D (Bui et al., 2016) (Figure 1.5B).

3.2 CCBE1 as a potential modulator of cardiac function

CCBE1 contains an N-terminal domain with three calcium binding EGF-like repeats and a C-terminal domain with two collagen-like repeats. Most known mutations of CCBE1 in humans are localized in its N-terminal domain associated to the Hennekam syndrome (Alders et al., 2009). Several reports have dissecting the importance of each terminal domain of CCBE1 using knock-in mice expressing different CCBE1 deletion mutants. These studies have shown two modes of action: CCBE1 accelerates the proteolytic cleavage of pro-VEGF-C – mediated by C-terminal domain, and localizes pro-VEGF-C mainly on the surface of endothelial cells to efficiently form the trimeric complex (pro-VEGF-C/CCBE1/ADAMTS3) – mediated by N-terminal domain (Jha et al., 2017; Roukens et al., 2015) (Figure 1.5B). It is highly expressed near to developing lymphatic vessels and particularly in the developing heart (Bos et al., 2011). CCBE1 was identified in early cardiac progenitors in chick embryos, and in heart precursors of first and second heart fields, and PE in mouse embryos from day E7.0 to E9.5 (Facucho-Oliveira et al., 2011). A recent study also showed a higher expression of CCBE1 in pericardium, epicardium and SV of the

embryonic mouse heart at E11.5 to E13.5, when coronary vessels stars to form (Bonet et al., 2018).

In mouse, CCBE1 have been shown to impact on the formation of SV-derived subepicardial coronary vasculature and coronary arteries during embryonic development (Sharma et al., 2017; Bonet et al., 2018). Interestingly, *Ccbe1* knockout mouse models displayed similar heart defects as in *Vegfc* mutants as well as in *Ela* or *Apj* mutants (Sharma et al., 2017). Indeed, CCBE1 is essential for the migration of the endocardial-derived ventral coronary vessels (Bonet et al., 2018). The ELABELA-APJ signaling axis is required for SV-derived progenitors and agonists of APJ would be considered as therapeutic agents to regulate cardiovascular homeostasis in adult. Accordingly, CCBE1 could also potentially be used as a therapeutic factor to promote neovascularization upon injury.

Given the embryonic lethal Ccbe1$^{-/-}$ phenotype at E14-14.5, the investigation of the complete loss-of-function of CCBE1 in adult heart, e.g. following MI, is only possible by conditional KO (Bui et al., 2016). Alternatively, the use of precise gene editing tools (e.g. CRISPR/Cas9) would greatly contribute for *in vivo* and *in vitro* studies uncovering the CCBE1 role in cardiac repair.

3.3 Gene editing tools

Understanding the regulatory networks driving specific cellular activities, in healthy or pathophysiological conditions, involves the use of precise and effective tools for specific gene manipulation. The combination of genome-engineering strategy and hiPSC technology enabled the generation of human cellular disease models in a precise and controlled manner, contributing also for predictable high-throughput drug screening platforms. Indeed, genome editing has been used to introduce genetic alterations to create disease models (e.g. cardiomyopathies and neurological disorders) or correct certain genetic mutations in iPSC-derivatives (Sayed et al., 2016).

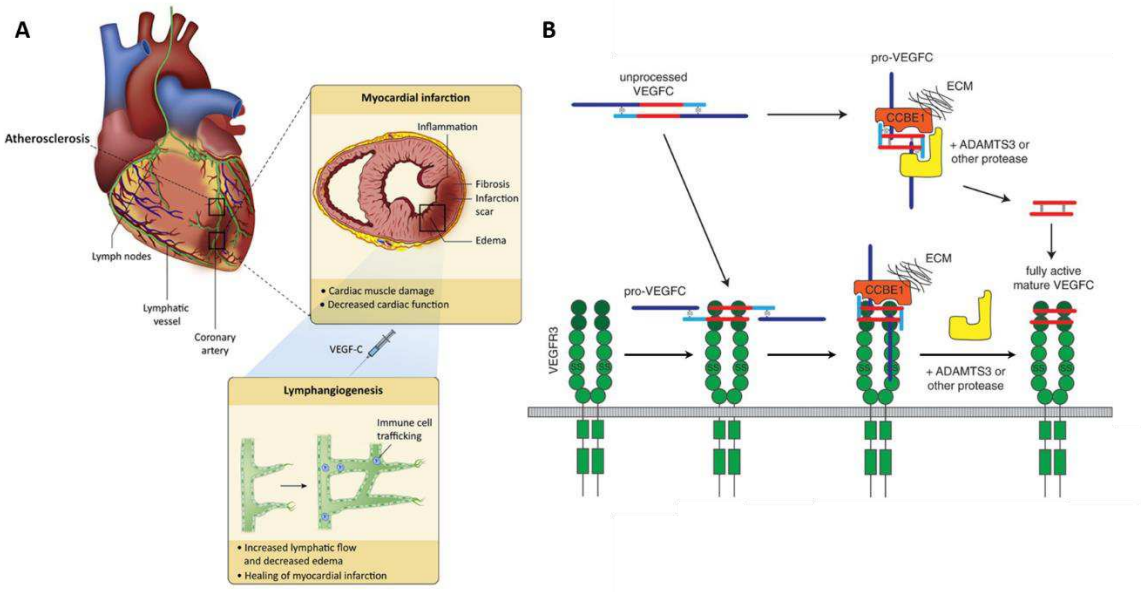

Figure 1.5. Lymphangiogenesis: VEGF-C role in myocardial infarction (MI) and its activation by CCBE1 and ADAMTS3. **A)** MI is followed by adverse remodeling of epicardial collector lymphatics and subsequent edema, severe inflammation and fibrosis. A therapeutic approach is based on VEGF-C administration to increase lymph flow and resolves inflammation, improving the cardiac function. **B)** CCBE1 secretion at sites of lymphatic vessel growth promotes the proteolytic cleavage of pro-VEGF-C form by the disintegrin/metalloprotease ADAMTS3. The mature form of VEGF-C can fully activate VEGFR-3. Most of the VEGF-C cleavage may occur on lymphatic endothelial cell (LEC) surface mediated by CCBE1 and ADAMTS3. Adapted from (Aspelund et al., 2016; Vuorio et al., 2017).

For that, it is crucial to create isogenic hiPSC line pairs, which have identical genetic backgrounds and differ in only a single genetic change, studying a specific mutation without confounding genetic background effects (Soldner et al., 2011; Y. Wang et al., 2014).

RNA-mediated interference (RNAi) was the first explored tool for studying gene function; however its inefficiency and non-specificity has limited their wide application (Jackson et al., 2003). For precise genetic modifications, custom-engineered and site-specific endonucleases were successfully developed: zinc-finger nucleases (ZFN) and transcription activation-like effector nucleases (TALEN) (Boch et al., 2009) (Figure 1.6). However, each DNA-binding protein needs to be individually designed and their construction and delivery is technically challenging. An emerging alterative based on RNA-guided nuclease surpass the above limitations. The type II Clustered Regularly Interspaced Short Palindromic Repeats (CRISPR) system uses a Cas9 derived from *Streptococcus pyrogenes* and a short non-coding CRISPR RNA sequence (single-guide RNA; sgRNA), which guides the Cas9 to the target sequence for site-specific double-stranded break (Jinek et al., 2012). CRISPR-Cas9 technology can also be explored as a gene regulation tool using a nuclease-deficient dCas9, which retains the ability to target specific sequences but unable to cleave DNA being a more versatile version of this technology. CRISPR/Cas9 system is a tremendously powerful tool for basic research applications, such as functional interrogation of new loci and generation of novel human cellular or animal disease models, as well as for novel clinical approaches. Currently, 14 studies exploring this technology are under clinical research, from the development of isogenic patient-derived stem cell lines towards disease treatment through genetic modification.

Heart embryonic development is tightly regulated showing gene activation and repression in a time-dependent manner, and dysregulation in the timing and dosage of critical transcription factors can lead to inherited congenital heart

defects (Takeuchi et al., 2011). The combination of CRISPR interference or activation technology (CRISPRi or CRISPRa) and iPSC lines can be exploited for temporal control of loss- or gain-of function phenotypes (Figure 1.6). Both CRISPR strategies were developed for gene regulation studies: the CRISPRi, where the dCas9 is fused with a repressor domain (e.g. KRAB), allowed the repression of a specific gene with a single sgRNA but might be limited by the presence of regulatory elements; and the CRISPRa, where the dCas9 is fused with activation domains (e.g. VP64), enabled the activation of reported or endogenous genes but requires multiple sgRNAs for effective activation (Dominguez, Lim, & Qi, 2016).

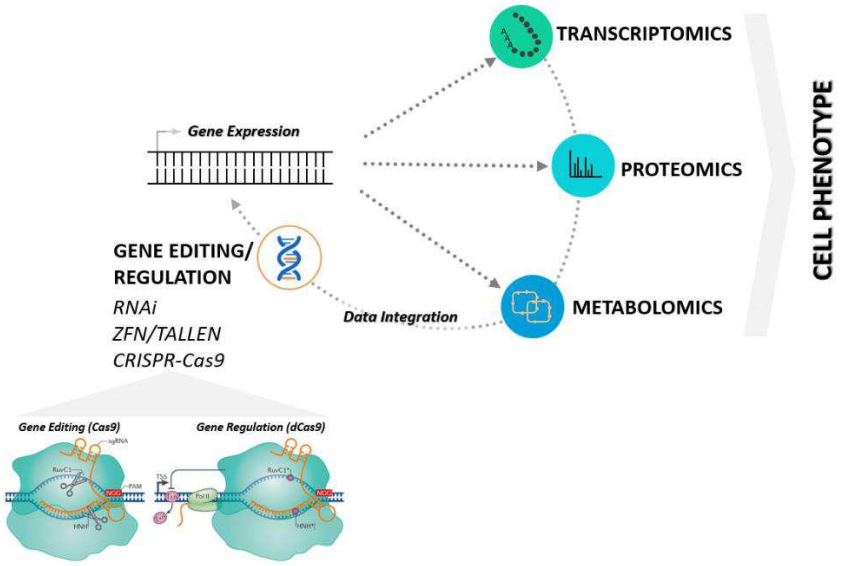

Figure 1.6. Gene editing tools. The identification of crucial cellular mechanisms through "omics" data integration and gene editing/regulation tools have been explored for the modulation of cell phenotype. Gene editing versus gene regulation strategies using Streptococcus pyogenes Cas9 and deactivated Cas9, respectively. Adapted from (Dominguez et al., 2016).

For loss-of function approaches, Mandegar and colleagues developed a versatile CRISPRi-based inducible system using iPSC lines to enable precise control of transcript silencing upon doxycycline addition, also amenable for studying cardiac development and disease mechanisms (Mandegar et al., 2016).

Genome editing has been used to introduce genetic alterations to create cardiac disease models or correct genetic mutations in iPSC-CMs to model cardiac diseases, such as Barth syndrome, mitochondrial disorder caused by mutation of the gene encoding tafazzin (G. Wang et al., 2014). In this study, Wang and colleagues combined patient-derived iPSC, CRISPR/Cas9, modified RNA and bioengineered microchips to mimic the pathophysiology of this disorder *in vitro* amenable for new target discovery. The CRISPR/Cas9 system has great potential to correct genetic defects in postnatal/adult mice. The ability of CRISPR/Cas9 system to disrupt a specific gene *in vivo* was recently demonstrated by Ding and colleagues (Ding et al., 2014). Here, the PCSK9 gene was efficiently disrupted in liver with no off-target mutagenesis, decreasing the risk of developing CHD due to higher LDL cholesterol levels (Ding et al., 2014). Recently, in Olson EN's group, a straightforward strategy was developed for rapidly edit genes of interest using a mouse model mimicking cardiomyopathy and heart failure diseases (Carroll et al., 2016). Thus, combining the multiplexing capacity of CRISPR/Cas9 and patient-specific iPSC technologies, more precise clinical trials would be performed towards precision medicine, identifying a subset of patients who optimally respond to the drugs under investigation, thereby reducing the attrition rates of developed drugs with clinical relevance.

4. Aims and Scope of Thesis

The overarching aim of this thesis was to implement strategies that could contribute for improved cardiac regenerative therapies. This work comprises two different parts: A) the development of robust and scalable approaches for manufacturing of stem cell therapy products, and (B) the interrogation of CCBE1 potential as a therapeutic factor, by unveiling its role on cardiac commitment (Figure 1.7).

The lack of robust protocols able to sustain production of high stem cell numbers, as required for regenerative medicine, has hindered its translation into clinical setting. Therefore, in the first part of this thesis, we explored different approaches aiming at improved stem cell expansion yields with high quality for clinical translation. For this, in **Chapter 2**, different culture matrices and conditions were tested to design an optimized protocol for the expansion of hESC. To assess the robustness of the optimized protocol using xeno-free microcarriers and stirred culture conditions, two different hESC lines, a feeder-dependent and a feeder-free, were expanded. Also, the impact of these conditions on hESC phenotype was evaluated exploring transcriptomic and metabolic tools. This work would provide physiological and metabolic insights of hESC expanded in different culture conditions that can also contribute to improved scale-up designs for such production systems. Given the proposed therapeutic potential of hMSC as a cell source for improving cardiac function following MI, in **Chapter 3**, we implemented a scalable protocol for the expansion of bone marrow-derived hMSC. For this, we used xeno-free microcarriers and a disposable low shear stress bioreactor (Vertical-Wheel^{TM} PBS-3 Air) that could effectively be translated into streamlined manufacturing platforms for clinical application. The impact of bioreactor design and hydrodynamics on hMSC growth profile and quality was also studied.

CCBE1 has been studied as a secreted protein critical for lymphatic/cardiac vascular development. Previous studies have proposed that CCBE1 may potentially be used to restore cardiac tissue upon heart injury, through CCBE1-mediated cardiac commitment and/or augmentation of lymphangiogenesis. Therefore, in **Chapter 4**, we conducted an *in vitro* study to investigate the CCBE1 molecular role on cardiac commitment, combining hPSC differentiation into cardiomyocytes (CM) and endothelial, and gene editing tools (CRISPR interference technology). We hypothesized that by understanding the CCBE1 role in each stage of CM or endothelial differentiation, we would be able to identify the CCBE1-

modulated signaling pathways for translation into CCBE1-based cardiac therapies. For this, we knocked down CCBE1 expression along hiPSC differentiation and its effect on CM and endothelial cells phenotype was assessed.

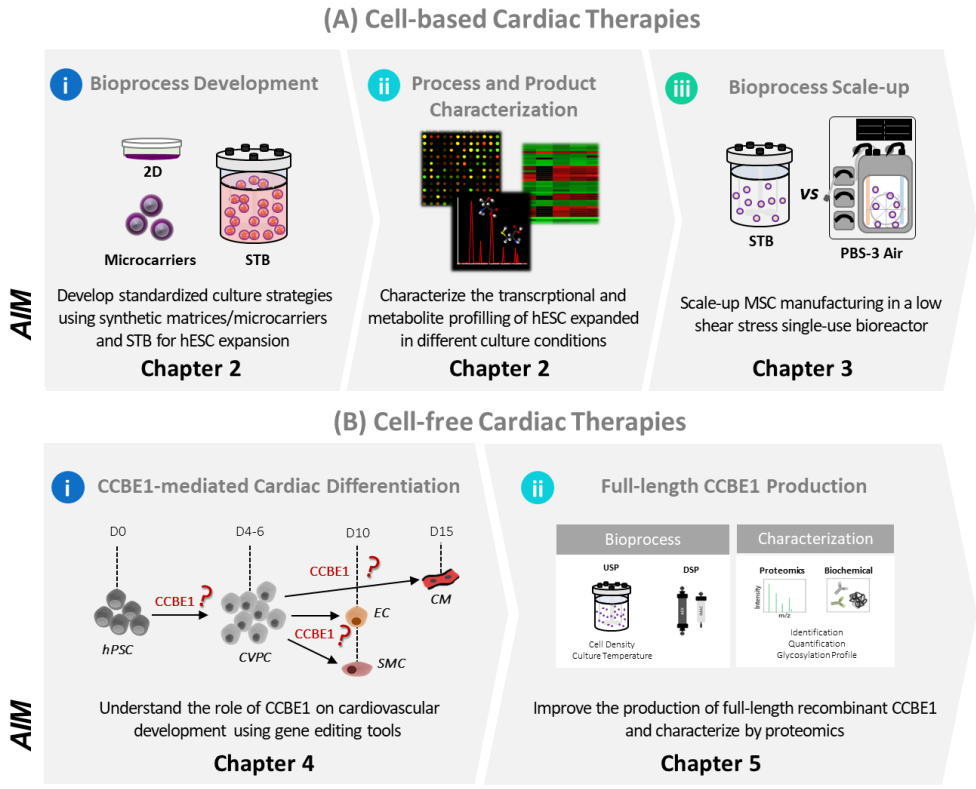

Figure 1.7. Schematic representation of the different strategies and major aims of this thesis on cellular- and noncellular-based cardiovascular therapies. 2D- two-dimensional culture; STB- stirred-tank bioreactors; PBS-3 Air- Vertical-Wheel^{TM} bioreactor (PBS Biotech®); hESC- human embryonic stem cells; hMSC- human mesenchymal stem cells; CVPC- cardiovascular progenitor cells; CM- cardiomyocytes; EC- endothelial cells; SMC- smooth muscle cells; USP- upstream bioprocess; DSP- downstream bioprocess.

Moreover, given CCBE1 therapeutic potential and the lack of efficient protocols to produce the full-length protein, in **Chapter 5** improved bioprocess strategies were pursued to maximize CCBE1 productivity. Product quality was comprehensively evaluated by mass spectrometry tools and complementary cell-based assays. This will support further studies to fully explore CCBE1 regenerative

therapeutic potential in *in vitro* and *in vivo* studies.

Finally, the results obtained in this thesis were discussed in **Chapter 6**, together with a perspective on how these can guide towards more efficacious cardiac regenerative therapies.

5. Author contribution & Acknowledgments

The author wrote this chapter based on the referred bibliography

6. References

Abraham, E., Ahmadian, B. B., Holderness, K., Levinson, Y., & McAfee, E. (2017). Platforms for Manufacturing Allogeneic, Autologous and iPSC Cell Therapy Products: An Industry Perspective. *In Advances in Biochemical Engineering/Biotechnology.*

Agathocleous, M., & Harris, W. A. (2013). Metabolism in physiological cell proliferation and differentiation. *Trends in Cell Biology*, 23(10), 484–492.

Alders, M., Hogan, B. M., Gjini, E., Salehi, F., Al-Gazali, L., Hennekam, E. A., Hennekam, R. C. (2009). Mutations in CCBE1 cause generalized lymph vessel dysplasia in humans. *Nature Genetics*, 41(12), 1272–1274.

Alders, M., Mendola, A., Adès, L., Al Gazali, L., Bellini, C., Dallapiccola, B., Hennekam, R. C. (2012). Evaluation of Clinical Manifestations in Patients with Severe Lymphedema with and without CCBE1 Mutations. *Molecular Syndromology*. 4(3):107-13.

Anker, P. S., Scherjon, S. A., Kleijburg-van der Keur, C., de Groot-Swings, G. M. J. S., Claas, F. H. J., Fibbe, W. E., & Kanhai, H. H. H. (2004). Isolation of Mesenchymal Stem Cells of Fetal or Maternal Origin from Human Placenta. *Stem Cells*, 22(7), 1338–1345.

Aspelund, A., Robciuc, M. R., Karaman, S., Makinen, T., & Alitalo, K. (2016). Lymphatic System in Cardiovascular Medicine. *Circulation Research*, 118(3), 515–530.

Bardy, J., Chen, A. K., Lim, Y. M., Wu, S., Wei, S., Weiping, H., Oh, S. K. W. (2013). Microcarrier Suspension Cultures for High-Density Expansion and Differentiation of Human Pluripotent Stem Cells to Neural Progenitor Cells. *Tissue Engineering Part C: Methods*, 19(2), 166–180.

Bellamy, V., Vanneaux, V., Bel, A., Nemetalla, H., Emmanuelle Boitard, S., Farouz, Y., Menasché, P. (2015). Long-term functional benefits of human embryonic stem cell-derived cardiac progenitors embedded into a fibrin scaffold. *The Journal of Heart and Lung Transplantation*, 34(9), 1198–1207.

Beltrami, A. P., Barlucchi, L., Torella, D., Baker, M., Limana, F., Chimenti, S., Anversa, P. (2003). Adult cardiac stem cells are multipotent and support myocardial regeneration. *Cell,* 114(6), 763–776.

Bergmann, O., Bhardwaj, R. D., Bernard, S., Zdunek, S., Barnabé-Heider, F., Walsh, S., Frisén, J. (2009). Evidence for Cardiomyocyte Renewal in Humans. *Science*, 324(5923), 98–102.

Boch, J., Scholze, H., Schornack, S., Landgraf, A., Hahn, S., Kay, S., Bonas, U. (2009). Breaking the Code of DNA Binding Specificity of TAL-Type III Effectors. *Science,* 326(5959), 1509–1512.

Bolli, R., Chugh, A. R., D'Amario, D., Loughran, J. H., Stoddard, M. F., Ikram, S., Anversa, P. (2011). Cardiac stem cells in patients with ischaemic cardiomyopathy (SCIPIO): initial results of a randomised phase 1 trial. *The Lancet*, 378(9806), 1847–1857.

Bolli, R., & Ghafghazi, S. (2017). Stem cells: Cell therapy for cardiac repair: what is needed to move forward? *Nature Reviews Cardiology*, 14(5), 257–258.

Bollini, S., Smart, N., & Riley, P. R. (2011). Resident cardiac progenitor cells: At the heart of regeneration. *Journal of Molecular and Cellular Cardiology*, 50(2), 296–303.

Bos, F. L., Caunt, M., Peterson-Maduro, J., Planas-Paz, L., Kowalski, J., Karpanen, T., … Schulte-Merker, S. (2011). CCBE1 is essential for mammalian lymphatic vascular development and enhances the lymphangiogenic effect of vascular endothelial growth factor-C in vivo. *Circulation Research*, 109(5), 486–491.

Bui, H. M., Enis, D., Robciuc, M. R., Nurmi, H. J., Cohen, J., Chen, M., …, Kahn, M. L. (2016). Proteolytic activation defines distinct lymphangiogenic mechanisms for VEGFC and VEGFD. *Journal of Clinical Investigation*, 126(6), 2167–2180.

Cahill, T. J., Choudhury, R. P., & Riley, P. R. (2017). Heart regeneration and repair after myocardial infarction: Translational opportunities for novel therapeutics. *Nature Reviews Drug Discovery*, 16(10), 699–717.

Cambria, E., Pasqualini, F. S., Wolint, P., Günter, J., Steiger, J., Bopp, A., … Emmert, M. Y. (2017). Translational cardiac stem cell therapy: advancing from first-generation to next-generation cell types. *Npj Regenerative Medicine*, 2(1), 17.

Caplan, A. I., & Correa, D. (2011). The MSC: an injury drugstore. *Cell Stem Cell*, 9(1), 11–15.

Carlsson, L., Clarke, J. C., Yen, C., Gregoire, F., Albery, T., Billger, M., … Fritsche-Danielson, R. (2018). Biocompatible, Purified VEGF-A mRNA Improves Cardiac Function after Intracardiac Injection 1 Week Post-myocardial Infarction in Swine. *Molecular Therapy - Methods and Clinical Development*, 330–346.

Carroll, K. J., Makarewich, C. A., McAnally, J., Anderson, D. M., Zentilin, L., Liu, N., … Olson, E. N. (2016). A mouse model for adult cardiac-specific gene deletion with CRISPR/Cas9. *Proceedings of the National Academy of Sciences*, 113(2), 338–343.

Chamuleau, S. A. J., van der Naald, M., Climent, A. M., Kraaijeveld, A. O., Wever, K. E., Duncker, D. J., … Bolli, R. (2018). Translational Research in Cardiovascular RepairTake-Home Messages. *Circulation Research*, 122(2), 310–318.

Chen, H. I., Poduri, A., Numi, H., Kivela, R., Saharinen, P., McKay, A. S., … Red-Horse, K. (2014a). VEGF-C and aortic cardiomyocytes guide coronary artery stem development. The *Journal of Clinical Investigation,* 124(11), 4899–4914.

Chen, H. I., Sharma, B., Akerberg, B. N., Numi, H. J., Kivelä, R., Saharinen, P., … Red-Horse, K. (2014b). The sinus venosus contributes to coronary vasculature through VEGFC-stimulated angiogenesis. *Development*, 141(23), 4500–4512.

Chien, K. R., & Olson, E. N. (2002). Converging Pathways and Principles in Heart Development and Disease. *Cell,* 110(2), 153–162.

Chien, K. R., Zangi, L., & Lui, K. O. (2015). Synthetic Chemically Modified mRNA (modRNA): Toward a New Technology Platform for Cardiovascular Biology and Medicine. *Cold Spring Harbor Perspectives in Medicine*, 5(1), a014035–a014035.

Chin, M. H., Mason, M. J., Xie, W., Volinia, S., Singer, M., Peterson, C., … Lowry, W. E. (2009). Induced Pluripotent Stem Cells and Embryonic Stem Cells Are Distinguished by Gene Expression Signatures. *Cell Stem Cell*, 5(1), 111–123.

Ding, Q., Strong, A., Patel, K. M., Ng, S.-L., Gosis, B. S., Regan, S. N., … Musunuru, K. (2014). Permanent Alteration of PCSK9 With In Vivo CRISPR-Cas9 Genome Editing. *Circulation Research*, 115(5), 488–492.

Doi, A., Park, I.-H., Wen, B., Murakami, P., Aryee, M. J., Irizarry, R., … Feinberg, A. P. (2009). Differential methylation of tissue- and cancer-specific CpG island shores distinguishes human induced pluripotent stem cells, embryonic stem cells and fibroblasts. *Nature Genetics*, 41(12), 1350–1353.

Dominguez, A. A., Lim, W. A., & Qi, L. S. (2016). Beyond editing: Repurposing CRISPR-Cas9 for precision genome regulation and interrogation. *Nature Reviews Molecular Cell Biology*, 17(1), 5–15.

Dominici, M., Le Blanc, K., Mueller, I., Slaper-Cortenbach, I., Marini, F., Krause, D., … Horwitz, E. (2006). Minimal criteria for defining multipotent mesenchymal stromal cells. The International Society for Cellular Therapy position statement. *Cytotherapy*, 8(4), 315–317.

Dos Santos, F., Campbell, A., Fernandes-Platzgummer, A., Andrade, P. Z., Gimble, J. M., Wen, Y., … Cabral, J. M. S. (2014). A xenogeneic-free bioreactor system for the clinical-scale expansion of human mesenchymal stem/stromal cells. *Biotechnology and Bioengineering*, 111(6), 1116–1127.

Facucho-Oliveira, J., Bento, M., & Belo, J.-A. (2011). Ccbe1 expression marks the cardiac and lymphatic progenitor lineages during early stages of mouse development. *The International Journal of Developmental Biolo*gy, 55(10–12), 1007–1014.

Faiella, W., & Atoui, R. (2016). Therapeutic use of stem cells for cardiovascular disease. *Clinical and Translational Medicine*, 5(1), 34.

Fan, Y., Hsiung, M., Cheng, C., & Tzanakakis, E. S. (2014). Facile Engineering of Xeno-Free Microcarriers for the Scalable Cultivation of Human Pluripotent Stem Cells in Stirred Suspension. *Tissue Engineering Part A*, 20(3–4), 588–599.

Farrell, A., McLoughlin, N., Milne, J. J., Marison, I. W., & Bones, J. (2014). Application of Multi-Omics Techniques for Bioprocess Design and Optimization in Chinese Hamster Ovary Cells. *Journal of Proteome Research*, 13(7), 3144–3159.

Fernandes, A. M., Marinho, P. A. N., Sartore, R. C., Paulsen, B. S., Mariante, R. M., Castilho, L. R., & Rehen, S. K. (2009). Successful scale-up of human embryonic stem cell production in a stirred

microcarrier culture system. *Brazilian Journal of Medical and Biological Research*, 42(6), 515–522.

Finkbeiner, S., Frumkin, M., & Kassner, P. D. (2015). Cell-Based Screening: Extracting Meaning from Complex Data. *Neuron*, 86(1), 160–174.

Florea, V., Rieger, A. C., DiFede, D. L., El-Khorazaty, J., Natsumeda, M., Banerjee, M. N., … Hare, J. M. (2017). Dose Comparison Study of Allogeneic Mesenchymal Stem Cells in Patients With Ischemic Cardiomyopathy (The TRIDENT Study) Novelty and Significance. *Circulation Research*, 121(11), 1279–1290.

Fraga, A. M., Souza de Araújo, É. S., Stabellini, R., Vergani, N., & Pereira, L. V. (2011). A Survey of Parameters Involved in the Establishment of New Lines of Human Embryonic Stem Cells. *Stem Cell Reviews and Reports*, 7(4), 775–781.

Gaebel, R., Furlani, D., Sorg, H., Polchow, B., Frank, J., Bieback, K., … Steinhoff, G. (2011). Cell origin of human mesenchymal stem cells determines a different healing performance in cardiac regeneration. *PloS One*, 6(2), e15652.

Gao, X., Yourick, J. J., & Sprando, R. L. (2017). Comparative transcriptomic analysis of endothelial progenitor cells derived from umbilical cord blood and adult peripheral blood: Implications for the generation of induced pluripotent stem cells. *Stem Cell Research*, 25, 202–212.

Guijarro, D., Lebrin, M., Lairez, O., Bourin, P., Piriou, N., Pozzo, J., … Roncalli, J. (2016). Intramyocardial transplantation of mesenchymal stromal cells for chronic myocardial ischemia and impaired left ventricular function: Results of the MESAMI 1 pilot trial. *International Journal of Cardiology*, 209, 258–265.

Gyöngyösi, M., Wojakowski, W., Navarese, E. P., & Moye, L. À. (2016). Meta-Analyses of Human Cell-Based Cardiac Regeneration TherapiesResponse to Gyöngyösi, Wojakowski, Navarese, Moyé, and the ACCRUE Investigators. *Circulation Research*, 118(8), 1254–1263.

Hare, J. M., Fishman, J. E., Gerstenblith, G., DiFede Velazquez, D. L., Zambrano, J. P., Suncion, V. Y., … Lardo, A. (2012). Comparison of allogeneic vs autologous bone marrow–derived mesenchymal stem cells delivered by transendocardial injection in patients with ischemic cardiomyopathy: the POSEIDON randomized trial. *JAMA*, 308(22), 2369–2379.

Hashimura, Y., Giroux, D., & Lee, B. (2012). Designing the ideal bioreactor with single-use technology. *BioProcess Int.*, 10, 36–29.

Heng, B. C., Li, J., Chen, A. K.-L., Reuveny, S., Cool, S. M., Birch, W. R., & Oh, S. K.-W. (2012). Translating Human Embryonic Stem Cells from 2-Dimensional to 3-Dimensional Cultures in a Defined Medium on Laminin- and Vitronectin-Coated Surfaces. *Stem Cells and Development*, 21(10), 1701–1715.

Henri, O., Pouehe, C., Houssari, M., Galas, L., Nicol, L., Edwards-Lévy, F., … Brakenhielm, E. (2016). Selective Stimulation of Cardiac Lymphangiogenesis Reduces Myocardial Edema and Fibrosis Leading to Improved Cardiac Function Following Myocardial Infarction: CLINICAL PERSPECTIVE. *Circulation*, 133(15), 1484–1497.

Hervy, M., Weber, J. L., Pecheul, M., Dolley-Sonneville, P., Henry, D., Zhou, Y., & Melkoumian, Z. (2014). Long Term Expansion of Bone Marrow-Derived hMSCs on Novel Synthetic Microcarriers in Xeno-Free, Defined Conditions. *PLoS ONE*, 9(3), e92120.

Higuchi, A., Ku, N.-J., Tseng, Y.-C., Pan, C.-H., Li, H.-F., Kumar, S. S., … Murugan, K. (2017). Stem cell therapies for myocardial infarction in clinical trials: bioengineering and biomaterial aspects. *Laboratory Investigation*, 00(300), 1–13.

Hogan, B. M., Bos, F. L., Bussmann, J., Witte, M., Chi, N. C., Duckers, H. J., & Schulte-Merker, S. (2009). Ccbe1 is required for embryonic lymphangiogenesis and venous sprouting. *Nature Genetics*, 41(4), 396–398.

Hu, B.-Y., Weick, J. P., Yu, J., Ma, L.-X., Zhang, X.-Q., Thomson, J. A., & Zhang, S.-C. (2010). Neural differentiation of human induced pluripotent stem cells follows developmental principles but with variable potency. *Proceedings of the National Academy of Sciences,* 107(9), 4335–4340.

Huang, Y., Wan, J., Guo, Y., Zhu, S., Wang, Y., Wang, L., … Wang, Z. (2017). Transcriptome Analysis of Induced Pluripotent Stem Cell (iPSC)-derived Pancreatic β-like Cell Differentiation. *Cell Transplantation*, 26(8), 1380–1391.

Iseoka, H., Miyagawa, S., Fukushima, S., Saito, A., Masuda, S., Yajima, S., … Sawa, Y. (2018). Pivotal Role of Non-cardiomyocytes in Electromechanical and Therapeutic Potential of Induced Pluripotent Stem Cell-Derived Engineered Cardiac Tissue. Tiss*ue Engineering Part A,* 24(3–4), 287–300.

Jackson, A. L., Bartz, S. R., Schelter, J., Kobayashi, S. V, Burchard, J., Mao, M., … Linsley, P. S. (2003). Expression profiling reveals off-target gene regulation by RNAi. *Nature Biotechnology*, 21(6), 635–637.

Jeltsch, M., Jha, S. K., Tvorogov, D., Anisimov, A., Leppänen, V.-M., Holopainen, T., … Alitalo, K. (2014). CCBE1 enhances lymphangiogenesis via A disintegrin and metalloprotease with thrombospondin motifs-3-mediated vascular endothelial growth factor-C activation. *Circulation*, 129(19), 1962–1971.

Jha, S. K., Rauniyar, K., Karpanen, T., Leppänen, V.-M., Brouillard, P., Vikkula, M., … Jeltsch, M. (2017). Efficient activation of the lymphangiogenic growth factor VEGF-C requires the C-terminal domain of VEGF-C and the N-terminal domain of CCBE1. *Scientific Reports*, 7(1), 4916.

Jinek, M., Chylinski, K., Fonfara, I., Hauer, M., Doudna, J. A., & Charpentier, E. (2012). A Programmable Dual-RNA-Guided DNA Endonuclease in Adaptive Bacterial Immunity. *Science*, 337(6096), 816–821.

Karra, R., & Poss, K. D. (2017). Redirecting cardiac growth mechanisms for therapeutic regeneration. *Journal of Clinical Investigation*, 127(2), 427–436.

Kehoe, D. E., Jing, D., Lock, L. T., Tzanakakis, E. S., & Ph, D. (2010). Scalable Stirred-Suspension Bioreactor Culture. Tiss*ue Engineering Part A*, 16(2), 405-21.

Kilpinen, H., Goncalves, A., Leha, A., Afzal, V., Alasoo, K., Ashford, S., … Gaffney, D. J. (2017). Common genetic variation drives molecular heterogeneity in human iPSCs. *Nature*, 546(7658), 370–375.

King, J. A., & Miller, W. M. (2007). Bioreactor development for stem cell expansion and controlled differentiation. *Current Opinion in Chemical Biology*, 11(4), 394–398.

Klopp, A. H., Zhang, Y., Solley, T., Amaya-Manzanares, F., Marini, F., Andreeff, M., … Kolonin, M. G. (2012). Omental Adipose Tissue-Derived Stromal Cells Promote Vascularization and Growth of

Endometrial Tumors. *Clinical Cancer Research*, 18(3), 771–782.

Klotz, L., Norman, S., Vieira, J. M., Masters, M., Rohling, M., Dubé, K. N., … Riley, P. R. (2015). Cardiac lymphatics are heterogeneous in origin and respond to injury. *Nature*, 522(7554), 62–67.

Kropp, C., Massai, D., & Zweigerdt, R. (2017). Progress and challenges in large-scale expansion of human pluripotent stem cells. *Process Biochemistry*, 59, 244–254.

Lam, A. T.-L., Li, J., Chen, A. K.-L., Reuveny, S., Oh, S. K.-W., & Birch, W. R. (2014). Cationic Surface Charge Combined with Either Vitronectin or Laminin Dictates the Evolution of Human Embryonic Stem Cells/Microcarrier Aggregates and Cell Growth in Agitated Cultures. *Stem Cells and Development*, 23(14), 1688–1703.

Le, T., & Chong, J. (2016). Cardiac progenitor cells for heart repair. *Cell Death Discovery*, 2(1), 16052.

Lee, J.-W., Lee, S.-H., Youn, Y.-J., Ahn, M.-S., Kim, J.-Y., Yoo, B.-S., … Hong, M. K. (2014). A Randomized, Open-Label, Multicenter Trial for the Safety and Efficacy of Adult Mesenchymal Stem Cells after Acute Myocardial Infarction. *Journal of Korean Medical Science*, 29(1), 23.

Lee, O. K. (2004). Isolation of multipotent mesenchymal stem cells from umbilical cord blood. *Blood*, 103(5), 1669–1675.

Linnekamp, J. F., Hooff, S. R. van, Prasetyanti, P. R., Kandimalla, R., Buikhuisen, J. Y., Fessler, E., … Medema, J. P. (2018). Consensus molecular subtypes of colorectal cancer are recapitulated in in vitro and in vivo models. Ce*ll Death & Differentiation*, 25(3), 616–633.

Lock, L. T., & Tzanakakis, E. S. (2009). Expansion and Differentiation of Human Embryonic Stem Cells to Endoderm Progeny in a Microcarrier Stirred-Suspension Culture. *Tissue Engineering Part A,* 15(8), 2051–2063.

Malik, N. N. (2012). Allogeneic Versus Autologous Stem-Cell Therapy. *BioPharm Int*. 25.

Mandegar, M. A., Huebsch, N., Frolov, E. B., Shin, E., Truong, A., Olvera, M. P., … Conklin, B. R. (2016). CRISPR Interference Efficiently Induces Specific and Reversible Gene Silencing in Human iPSCs. *Cell Stem Cell,* 18(4), 541–553.

Manzoni, C., Kia, D. A., Vandrovcova, J., Hardy, J., Wood, N. W., Lewis, P. A., & Ferrari, R. (2018). Genome, transcriptome and proteome: the rise of omics data and their integration in biomedical sciences. *Briefings in Bioinformatics*, 19(2), 286–302.

Marchetto, M. C. N., Winner, B., & Gage, F. H. (2010). Pluripotent stem cells in neurodegenerative and neurodevelopmental diseases. *Human Molecular Genetics*, 19(R1), R71-6.

Mateos, J., Pernas, P., Labora, J., Blanco, F., & Arufe, M. (2014). Proteomic Applications in the Study of Human Mesenchymal Stem Cells. *Proteomes*, 2(1), 53–71.

McShane, L. M., Cavenagh, M. M., Lively, T. G., Eberhard, D. A., Bigbee, W. L., Williams, P. M., … Conley, B. A. (2013). Criteria for the use of omics-based predictors in clinical trials. *Nature*, 502(7471), 317–320.

Menasché, P. (2018). Cell therapy trials for heart regeneration — lessons learned and future directions. *Nature Reviews Cardiology*.

Menasché, P., Vanneaux, V., Hagège, A., Bel, A., Cholley, B., Cacciapuoti, I., … Larghero, J. (2015). Human embryonic stem cell-derived cardiac progenitors for severe heart failure treatment: first clinical case report. *European Heart Journal*, 36(30), 2011–2017.

Menasché, P., Vanneaux, V., Hagège, A., Bel, A., Cholley, B., Parouchev, A., … Larghero, J. (2018). Transplantation of Human Embryonic Stem Cell–Derived Cardiovascular Progenitors for Severe Ischemic Left Ventricular Dysfunction. Journal of the American College of Cardiology, 71(4), 429–438.

Mohyeldin, A., Garzón-Muvdi, T., & Quiñones-Hinojosa, A. (2010). Oxygen in Stem Cell Biology: A Critical Component of the Stem Cell Niche. *Cell Stem Cell*, 7(2), 150–161.

Murphy, M. B., Moncivais, K., & Caplan, A. I. (2013). Mesenchymal stem cells: environmentally responsive therapeutics for regenerative medicine. *Experimental & Molecular Medic*ine, 45(11), e54–e54.

Nie, Y., Bergendahl, V., Hei, D. J., Jones, J. M., & Palecek, S. P. (2009). Scalable culture and cryopreservation of human embryonic stem cells on microcarriers. *Biotechnology Progress,* 25(1), 20–31.

Niss, K., Sunil, N., Murrel, J., Punreddy, S., Kehoe, D., Rook, M., … Aysola, M. (2013). Growth Kinetics of Human Mesenchymal Stem Cells in a 3L Single-Use, Stirred Tank Bioreactor. *BioPharm Int.*

Oh, H., Bradfute, S. B., Gallardo, T. D., Nakamura, T., Gaussin, V., Mishina, Y., … Schneider, M. D. (2003). Cardiac progenitor cells from adult myocardium: Homing, differentiation, and fusion after infarction. *Proceedings of the National Academy of Sciences*, 100(21), 12313–12318.

Park, I.-H., Arora, N., Huo, H., Maherali, N., Ahfeldt, T., Shimamura, A., … Daley, G. Q. (2008). Disease-Specific Induced Pluripotent Stem Cells. *Cell,* 134(5), 877–886.

Pittenger, M. F., Mackay, A. M., Beck, S. C., Jaiswal, R. K., Douglas, R., Mosca, J. D., … Marshak, D. R. (1999). Multilineage potential of adult human mesenchymal stem cells. *Science*, 284(5411), 143–147.

Rafiq, Q. A., Brosnan, K. M., Coopman, K., Nienow, A. W., & Hewitt, C. J. (2013). Culture of human mesenchymal stem cells on microcarriers in a 5 l stirred-tank bioreactor. *Biotechnology Letters*, 35(8), 1233–1245.

Richard, C. (2003). Selection of autologous or allogeneic transplantation. In W. R. Kufe DW, Pollock RE (Ed.), Holland-Frei Cancer Medicine (6th ed.). BC Decker.

Robinton, D. A., & Daley, G. Q. (2012). The promise of induced pluripotent stem cells in research and therapy. *Nature,* 481(7381):295-305.

Roukens, M. G., Peterson-Maduro, J., Padberg, Y., Jeltsch, M., Leppanen, V.-M., Bos, F. L., … Schulte, D. (2015). Functional Dissection of the CCBE1 Protein: A Crucial Requirement for the Collagen Repeat Domain. *Circulation Research*, 116(10), 1660–1669.

Sayed, N., Liu, C., & Wu, J. C. (2016). Translation of Human-Induced Pluripotent Stem Cells. *Journal of the American College of Cardiology*, 67(18), 2161–2176.

Schirmaier, C., Jossen, V., Kaiser, S. C., Jüngerkes, F., Brill, S., Safavi-Nab, A., … Eibl, R. (2014). Scale-up of adipose tissue-derived mesenchymal stem cell production in stirred single-use bioreactors under low-serum conditions. *Engineering in Life Sciences*, 14(3), 292–303.

Serra, M., Brito, C., Correia, C., & Alves, P. M. (2012). Process engineering of human pluripotent stem cells for clinical application. *Trends in Biotechnology*, 30(6), 350–359.

Serra, M., Brito, C., Sousa, M. F. Q., Jensen, J., Tostões, R., Clemente, J., … Alves, P. M. (2010). Improving expansion of pluripotent human embryonic stem cells in perfused bioreactors through oxygen control. *Journal of Biotechnology*, 148(4), 208–215.

Sharma, B., Ho, L., Ford, G. H., Chen, H. I., Goldstone, A. B., Woo, Y. J., … Red-Horse, K. (2017). Alternative Progenitor Cells Compensate to Rebuild the Coronary Vasculature in Elabela - and Apj - Deficient Hearts. *Developmental Cell*, 42(6), 655–666.e3.

Simaria, A. S., Hassan, S., Varadaraju, H., Rowley, J., Warren, K., Vanek, P., & Farid, S. S. (2014). Allogeneic cell therapy bioprocess economics and optimization: single-use cell expansion technologies. *Biotechnology and Bioengineering*, 111(1), 69–83.

Simões, F. C., & Riley, P. R. (2018). The ontogeny, activation and function of the epicardium during heart development and regeneration. *Development*, 145(7), dev155994.

Smart, N., Dubé, K. N., & Riley, P. R. (2009). Coronary vessel development and insight towards neovascular therapy. International *Journal of Experimental Pathology*, 90(3), 262–283.

Smart, N., Risebro, C. A., Melville, A. A. D., Moses, K., Schwartz, R. J., Chien, K. R., & Riley, P. R. (2007). Thymosin β4 induces adult epicardial progenitor mobilization and neovascularization. *Nature*, 445(7124), 177–182.

Smits, A. M., Dronkers, E., & Goumans, M.-J. (2018). The epicardium as a source of multipotent adult cardiac progenitor cells: Their origin, role and fate. *Pharmacological Research*, 127, 129–140.

Soldner, F., Laganière, J., Cheng, A. W., Hockemeyer, D., Gao, Q., Alagappan, R., … Jaenisch, R. (2011). Generation of Isogenic Pluripotent Stem Cells Differing Exclusively at Two Early Onset Parkinson Point Mutations. *Cell*, 146(2), 318–331.

Taimeh, Z., Loughran, J., Birks, E. J., & Bolli, R. (2013). Vascular endothelial growth factor in heart failure. *Nature Reviews Cardiology*, 10(9), 519–530.

Takahashi, K., Tanabe, K., Ohnuki, M., Narita, M., Ichisaka, T., Tomoda, K., & Yamanaka, S. (2007). Induction of Pluripotent Stem Cells from Adult Human Fibroblasts by Defined Factors. *Cell*, 131(5), 861–872.

Takahashi, K., & Yamanaka, S. (2006). Induction of Pluripotent Stem Cells from Mouse Embryonic and Adult Fibroblast Cultures by Defined Factors. *Cell,* 126(4), 663–676.

Takahashi, K., & Yamanaka, S. (2016). A decade of transcription factor-mediated reprogramming to pluripotency. *Nature Reviews Molecular Cell Biology*, 17(3), 183–193.

Takeuchi, J. K., Lou, X., Alexander, J. M., Sugizaki, H., Delgado-Olguín, P., Holloway, A. K., … Bruneau, B. G. (2011). Chromatin remodelling complex dosage modulates transcription factor function in heart development. *Nature Communications*, 2, 187.

Tang, X.-L., Li, Q., Rokosh, G., Sanganalmath, S. K., Chen, N., Ou, Q., … Bolli, R. (2016). Long-Term Outcome of Administration of c-kit POS Cardiac Progenitor Cells After Acute Myocardial InfarctionNovelty and Significance. *Circulation Research*, 118(7), 1091–1105.

Tang, X., Nakamura, S., Li, Q., Wysoczynski, M., Gumpert, A. M., Wu, W., … Bolli, R. (2018). Repeated Administrations of Cardiac Progenitor Cells Are Superior to a Single Administration of an Equivalent Cumulative Dose. *Journal of the American Heart Association*, 7(4).

Taylor, C. J., Bolton, E. M., Pocock, S., Sharples, L. D., Pedersen, R. A., & Bradley, J. A. (2005). Banking on human embryonic stem cells: estimating the number of donor cell lines needed for HLA matching. *The Lancet*, 366(9502), 2019–2025.

Tian, X., Pu, W. T., & Zhou, B. (2015). Cellular Origin and Developmental Program of Coronary Angiogenesis. *Circulation Research*, 116(3), 515–530.

Tiburcy, M., Hudson, J. E., Balfanz, P., Schlick, S., Meyer, T., Chang Liao, M.-L., … Zimmermann, W.-H. (2017). Defined Engineered Human Myocardium With Advanced Maturation for Applications in Heart Failure Modeling and RepairClinical Perspective. *Circulation,* 135(19), 1832–1847.

Ting, S., Chen, A., Reuveny, S., & Oh, S. (2014). An intermittent rocking platform for integrated expansion and differentiation of human pluripotent stem cells to cardiomyocytes in suspended microcarrier cultures. *Stem Cell Research*, 13(2), 202–213.

Trounson, A., & DeWitt, N. D. (2016). Pluripotent stem cells progressing to the clinic. *Nature Reviews Molecular Cell Biology*, 17(3), 194–200.

Varum, S., Rodrigues, A. S., Moura, M. B., Momcilovic, O., Easley, C. a, Ramalho-Santos, J., … Schatten, G. (2011). Energy metabolism in human pluripotent stem cells and their differentiated counterparts. *PloS One*, 6(6), e20914.

Vivien, C. J., Hudson, J. E., & Porrello, E. R. (2016). Evolution, comparative biology and ontogeny of vertebrate heart regeneration. *Npj Regenerative Medicine*, 1(1), 16012.

Vuorio, T., Tirronen, A., & Ylä-Herttuala, S. (2017). Cardiac Lymphatics – A New Avenue for Therapeutics? *Trends in Endocrinology and Metabolism*, 28(4), 285–296.

Wang, G., McCain, M. L., Yang, L., He, A., Pasqualini, F. S., Agarwal, A., … Pu, W. T. (2014). Modeling the mitochondrial cardiomyopathy of Barth syndrome with induced pluripotent stem cell and heart-on-chip technologies. *Nature Medicine*, 20(6), 616–623.

Wang, Y., Liang, P., Lan, F., Wu, H., Lisowski, L., Gu, M., … Wu, J. C. (2014). Genome editing of isogenic human induced pluripotent stem cells recapitulates long QT phenotype for drug testing. *Journal of the American College of Cardiology*, 64(5), 451–459.

Warren, L., Manos, P. D., Ahfeldt, T., Loh, Y.-H., Li, H., Lau, F., … Rossi, D. J. (2010). Highly Efficient Reprogramming to Pluripotency and Directed Differentiation of Human Cells with Synthetic Modified mRNA. *Cell Stem Cell*, 7(5), 618–630.

Wei, K., Serpooshan, V., Hurtado, C., Diez-Cuñado, M., Zhao, M., Maruyama, S., … Ruiz-Lozano, P. (2015). Epicardial FSTL1 reconstitution regenerates the adult mammalian heart. *Nature*, 525(7570), 479–485.

Wu, R., Hu, X., & Wang, J. (2018). Concise Review: Optimized Strategies for Stem Cell-Based Therapy in Myocardial Repair: Clinical Translatability and Potential Limitation. *Stem Cells,* 36(4), 482–500.

Ye, J., Bates, N., Soteriou, D., Grady, L., Edmond, C., Ross, A., … Brison, D. R. (2017). High quality clinical grade human embryonic stem cell lines derived from fresh discarded embryos. *Stem Cell Research & Therapy*, 8(1), 128.

Yugi, K., Kubota, H., Hatano, A., & Kuroda, S. (2016). Trans-Omics: How To Reconstruct Biochemical Networks Across Multiple 'Omic' Layers. *Trends in Biotechnology*, 34(4), 276–290.

Zhou, L., Kong, J., Zhuang, Y., Chu, J., Zhang, S., & Guo, M. (2013). Ex vivo expansion of bone marrow mesenchymal stem cells using microcarrier beads in a stirred bioreactor. *Biotechnology and Bioprocess Engineering*, 18(1), 173–184.

Zuk, P. A., Zhu, M., Ashjian, .P, De Ugarte, D. A., Huang, J. I., Mizuno, H., … Hedrick, M. H. (2002). Human Adipose Tissue Is a Source of Multipotent Stem Cells. *Molecular Biology of the Cell*, 13(12), 4279–4295.

2

"Omics" Characterization of Human Pluripotent Stem Cells

This chapter was adapted from:

Silva MM*, Rodrigues AF*, Correia C, Sousa MF, Brito C, Coroadinha AS, Serra M, Alves PM. (2015) Robust expansion of human pluripotent stem cells: integration of bioprocess design with transcriptomic and metabolomic characterization. *Stem Cells Transl Med.* 4(7):731-42.

* Authors contributed equally

Abstract

Human embryonic stem cells (hESC) have an enormous potential as a source for cell replacement therapies, tissue engineering and in vitro toxicology applications. The lack of standardized and robust bioprocesses for hESC expansion in relevant quantities while maintaining their pluripotency has hindered the application of hESC and their derivatives in clinical setting. Here, we developed a scalable and well-characterized bioprocess for hESC expansion under fully-defined conditions and explored the potential of transcriptomic and metabolomic tools to evaluate the impact of culture system on hESC phenotype. Two different hESC lines (feeder-dependent and feeder-free lines) were efficiently expanded on xeno-free microcarriers in stirred culture systems. Both hESC lines maintained the expression of stemness markers such as Oct-4, Nanog, SSEA-4 and TRA1-60, and the ability to spontaneously differentiate into the three germ layers. Whole-genome transcriptome profiling revealed a phenotypic convergence between both hESC lines along the expansion process in stirred-tank bioreactor cultures, providing strong evidence on the robustness of the cultivation process to homogenize cellular phenotype. Under low oxygen tensions, results showed a metabolic rearrangement with the up-regulation of the glycolytic machinery favoring an anaerobic glycolysis Warburg-effect like phenotype, with no evidence of hypoxic stress response, in contrast to 2-dimensional culture. Overall, we report a scalable and fully-defined bioprocess for the propagation of hESC while guaranteeing product quality. Furthermore, the “omics” tools herein used provided relevant findings on the physiological/metabolic changes during the hESC expansion in environmentally-controlled stirred-tank bioreactors, which can contribute for more standardized production systems.

Table of Contents

1.Introduction

Human pluripotent stem cells (hPSCs), including embryonic (hESCs) and induced pluripotent stem cells, are an extremely attractive cell source for cellular therapy (Robinton & Daley, 2012), drug discovery and disease modeling applications (Inoue & Yamanaka, 2011), due to their ability to proliferate indefinitely and to differentiate into all cell types of the three germ layers. Many of their biomedical applications require massive numbers of hPSC and their derivatives. Therefore, there is a need for robust protocols for scalable cell production under well-defined conditions, and compliant to good manufacturing practices (GMP).

In the past decade, methods for hPSC production have rapidly evolved along with the development of novel culture media formulations and supplements (Chen, Mallon, McKay, & Robey, 2014). Additionally, the use of extracellular components and synthetic surfaces has shown to provide safer and more defined culture conditions for long-term expansion of undifferentiated hPSCs in either adhesion or suspension (Serra, Brito, Correia, & Alves, 2012; Sun et al., 2014). Concerning suspension culture systems, different strategies for expansion and/or differentiation of hPSCs have been explored, including the cultivation of cells as aggregates (Abbasalizadeh, Larijani, Samadian, & Baharvand, 2012), immobilized on microcarriers (Serra et al., 2010) or using hydrogels (Lei & Schaffer, 2013). With well-designed robotic automated systems or environmentally controlled bioreactors (e.g. stirred-tank bioreactors), the production of a clinically relevant quantities of hPSCs will hopefully be achieved in the near future.

The combination of stirred culture systems and microcarrier technology offers great advantages in process scale-up over the standard 2-dimensional (2D) static culture (i.e. planar technologies), providing a high surface-to-volume ratio in a more controlled and homogeneous microenvironment. Because massive

numbers of hPSCs may be needed to address the biomedical demands, namely, for cell therapy (e.g. 10^9 - 10^{10} cells are required for heart or hepatic failure therapies) or drug discovery pipelines (requiring approximately 10^{10} cells to screen a 1 million-compound library at once), the use of microcarrier-based bioreactors offers a more cost-effective system for high production scales than planar technologies, as reported recently (Simaria et al., 2014). Our group and others have demonstrated successful expansion of hPSCs in stirred tank bioreactors using different types of microcarriers (Kehoe, Jing, Lock, & Tzanakakis, 2010; Krawetz et al., 2010; Serra et al., 2010). Moreover, in order to meet regulatory safety concerns, Yongjia F. *et al.* engineered xeno-free microcarriers for hPSC propagation in stirred suspension vessels making the hPSCs more suitable for clinical applications (Fan, Hsiung, Cheng, & Tzanakakis, 2014). In particularly, Hervy *et al.* reported long term culture of human mesenchymal stem cells on novel synthetic Synthemax II microcarriers (Corning Inc., Corning, NY, http://www.corning.com) (Hervy et al., 2014). This synthetic surface (VN-PAS; Corning Synthemax® Surface) was already tested to expand and differentiate hESCs in 2D static culture system (Melkoumian et al., 2010); however, its use in dynamic conditions has not yet been reported for hPSCs.

Identifying the key regulatory mechanisms/pathways associated to the stem cell self-renewal and maintenance of pluripotent phenotype during hPSC production is critical. Growing attention has been directed towards the significance of stem cell metabolism in pluripotency and differentiation. It is reported that highly proliferative stem cells have unique energetic demands compared to differentiated cells, presenting high glycolytic flux (Prigione, Fauler, Lurz, Lehrach, & Adjaye, 2010) that can be controlled by transcription factors and signaling network molecules, including the phosphatidylinositol 3-kinase/Akt/mammalian target of rapamycin system (Agathocleous & Harris, 2013; DeBerardinis, Lum, Hatzivassiliou, & Thompson, 2008). Characterization of stem

cell phenotype during the expansion bioprocess and differentiation, however, has been restricted to the assessment of stemness markers using immunofluorescence microscopy and quantitative real-time polymerase chain reaction. Transcriptional and metabolite profiling provided important insights about stem cell phenotype in characterizing the final cell-based product so as to facilitate bioprocess optimization for different culture conditions (Varum et al., 2011). Still, the use of such tools to evaluate the influence of culture strategies, such as extracellular matrices or environmental factors, on hPSC phenotype and metabolic signatures has not been considered aiming at improvement in hPSC bioprocesses.

This study reports the use of transcriptomic and metabolomic tools for hESC culture characterization. These were herein used to evaluate the impact of the developed bioprocess on hESC proliferation and phenotype of two hESC lines displaying different growth characteristics: a feeder-dependent hESC line (growing as a colony) and a feeder-free hESC line (growing as a monolayer). Large-scale transcriptional profiling and metabolite analysis tools were used to support process and product characterization by comparing 2D culture systems with microcarrier-based stirred tank bioreactors using synthetic beads.

2. Material & Methods

2.1 Human embryonic stem cell culture

Two different hESC lines were used: a feeder-dependent hESC line (SCED461; Cellectis Bioresearch, Romainville, France, http://www.cellectis.com) that grows as a colony-type culture (hereafter referred to as hESC-C) and a feeder-free hESC line (SA181; Cellectis Bioresearch) that proliferates in a single-cell-based non colony monolayer (hereafter referred to as hESC-M) culture.

2.1.1 Culture of hESC in 2D culture systems

hESC-C cells were routinely propagated as colonies in static systems (six-well plates; 2D culture) on a feeder layer of human foreskin fibroblasts (hFFs; catalog no. CRL-2429, ATCC collection), inactivated with mitomycin C (Sigma-Aldrich, Steinheim, Germany, https://www.sigmaaldrich.com), in knockout Dulbecco's modified Eagle's medium (DMEM) culture medium (knockout DMEM supplemented with 20% [vol/vol] knockout serum replacement, 1% [vol/vol] minimum essential medium nonessential amino acids, 0.1 mM 2-mercaptoethanol, 2 mM GlutaMAX, 1% [vol/vol] penicillin/streptomycin, 0.5% [vol/vol] gentamycin; all from Life Technologies, Paisley, UK, https://www.lifetechnologies.com) and 10 ng/ml basic fibroblast growth factor (Peprotech, Neuilly-Sur-Seine, France, https://www.peprotech.com), as reported previously [19]. hESC-C propagation was performed as described by Serra et al. [20]. Extracellular components were also evaluated for the expansion of hESC-C: Matrigel (diluted 1:35 in mouse embryonic fibroblast-conditioned medium [MEF-CM]; BD Biosciences, Franklin Lakes, NJ, https://www.bdbiosciences.com), CELLstart (diluted 1:50 in Dulbecco's phosphate-buffered saline with CaCl2 and MgCl2; Life Technologies), StemAdhere matrix (diluted 1:25; Stemcell Technologies, Grenoble, France, http://www.stemcell.com), and Synthemax® six-well plates (Corning Inc.). hESC-C cells were inoculated at 53 104 cells per cm^2 under defined culture medium mTeSR1 (Stemcell Technologies) and MEF-CM [7], both supplemented with 10 mM Rock inhibitor (Calbiochem; EMD Millipore, Billerica, MA, http://www.emdmillipore.com). The culture medium was replaced every 2 days.

hESC-M cells were routinely propagated in Coat-1-coated tissue culture flasks (2D culture) using DEF-CS basal medium(DEF-CS system; Cellectis Bioresearch), according to the manufacturer's protocols. Synthemax® six-well plates (Corning Inc.) were also used as an extracellular component to propagate

hESC-M cells in comparison with 2D culture using Coat-1. hESC-M cells were inoculated at 3.53104 cells per cm2 using DEF-CS basal medium; culture medium was replaced daily.

2.1.2 Culture of hESC on microcarriers in 24 well plates

Cells were inoculated (3.5–5 3 104 cells per cm2) with empty microcarriers (3 cm2 per well) in ultra-low-attachment 24-well plates (Corning Inc.) in 0.5 ml of culture medium per well. Seven different synthetic microcarriers prototypes (Corning Inc.) were tested, Matrigel-coated Cytodex 3 and Coat-1-coated Cytodex 1 were used as controls for hESC-C and hESC-M cells, respectively. The cells were cultured in these conditions for up to 5 days; medium was replaced every 2 days. All microcarriers tested are listed in supplemental online Table 1. hESC-C cells were expanded in mTeSR1 (Stemcell Technologies) and MEF-CM, both supplemented with 10 mMRock inhibitor (Calbiochem; EMD Millipore). hESC-M were expanded in DEF-CS basal medium. The culture medium was replaced every 2 days for hESC-C cells and daily for hESC-M cells.

2.1.3 Culture of hESC on microcarriers in in stirred vessels

hESC-C and hESC-Mcellswere inoculated at 3 and 2 × 10^5 cells per milliliter, respectively, into 125-ml spinner vessels (Corning Inc.) containing synthetic microcarriers (Synthemax II-hydrogel [4 g/l] and Synthemax II-polysterene [16 g/l], Corning Inc.). Cells and beads were inoculated in 50% of the final working volume of medium under intermittent stirring, as described previously by Serra et al. [7]. After 6 hours, fresh medium was added to cultures to a final working volume of 60 ml, and the agitation rate was set to 20 rotations per minute (rpm). Partial medium exchange was performed daily (50% in hESC-C cultures and 80% in hESC-M cultures).

hESC-M cells were cultivated in computer-controlled stirred tank bioreactors (Cellferm-pro bioreactor system, working volume 180 ml; Eppendorf

AG, Hamburg, Germany, http://www.eppendorf.com) under defined culture conditions (pH 7.2; partial pressure of oxygen 30% air saturation; temperature 37°C). Cells were inoculated (23105 cells per milliliter) into a bioreactor containing empty microcarriers in 50% of initial working volume (90 ml) under intermittent stirring. After 6 hours, the remaining volume of culture medium was added. By day 3 onward, the agitation rate was set to continuous at 20 rpm. Partial (80%) medium exchange was performed daily after day 2.

2.2 Evaluation of cell viability, cell concentration and metabolic activity

2.2.1 Cell viability & Metabolic activity

Cell viability was evaluated by using two methods, as described by Serra *et al.* (Serra et al., 2011): (a) the enzyme substrate fluorescein diacetate (FDA; Sigma-Aldrich) and the DNA-dye propidium iodide (PI; Sigma-Aldrich) and (b) the trypan blue (Life Technologies) exclusion method.

hESC metabolic activity was assessed using the metabolic indicator alamarBlue, according to the manufacture's recommendation (Life Technologies). Fold increase in metabolic activity was estimated based on the ratio of $fluorescence_{MAX}$/ $fluorescence_i$, in which $fluorescence_{MAX}$ represents the fluorescence at day 4 of culture and $fluorescence_i$ represents the fluorescence at day 1 of culture.

2.2.2 Cell concentration

For the 2D culture system and static culture on microcarriers, the cell concentration was determined by the trypan blue exclusion method after the cell harvesting using TrypLE^{TM} Select (Life Technologies) for 5-10 minutes. For stirred culture conditions, the cell concentration was determined using crystal violet staining, as described previously (Serra, Brito, Leite, Gorjup, von Briesen, et al., 2009). Fold increase in cell concentration was evaluated based on the ratio

X_{MAX}/X_0, in which X_{MAX} is the peak of cell concentration (cells per milliliter) and X_0 is the initially attached cells at day 0 (cells per milliliter). The specific rate of cell growth (μ) was determined using a simple first order kinetic model $dX/dt = \mu X$, as described elsewhere (Serra et al., 2010; Serra, et al., 2009).

2.3. RNA extraction, amplification, labelling and BeadChip hybridization of RNA samples

Total RNA from hESC-C and hESC-M after expansion on Synthemax II-polystyrene in stirred culture or 2D culture systems were extracted using RNeasy mini kit (Qiagen, Venlo, The Netherlands, https://www.qiagen.com), according to the manufacturer instructions. RNA quality was characterized by the quotient of the 28S to 18S ribosomal RNA electropherogram peak using an Agilent 2100 bioanalyzer and the RNA Nano Chip (Agilent, Santa Clara, CA, http://www.agilent.com). Transcriptional profiling was assessed using Illumina HumanHT-12 v4 Expression BeadChip microarray technology (Illumina, San Diego, CA, http://www.illumina.com). Illumina TotalPrep RNA Amplification Kit (Ambion; Life Technologies) was used to transcribe 200 ng of RNA according to the manufacturer's recommendation. A total of 700 ng of cRNA was hybridized at 58°C for 16 hours to the Illumina HumanHT-12 v4 Expression BeadChips (Illumina). BeadChips were scanned using an Illumina BeadArray Reader and the Bead Scan Software (Illumina). To assess the pluripotency *via* microarray-based gene expression, data was processed using online PluriTest platform (www.pluritest.org/), according to Müller et al. (Müller et al., 2011). To evaluate the gene expression profile along culture time and the differences between both hESC lines, data was processed using Environment for Statistical Computing (R) 2.7.0 (R Foundation for Statistical Computing, Vienna, Austria, http://www.r-project.org) in combination with Bioconductor 2.2 (Gentleman et al., 2004). The Bioconductor lumi package (Du, Kibbe, & Lin, 2008) was used for quality control.

Raw data was log2-transformed using the *lumiT()* function and no background correction was performed (Schmid et al., 2010). Data was transformed using variance-stabilizing transformation (Lin, Du, Huber, & Kibbe, 2008) and quantile normalized (Bolstad, Irizarry, Astrand, & Speed, 2003). All methods used are implemented in the R package lumi. Data of both static and dynamic cultures was analyzed and the dynamic changing genes were selected based on the coefficient of variation (CV), $|CV| \geq 20\%$ defined as the ratio of the standard deviation to the mean (average) providing a normalized estimation of the variation in gene expression changes. Hierarchical clustering was performed in transformed/normalized data using Spotfire® Decision Site™ software (www.spotfire.com). Pathway analysis was performed using Ingenuity Pathway Analysis (IPA) (Ingenuity® Systems, www.ingenuity.com). The entire microarray data set was submitted to the Gene Expression Omnibus repository with the accession number GSE63192.

2.4 Metabolic Profiling

In both 2D culture and bioreactor culture systems, the hESC metabolic profile was evaluated. Glucose and lactate concentrations were measured using YSI 7100 MBS system (YSI Life Sciences, Yellow Springs, OH, http://www.ysilifesciences.com). Ammonia concentration was quantified using an enzymatic kit (catalog no.AK00091; NZYTech, Lisboa, Portugal, https://www.nzytech.com). Amino acids were quantified by high performance liquid chromatography (HPLC) using the protocol described by Carinhas *et al.* (Carinhas et al., 2010). The specific metabolic rates (q_{Met}, $mol \cdot 10^6\ cells^{-1} \cdot hour^{-1}$) were estimated, as described elsewhere (Serra, et al., 2009).

2.5 hESC Phenotype Characterization

2.5.1 Alkaline Phosphatase (AP) staining

Cultures were stained using an AP activity detection kit (Millipore, Billerica, MA, USA) according to the manufacturer's instructions and observed using an inverted phase contrast microscope (Leica Microsystems GmbH).

2.5.2 Immunocytochemistry

The detection of stemness markers in hESC immobilized on microcarriers was performed as described by Serra *et al.* (Serra et al., 2011). Primary antibodies used were: Tra-1-60 and Oct-4 (from Santa Cruz Biotechnology, CA, USA). Secondary antibodies used were: goat anti-mouse IgM-AlexaFluor488 and goat anti-mouse IgG-AlexaFluor 488 (all from Life Technologies™, Paisley, UK).

2.5.3 Flow cytometry

Cells were dissociated from microcarriers with TrypLE™ Select and the sample preparation protocol was based on previous reported work (Serra et al., 2011). Primary antibodies used were Tra-1-60, SSEA-4, SSEA-1, isotype control antibodies (all Santa Cruz Biotechnology, Santa Cruz, CA, USA), SSEA-5 (Abcam, Cambridge, UK) and hESCellect™ (Cellartis AB, Göteborg, Sweden). Secondary antibodies used were goat anti-mouse IgM-AlexaFluor488 and goat anti-mouse IgG-AlexaFluor 488 (all from Life Technologies™).

2.5.4 RT-qPCR analysis

Total RNA was isolated with High Pure RNA Isolation Kit (Roche Applied Science), according to the manufacturer instructions, and reverse transcription was performed using High Fidelity cDNA Synthesis Kit (Roche Applied Science). The resulting cDNA was quantified and used directly for qPCR analysis. qPCR was performed in triplicates according to LightCycler® 480 SYBR Green I Master Kit (Roche Applied Science) on LightCycler® Carousel-Based System (Roche Applied Science), in 20µL reactions with diluted 1:2 cDNA template and 5 µM Primers

(listed in Table S2). Cycles threshold (Ct's) and melting curves were determined using LightCycler® 480 Software version 1.5 (Roche Applied Science). All data was analyzed using the $2^{-\Delta\Delta}$Ct method for relative gene expression analysis (Livak & Schmittgen, 2001). The changes in gene expression (*Oct-4 and Nanog*) were normalized using the housekeeping gene *RPL22* (Ribosomal Protein L22) as internal control. Statistical analysis was carried out using GraphPad Prism 5 software.

2.5.5 *In vitro* pluripotency analysis via embryoid body (EB) formation

hESC pluripotency was evaluated *in vitro* via embryoid body (EB) formation and spontaneous differentiation as described by Serra *et al.*(Serra et al., 2010).

3. Results

To implement a robust and standardized bioprocess for the expansion of hESCs, an initial screening of several xeno-free matrices for the cultivation of two phenotypically different hESC lines in chemically defined culture media was performed using static 2D culture systems. The best xeno-free matrix was then selected for the development of a scalable protocol using microcarrier-based stirred culture systems. Finally, transcriptomic and metabolic profiles of hESCs in stirred-tank bioreactors and static 2D cultures were analyzed and compared to better understand the biological changes induced by the culture system (Figure 2.1).

3.1 Xeno-free matrices screening allowed the hESC expansion under fully-defined conditions

We assessed the culture of hESC-C, typically grown as colonies on Matrigel using MEF-CM (control culture) in the chemically defined medium mTeSR1 and on the following xeno-free matrices: vitronectin-based peptide (Synthemax®; Life

Technologies), recombinant human E-cadherin (StemAdhere; Stemcell Technologies), and substrate composed mainly of fibronectin and albumin (CELLstart™; Life Technologies). The vitronectin-based peptide surface induced the highest-fold increase in cell concentration during expansion. Indeed, cells cultured on this matrix showed similar proliferation capacity (Figure 2.2B) and metabolic activity (Figure 2.2C) compared with control culture. The same outcome was observed for the second cell line used, hESC-M (not shown). These results showed the effectiveness of a vitronectin-based peptide surface for the expansion of both hESC lines, which was selected for the development of a scalable protocol using microcarrier-based stirred culture systems.

3.2 A fully defined microcarrier-based stirred culture system increases hESC expansion yields while maintaining the undifferentiated phenotype

Six different microcarrier prototypes were screened for growth of hESC-C and hESC-M using small scale culture systems (as described in Material and Methods) (supplemental Table 1). Most microcarriers evaluated allowed efficient cell attachment and growth for both cell lines (supplemental Table 1). For enhanced-attachment polystyrene and Coating K microcarriers very low cell attachment efficiency was observed (supplemental Table 1). Synthemax II-hydrogel and Synthemax II-polystyrene microcarriers were selected for use in stirred culture systems because they allowed the highest cell attachment efficiency and growth and efficient microcarrier colonization during culture time (supplemental Table 1).

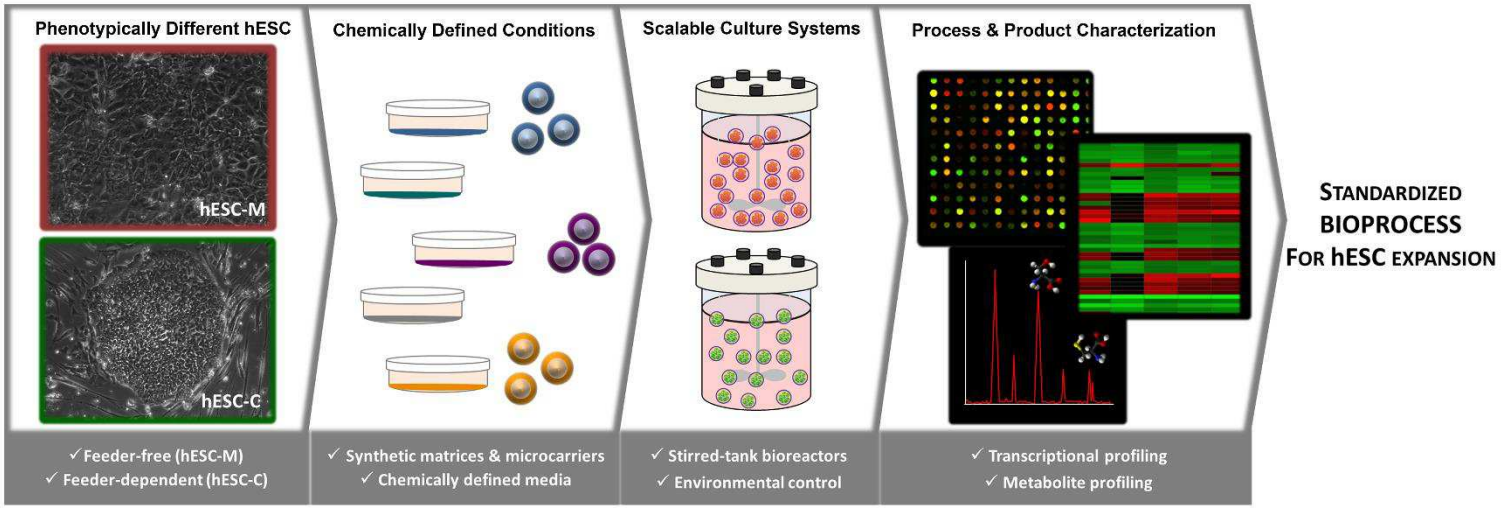

Figure 2.1. Implementation and characterization of a standardized protocol for hESC expansion. Schematic representation of the hESC expansion bioprocess herein developed. Two hESC lines, a feeder-dependent line (hESC-C, in green) and a feeder-free line (hESC-M, in red), were expanded under fully defined conditions using stirred-tank bioreactors and characterized by transcriptomic and metabolic tools toward implementation of a standardized and robust protocol for hESC expansion.

The expansion of hESCs on the two selected microcarriers was evaluated in stirred culture systems using spinner vessels. Our results showed that Synthemax II-polysterene microcarriers were the most suitable beads for the expansion of both hESCs (Figure 2.3A-B). In these microcarriers, hESC-C and hESC-M achieved maximum cell concentration of 20.7 ± 0.6 × 10^5 cell/mL and 10.6 ± 0.3 × 10^5 cell/mL (Figure 2.3B), respectively. In addition, higher cell-recovery yields (>80%) (Figure 2.3C) were attained after cell detachment from these microcarriers without compromising cell viability (>90%).

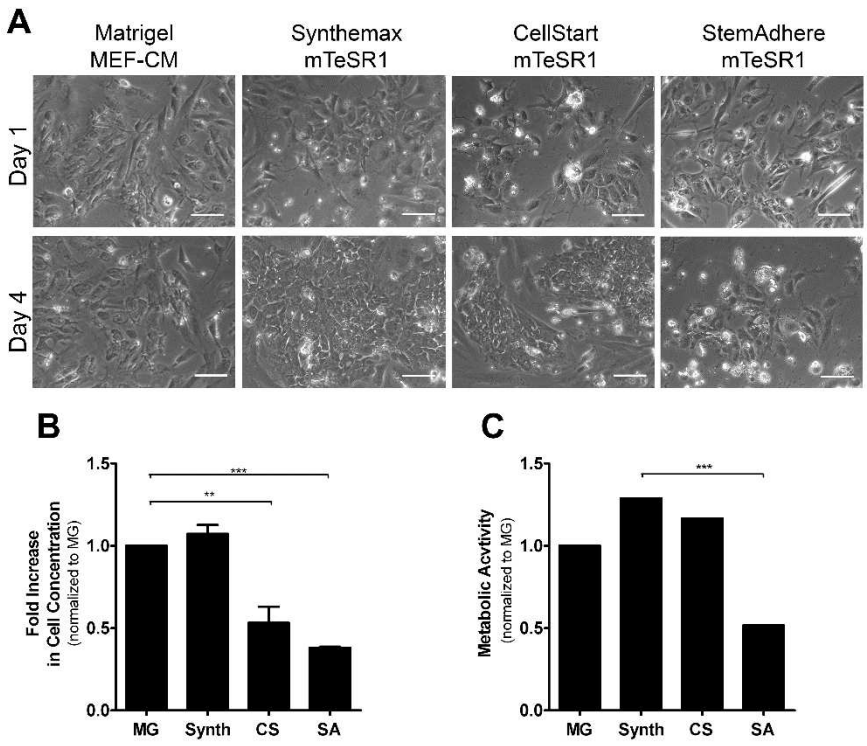

Figure 2.2. Human embryonic stem cell attachment and growth on different extracellular matrices. **A)** Representative images from phase-contrast microscopy at days 1 and 4 of hESC-C cells expanded on different extracellular matrices. Scale bars = 100 mm. Fold increase in cell concentration **(B)** and metabolic activity **(C)** measured by alamarBlue assay for hESC-C cells. Error bars denote the mean ± SD of four measurements. **, $p < .01$; ***, $p < .001$ determined by one-way analysis of variance. Abbreviations: CS, CELLstart™; MEF-CM, mouse embryonic fibroblast conditioned medium; MG, Matrigel™; Synth, Synthemax®; SA, StemAdhere.

In contrast, Synthemax II-hydrogel microcarriers did not support the expansion of hESCS-C cells in stirred culture system (Figure 2.3A, upper right panel). Although efficient cell growth was achieved in hESC-M culture (24.0 ± 1.2 × 10^5 cell/mL), a low percentage of recovered cells after cell detachment from the microcarriers was achieved (45.5 ± 0.5%) (Figure 2.3C). Importantly, the differences observed on cell attachment efficiency (28.5 ± 4.5% vs. 53 ± 3% for hESC-C and hESC-M, respectively) and on colonization (Figure 2.3A) of Synthemax II-polystyrene microcarriers in both hESC lines might be explained by the physical properties of each line (colony culture mode or monolayer culture mode, (Chen et al., 2014)).

After expansion on synthetic microcarriers, both hESC lines retained their undifferentiated phenotype and pluripotency. Both nuclear (Oct-4) and surface (TRA-1-60) markers were detected at the last day of culture, as was positive staining for alkaline phosphatase (Figure 2.3D). The expression of stemness markers (TRA-1-60, SSEA-4, and hES-Cellect [Cellartis, Göteborg, Sweden, http://www.cellartis.com])along with very low percentage of positive cells for SSEA-1 (early differentiation marker) was maintained (Figure 2.3E), and no significant differences were observed in relative gene expression of Oct-4 and Nanog compared with 2D culture systems (control) (Figure 2.3F).

Both hESC were able to form embryoid bodies and spontaneously differentiated into cells from the three germ layers (mesoderm, ectoderm, and endoderm) (Figure 2.3G). Our results also demonstrate that these cells presented strong pluripotency signatures, according to PluriTest bioinformatic platform (Müller et al., 2011), showing high and similar scores (supplemental Figure 1) compared with 2D culture.

Hierarchical clustering of hESC-C expansion on Synthemax II-polystyrene microcarriers (day 12), on Synthemax® 2D surface (day 12) and on hFF feeder (static 2D culture; day 12) showed divergence of hESC-C cells in 2D culture (day 0 and day 12) and cultured on Synthemax® surface (2D and microcarriers) (Figure

2.3H). Interestingly, hESC-M cells on Synthemax II-polystyrene microcarriers (day 8) clustered with hESC-M cells at day 0, but with a clear approximation to hESC-C cells on the Synthemax® surface (2D and microcarriers) (Figure 2.3H). These results demonstrated approximation of hESC lines, providing evidence of the robustness of the cultivation process to homogenize cellular phenotype. The removal of feeder cells in hESC-C culture appeared to be an important driving force for this output because the cultures in which the feeder was present clustered in an isolated group, regardless the culture day.

3.3 Synthemax II-polystyrene microcarriers and fully defined conditions shifted central carbon metabolism

For the cultivation of hESC in a fully controlled environment, we used stirred-tank bioreactors operating at specific culture conditions, such as low O_2 tensions (as described in Material and Methods), as optimized previously by our group (Serra et al., 2010). The results obtained were similar to those described for the cultures in spinner vessels, both in terms of growth profile and cell characteristics, proving that the culture strategy was successfully implemented in stirred-tank bioreactors (results not shown). In the following sections, we reported and compared the transcriptomic and metabolomic profiles of hESC-M cells cultured in stirred-tank bioreactors (using Synthemax II-polysterene microcarriers) and 2D culture system, aiming at a thorough and comparative characterization of hESC expansion.

3.3.1 Transcriptome analysis

For transcriptome analysis, genes showing dynamic expression along the culture period (based on a coefficient of variation CV ≥ 20% [day 8 vs. day 0]) were selected both for 2D and bioreactor culture systems.

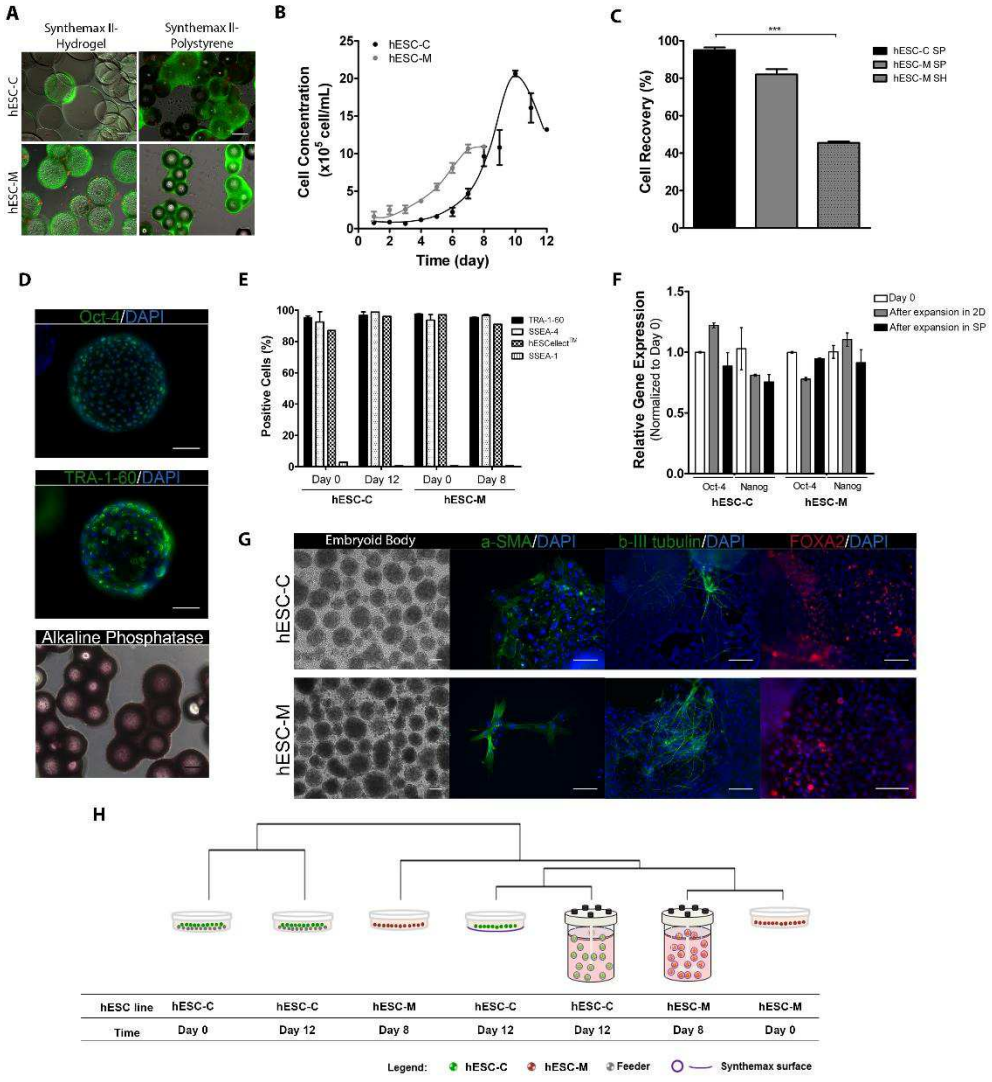

Figure 2.3. Expansion and characterization of hESC on synthetic microcarriers in stirred culture conditions. .**A)** Representative images from cell viability assays (FDA-live cells in green; PI – dead cells in red) of hESC-C and hESC-M on microcarriers at the last day of culture. Scale bars: 100 µm. **B)** Growth curves of hESC-C and hESC-M in spinner vessels on SP microcarriers. **C)** Percentage of cell recovery after the harvesting process, using TrypLE Select. **D)** Immunofluorescence images of Oct-4 and TRA-1-60 labeling of hESC-M on SH microcarriers, and phase contrast images of alkaline phosphatase activity staining of hESC-M on SP microcarriers. **E)** Flow cytometry analysis: percentages of TRA-1-60, SSEA-4, hESCellect^{TM} and SSEA-1 positive cells at Day 0 and at the last day of culture on SP microcarriers. Error bar denotes SD of 2 measurements. **F)** Gene expression of stemness markers *Oct-4* and *Nanog* relative to Day 0 of both hESC-C and hESC-M cultured on SP microcarriers and 2D culture (2D). Gene expression was quantified using $\Delta\Delta C_t$ method (housekeeping: *RPL22*). Error bar denotes SD of 3 replicates. **G)** Images of embryoid bodies of both hESC (after expansion on SP microcarriers) and the differentiated cultures labeled for α–SMA (α

smooth muscle actin, *mesoderm*), FOXA2 (Forkheadbox A2, *endoderm*) and β III-Tub (β tubulin type III, *ectoderm*). Nuclei were stained with DAPI (blue). Scale bars: 100 µm. **H)** Hierarchical clustering given by person correlation method implemented in SpotFire of initial and final samples for both hESC lines in 2D culture system (feeder layer for hESC-C and Coat1 for hESC-M) and on Synthemax synthetic surface. Legend: SP-Synthemax II-polystyrene; SH-Synthemax II-hydrogel. (***p*<0.01 and ****p*<0.001 determined by two-way ANOVA).

A total of 1,796 probes, presenting CV ≥ 20%, was selected (supplemental file SFA) and analyzed by Ingenuity Pathway Analysis for significantly enriched pathways. The most significantly enriched pathways – glycolysis, amino acid metabolism, cytoskeleton rearrangements and stress resistance – were further analyzed throughout culture time (Figure 2.4A; supplemental file SFB). For both 2D and bioreactor systems, transcriptional signatures associated to high glycolytic rates were identified (Figure 2.4A); however, bioreactor samples presented consistently higher expression of the glycolytic enzymes, prominently aldolase A (ALDOA), enolase 2 (ENO2), glucose phosphate isomerase (GPI) and phosphoglycerate kinase 1 (PGK1). Glucose transporters were also consistently up-regulated in bioreactor culture, although only SLC2A1 (also known as GLUT1) presented CV ≥20%. Finally, lactate dehydrogenase A (LDHA) was found to be drastically increased in the bioreactor, sustaining high expression levels until the end of culture time (Figure 2.4A). These results led to the hypothesis that, given the low oxygen levels maintained in bioreactor (6% O_2), hESC-M cells could be facing hypoxic stress; however, we found that, although all the downstream response associated to hypoxia was changing substantially, the upstream hypoxia responsive machinery, in particular hypoxia inducible factor 1 (HIF1) was relatively unchanged (CV=1.3%) (supplemental Figure 2; supplemental file SFC).

In the category of amino acid metabolism, the SLC3A2 and SLC7A5 transporter subunits were the most highly changing along time and presented increased expression rates in bioreactor culture (Figure 2.4A). Many amino acid catabolic enzymes were also highly dynamic and showed increased expression levels in bioreactor culture, including asparagine synthetase (ASNS), branched chain

aminotransferase 1 (BCAT1), glutamic pyruvate transaminase 2 (GPT2, also known as alanine aminotransferase) (Figure 2.4A). Altogether, this transcriptional signature indicated a more active amino acid metabolism under fully defined conditions. Cytoskeleton rearrangements category was also extensively enriched. Genes like vimentin (VIM), actin alpha 1 (ACTA1) and transgelin (TAGLN), appeared as highly dynamic during culture time and presented increased expression levels in bioreactor culture (Figure 2.4A). In fact, the hESC-M cultivation on synthetic microcarriers combined with fully defined conditions resulted in the up-regulation of all cytoskeleton filament types: i) microfilaments (actins, transgelins); ii) intermediate filaments (vimentin, keratins and lamins) and iii) microtubules (tubulins) (Figure 2.4A). In stress resistance category, we found a set of genes displaying a common behavior: metallotionines (MTs, Figure 2.4A). In general, in bioreactor culture, MTs presented lower expression relatively to 2D culture, sustained until the end of the culture. As metallotionines are robust stress markers, this data suggests that fully defined conditions provide a more adequate environment for cell cultivation.

The lack of standardization and reproducibility is a major problem in the protocols for hESC expansion derived from academic and research labs. Apart from the operator associated variability, the cell line origin (feeder dependence) and the culture process parameters (matrix, medium, O2, pH, etc) are the main causes of this problem. Therefore, we evaluated the robustness of the herein presented process to reduce such variability. Transcriptome signatures of both hESC lines used in this work were compared in the beginning and in the end of the process, showing a clear convergence of both hESC lines when cultured on synthetic microcarriers using stirred culture systems (Figure 2.3H). We further inquired on the biological pathways steering such convergence, and the most significantly enriched pathways were cytoskeleton/extracellular matrix rearrangements, glycolysis and carbohydrate metabolism, nucleotide metabolism,

cell cycle, transcription and RNA processing and stress and apoptosis (Figure 4B and supplemental file SFD). Interestingly, many of these pathways were found to be enriched for hESC-M expansion in bioreactor (Figure 2.4A) including the transcriptional signatures associated to high glycolytic rates, substantiating the importance of culturing under fully defined conditions to homogenize and standardize the final cell phenotype.

3.3.2 Central carbon metabolism analysis

To further characterize the metabolic changes occurring within the bioreactor microenvironment, central carbon metabolism dynamics of hESC-M were analyzed in both bioreactor and 2D culture systems. Figure 2.5 summarizes the specific consumption/production rates of glucose, lactate and amino acids, and Figure 2.6 illustrates the main reactions of central carbon metabolism integrating transcriptional changes data.

In bioreactor culture we observed higher ratios of lactate production to glucose consumption in comparison to 2D culture (Table 1), in line with the extensive up-regulation of the glycolytic machinery and LDHA given by transcriptome analysis (Figure 2.4A and Figure 2.6). Yet, ratios of LAC/GLC greater than 2, as those obtained in bioreactor (Table 2.1), suggested an alternative source for lactate production. An alternative source of lactate through pyruvate can be derived from amino acid catabolism (Figure 2.6). Glucose as well as amino acid consumption (Figure 2.5), was higher in 2D culture, however, the ratios of LAC/GLC and ammonia production to amino acid consumption (AMN/NET, Table 2.1) were lower. This suggests that these macromolecules are being channeled to biomass synthesis in 2D culture (with less formation of by-products), while shifting to energy production in the bioreactor culture. This hypothesis is corroborated by higher specific cell growth rate in 2D culture (0.02 h^{-1}) than in bioreactor (0.01 h^{-1}).

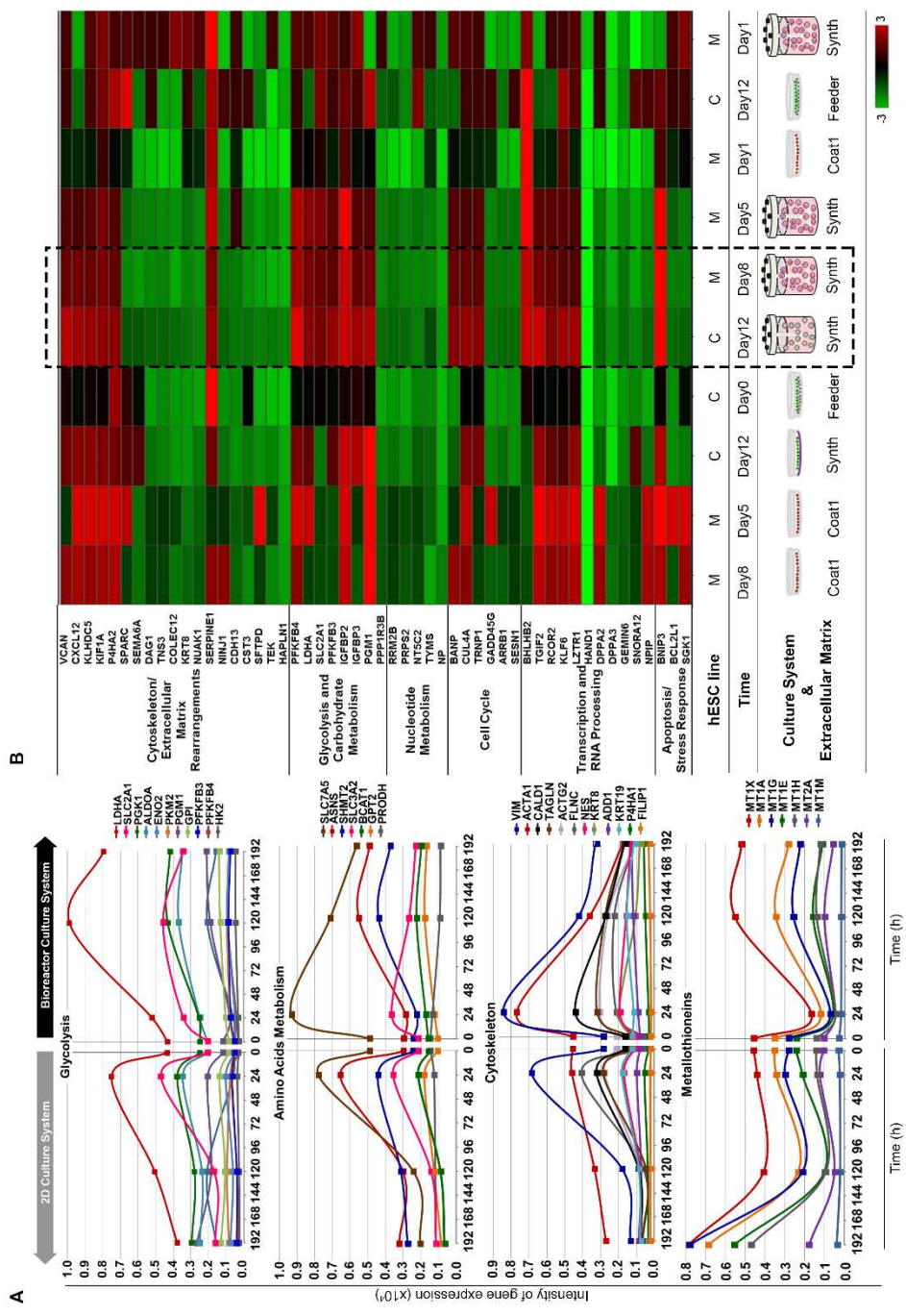
A
B
2D Culture System
Bioreactor Culture System
Glycolysis
Amino Acids Metabolism
Cytoskeleton
Metallothioneins
Intensity of gene expression (x10⁴)
Time (h)
LDHA
SLC2A1
PGK1
ALDOA
ENO2
PGAM2
PGM1
GPI
PFKFB3
PFKFB4
HK2
SLC7A5
ASNS
SLC1A5
SLC7A2
BCAT1
GPT2
PRODH
VIM
ACTA1
CALD1
TAGLN
ACTG2
FLNC
KRT8
KRT18
ADD1
DPYSL3
KRT19
P4HA1
FILIP1
MT1X
MT1A
MT1G
MT1E
MT1H
MT2A
MT1M
VCAN
CXCL12
KIF16C
KIF4A
P4HA2
SPARC
SEMA6A
DAG1
TNS3
COLEC12
KRT8
NUAK1
SERPINE1
NINJ1
CD13
CST3
SFTPD
TEK
HAPLN1
Cytoskeleton/ Extracellular Matrix Rearrangements
PFKFB4
LDHA
SLC2A1
PFKFB3
IGFBP2
IGFBP3
PGM1
PPP1R3B
Glycolysis and Carbohydrate Metabolism
RRM2B
PRPS2
NT5C2
TYMS
NP
Nucleotide Metabolism
BANP
CUL4A
TRNP1
CDC45G
ARRB1
SESN1
Cell Cycle
BHLHB2
TGIF2
RCOR2
KLF6
LZTR1
HAND1
DPPA2
DPPA3
CELF6
SNORA12
NPIP
Transcription and RNA Processing
BNIP3
BCL2L1
SGK1
Apoptosis/ Stress Response
hESC line
Time
Culture System & Extracellular Matrix
M
Day8
Coat1
M
Day5
Coat1
C
Day12
Synth
C
Day0
Feeder
C
Day12
Synth
M
Day8
Synth
M
Day5
Synth
M
Day1
Coat1
C
Day12
Feeder
M
Day1
Synth
3
-3

Figure 2.4. Whole-genome transcriptome analysis of hESCs expanded on Synthemax II-polystyrene microcarriers. A) Transcriptional profiling of selected genes with dynamically changing expression over culture time. hESC-M cells in the 2D culture system (left) versus the bioreactor culture system (right) of glycolysis, amino acid metabolism, cytoskeleton rearrangements, and metallothionein genes. Genes were considered dynamically changing for coefficient of variation CV≥20% over the 192 hours of culture. A complete list of all genes with CV≥20% can be found in supplemental online file SFA. A list of the genes composing this figure, fold-change values, CV statistics, and gene abbreviation definitions is provided in supplemental online file SFB. **B)** Heat map of converging genes in both hESC lines across significantly enriched pathways given by Ingenuity Pathway Analysis. Heat map of probes with transcriptional convergence during the expansion process. Color gradient indicates gene expression fold-change between the referred samples and "hESC-M day 0." Dashed box highlights the similarity of gene expression patterns between hESC-C and hESC-M cells by the end of expansion process in Synthemax II-polystyrene microcarriers. A complete list of the genes composing this figure, expression values, fold-change, and gene abbreviation definitions can be found in supplemental online file SFD. The microarray dataset presented in this figure was submitted to the Gene Expression Omnibus repository with the accession number GSE63192. Abbreviations: 2D, two-dimensional; C, hESC-C cell line; M, hESC-M cell line.

The dynamics in amino acid metabolism, could be divided into three groups (Figure 2.5B-D). The first group (Figure 2.5B), comprising consumed amino acids, showed reduced uptake in bioreactor culture. Given that amino acid metabolic genes appeared extensively enriched and up-regulated in transcriptional profiling (Figure 2.4A and Figure 2.6), these results suggested a shifting/rearrangement of amino acid metabolism, with less consumption and increased channeling towards catabolic routes. This observation was substantiated by extremely high ratios of AMN/NET (Table 2.1), indicating amino acid catabolism to be used as feeding of TCA intermediates (Figure 2.6). The second group includes amino acids accumulating in the extracellular, glycine, alanine and glutamate, which were found to be produced in higher extent in bioreactor culture (Figure 2.5C). Increased production of glycine was in agreement with the up-regulation of serine hydroxymethyltransferase 2 (mitochondrial) (SHMT2, Figure 2.6). This reaction also supports folate recycling, essential to sustain amino acid catabolism (Figure 2.6).

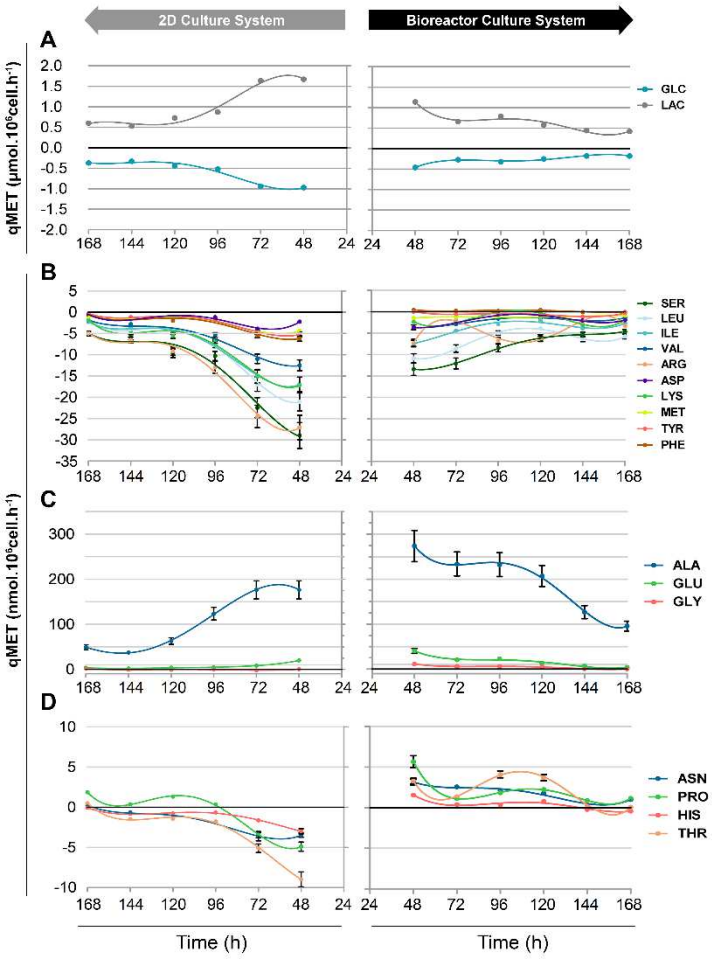

Figure 2.5. Metabolic profiling of hESC-M in the 2D culture system versus stirred-tank bioreactors. hESC-M cells in the 2D culture system (left- sided charts) and the bioreactor culture system (right). **A)** Specific rates of glucose consumption and lactate production. Specific amino acid uptake/production rates of group 1, consumed amino acids (**B**); group 2, produced amino acids (**C**); and group 3, amino acids with inverted uptake/production profiles (**D**). For specific rates, negative values denote uptake and positive values denote production. Error bars represent the propagation of error. The curves represent the best fit to points using the fourth order polynomial. Abbreviation: 2D, two- dimensional.

Increased glutamate accumulation, corroborated the shifting of amino acid metabolism towards catabolic routes, as glutamate is a common intermediate in the degradation of many amino acids, before it is finally converted to α-ketoglutarate releasing ammonia (Figure 2.6). Glutamate can also be transaminated by glutamic

pyruvate transaminase (GPT2), up regulated by 2-fold in bioreactor culture (Figure 6), contributing to the increased accumulation of alanine observed (Figure 2.5C).

Table 1. Amino acid metabolism of hESC-M during expansion process in 2D culture system and stirred-tank bioreactors.

Culture	NET consumption		AMN/NET consumption		YLAC/GLC	
Time (h)	2D	BR	2D	BR	2D	BR
48	162 ± 17	50 ± 6	0.209 ± 0.001	1.438 ± 0.002	1.7 ± 0.2	2.5 ± 0.3
72	140 ± 15	37 ± 4	0.310 ± 0.001	1.344 ± 0.003	1.7 ± 0.2	2.4 ± 0.2
96	61 ± 6	28 ± 3	0.261 ± 0.002	1.880± 0.004	1.7 ± 0.2	2.5 ± 0.3
120	49 ± 5	22 ± 2	0.407 ± 0.002	1.828 ± 0.005	1.7 ± 0.2	2.3 ± 0.2
144	36 ± 4	28 ± 3	0.398 ± 0.003	0.920 ± 0.004	1.6 ± 0.2	2.4 ± 0.2
168	18 ± 3	23 ± 2	1.115 ± 0.008	0.455 ± 0.005	1.6 ± 0.2	2.4 ± 0.2

NET denotes the sum of specific rates determined for all consumed amino acids, excluding glutamine uptake, and AMN/NET consumption denotes the ratio between ammonia production (AMN) and NET consumption. Glutamine consumption could not be quantified but it was estimated to be identical in both culture systems since the levels of glutamine accumulation in the culture medium – derived from GlutaMAX® peptidase degradation – when normalized to the cell concentration were similar. Peptidases expression was also similar evaluated by transcriptome analysis. Legend: 2D-2D culture system; BR-stirred-tank bioreactor.

Finally, the third group comprised amino acids where the uptake/production profile was found to be inverted between 2D and bioreactor cultures. For histidine and threonine, the positive rates cannot reflect production as these are essential amino acids in human cells. Therefore, either they reflect: i) protein degradation (supported by transcriptional data), or ii) it might translate reduced consumption of these amino acids, if they are provided by medium proteins/peptides, since the media herein used is not protein free. For proline and asparagine, the increased production observed was supported by the up-regulation of their synthesizing enzymes, pyrroline-5-carboxylate reductase (PYCR) and asparagine synthase (ASNS), respectively (Figure 2.6).

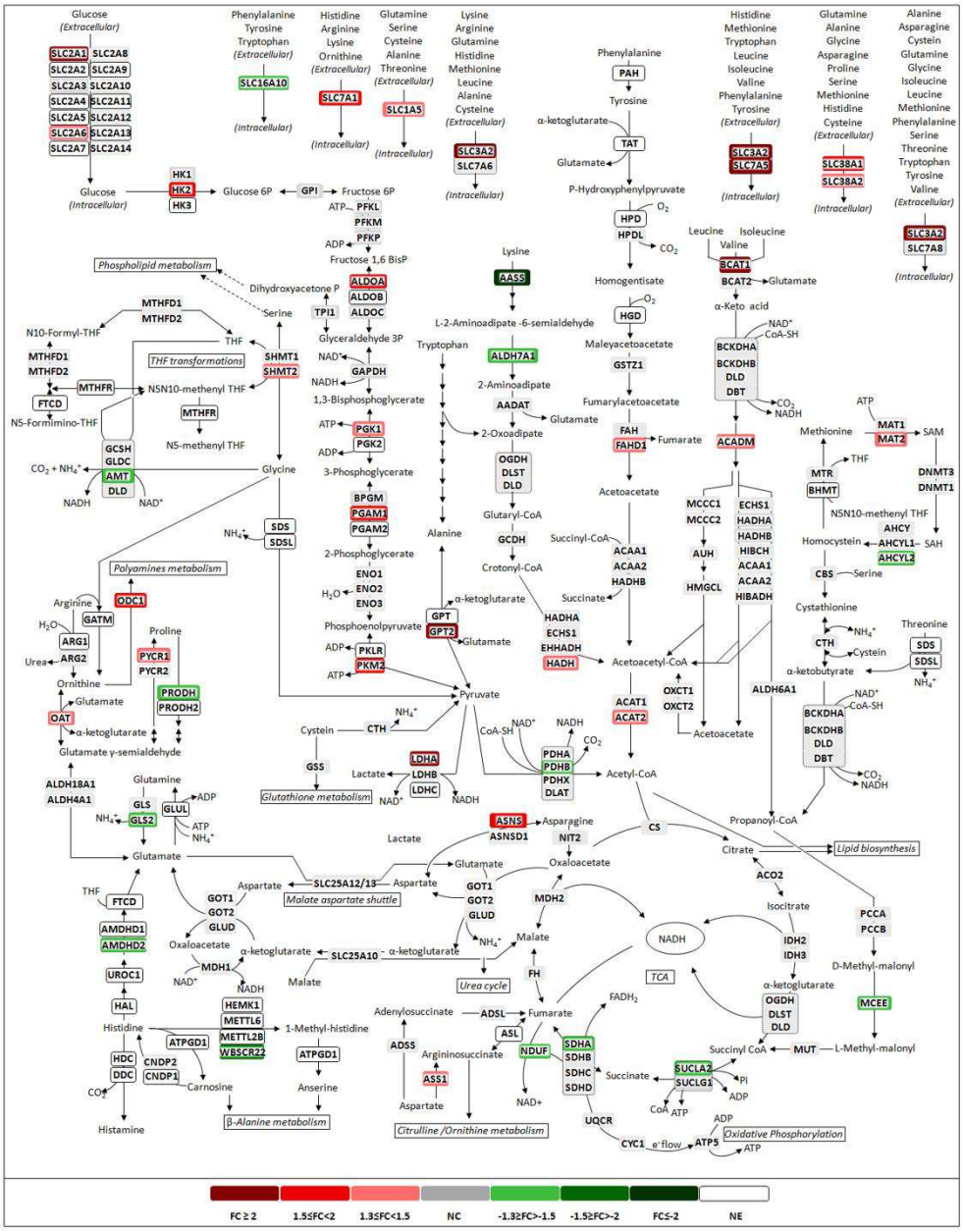

Figure 2.6. Central carbon metabolism of hESC-M cells expanded in 2D culture system versus stirred-tank bioreactors. Schematic representation of the main reactions of central carbon metabolism, highlighting transcriptome changes of hESC-M cells in the 2D culture system and the bioreactor culture system. Transcriptome changes correspond to fold-change in both culture conditions at the last day of culture, colored according the graphic legend. Each arrow represents a single reaction; reversibility is indicated by a two-arrow line according to the BioCyc database (Caspi et al., 2010). Dashed arrows are a general representation of metabolites being channeled from or into the indicated pathways. Reactions

are shown as a schematic representation and do not necessarily represent a unique possibility for the presented metabolites. For simplicity, only the main metabolites and cofactors are shown, thus the reactions are not necessarily balanced. Not all reactions (arrows) are assigned to an enzyme, either for clarity or because no specific enzyme has been described in the BioCyc database. Genes are shown in corner-rounded boxes, colored according to fold-change, and metabolites are shown unboxed. Enzymatic complexes and multigene-composed proteins are identified by a corner-rounded dashed line surrounding the gene set. Gene sets not surrounded by this line represent different enzymes and/or enzyme isoforms catalyzing the same reaction. Genes were considered to be expressed for average expression level above 1.5-fold the average expression of the background probes. Metabolic map adapted from (Rodrigues et al., 2013). The microarray dataset presented in this figure was submitted to the Gene Expression Omnibus repository with the accession number GSE63192. Abbreviations: 2D, two-dimensional; CoA, coenzyme A; DHF, dihydrofolate; FC, fold change; NC, no change; NE, not expressed; Pi, inorganic phosphate; PLP, pyridoxal-5-phosphate; SAH, S-adenosylhomocysteine; SAM, S-adenosylmethionine; THF, tetrahydrofolate.

4. Discussion

The implementation of fully defined scalable bioprocesses for the production of hESCs, along with proper process and product characterization, are important steps for meeting regulatory demands. In previous work, our group reported a scalable expansion protocol to expand a feeder-dependent hESC line on Matrigel-coated Cytodex-3 microcarriers (Serra et al., 2010, 2011). In this work, we evaluated the ability of synthetic and fully defined surfaces to expand two different hESC lines providing detailed transcriptomic and metabolic characterization. The differences in cell propagation on Synthemax II-polystyrene under fully defined conditions comparatively to the control condition (supplemental online Table1) can be related to the diversity of microcarrier surface composition. The interaction of hESCs with the Synthemax® surface (engaging vitronectin-derived short peptide), for example, ismediated by integrin-αvβ5 (Jin, Yao, Weber, Melkoumian, & Ye, 2012), whereas that connection on Matrigel-coated Cytodex-3 could be mediated by several extracellular matrix proteins (ECMPs) such as laminin, vitronectin, collagen, and fibronectin. In general, and as recently reviewed, the cell-adhesion molecules and ECMPs might be involved in cell-surface interactions to maintain the homeostasis and self-renewal of hPSCs (Lambshead, Meagher, O´Brien, & Laslett, 2013). Consequently, it is crucial to

expand hPSCs in a xeno-free and fully defined culture surface for the establishment of a well-characterized cell production platform to overcome some clinical concerns.

In stirred culture conditions, Synthemax II microcarriers presented very distinct abilities in supporting cell growth of both hESC lines (Figure 2.3). The microcarrier surface functional property might be related to this outcome: only Synthemax II-polystyrene microcarriers could efficiently support the attachment and proliferation of both hESC lines. Synthemax II-hydrogel showed very low cell-recovery yields, suggesting the presence of strong cell- ECM interactions that might hamper efficient cell harvesting. The pluripotent phenotype of both hESC cell lines was confirmed by the detection of stemness markers (Figure 2.3D–3F), by *in vitro* oxygen levels have been reported as a key process parameter in the maintenance of pluripotency (Agathocleous & Harris, 2013; Folmes, Dzeja, Nelson, & Terzic, 2012; Zhang, Nuebel, Daley, Koehler, & Teitell, 2012). Our data showed that the culture conditions used, including low oxygen levels, do not activate the hypoxia response machinery while maintaining the downstream hypoxia-response signature including an anaerobic glycolysis phenotype, a stemness feature that was less evident with the 2D culture system. Under hypoxic conditions, anaerobic glycolysis will be favored over oxidative phosphorylation as an energy-generation source. This is in agreement with the upregulation of the glycolytic machinery and LDHA, with the downregulation of the TCA reactions preceding oxidative phosphorylation, and stands for the evidently higher ratios of lactate production to glucose consumption (Table 1). In this context, amino acid catabolism can function as a feeding source of the remaining TCA reactions, substantiated by the extremely high ratios of ammonia production to amino acid consumption (Table 1). Intriguingly, although membrane transporters of both glucose and the majority of the amino acids were found to be extensively upregulated in the bioreactor, specific consumption rates of both were lower (Figure 2.5). The reason why increased upregulation did not translate into higher consumption is not clear, and although it is worth investigating, it was outside the scope of this work. A

direct correlation is not compulsory; for example, for glucose transporters, it has been shown that increased gene expression does not necessarily lead to higher glucose uptake rates, which better correlate with mitochondrial phosphorylation activity (Aloj et al., 1999). For amino acid consumption, a recent study reported substantial gene expression variation for amino acid transporters among different CHO cell lines, whereas the rates of consumption and production remained unchanged (Kyriakopoulos, Polizzi, & Kontoravdi, 2013). The crosstalk between metabolic plasticity, cellular signaling and genetic/epigenetic network has been studied extensively to understand and identify the key molecular mechanism linked to the maintenance of pluripotency in hPSCs (Folmes et al., 2012; Smith, Ladi, Mayer-Proschel, & Noble, 2000). In accordance, we highlight the importance of using transcriptional and metabolic tools to further characterize the final cell phenotype. In this study, we showed, for the first time, the phenotypic approximation of two different hESC lines, driven by a fully defined and standardized expansion bioprocess, while maintaining pluripotency markers. The results presented offer valuable insights into the transcriptomic and metabolic hallmarks of hPSC expansion using a fully defined manufacturing bioprocess, a subject underexplored because much of the currently available data derive from academia and research protocols. Such insights can help guide process design and media optimization toward higher cell densities of pluripotent human stem cells.

5. Conclusion

In this study, we implemented a fully defined bioprocess for the expansion of undifferentiated pluripotent hESCs. Transcriptomic and metabolomic tools further confirmed the robustness and standardization capacity of the developed bioprocess by showing phenotype convergence between two different hESC lines. Consequently, the bioprocess established in this study to expand hESCs can contribute to the

implementation of manufacturing systems to efficiently produce hESCs for high-throughput drug screening and stem cell-based therapies.

6. Author contribution & Acknowledgments

Marta M. Silva participated on the conception and design, collection and assembly of data, data analysis and interpretation, and wrote the chapter. The transcriptomic data was analyzed by Ana Filipa Rodrigues (co-author of this work).

7. Supplemental data

All the supplemental data (tables and figures) are available on online version of the paper.

8. References

Abbasalizadeh, S., Larijani, M. R., Samadian, A., & Baharvand, H. (2012). Bioprocess Development for Mass Production of Size-Controlled Human Pluripotent Stem Cell Aggregates in Stirred Suspension Bioreactor. *Tissue Engineering Part C: Methods*. 18:831–851.

Agathocleous, M., & Harris, W. a. (2013). Metabolism in physiological cell proliferation and differentiation. *Trends in Cell Biology*, 23, 484–492.

Aloj, L., Caracó, C., Jagoda, E., Caraco, C., Eckelman, W. C., & Neumann, R. D. (1999). Glut-1 and Hexokinase Expression: Relationship with 2-Fluoro-2-deoxy-d-glucose uptake in A431 and T47D cells in culture. Cancer Res, 4709–4714.

Bolstad, B. M., Irizarry, R. A., Astrand, M., & Speed, T. P. (2003). A comparison of normalization methods for high density oligonucleotide array data based on variance and bias. *Bioinformatics (Oxford, England)*, 19(2), 185–193.

Carinhas, N., Bernal, V., Monteiro, F., Carrondo, M. J. T., Oliveira, R., & Alves, P. M. (2010). Improving baculovirus production at high cell density through manipulation of energy metabolism. *Metabolic Engineering*, 12(1), 39–52.

Caspi, R., Altman, T., Dale, J. M., Dreher, K., Fulcher, C. a, Gilham, F., … Karp, P. D. (2010). The MetaCyc database of metabolic pathways and enzymes and the BioCyc collection of pathway/genome databases. *Nucleic Acids Research*, 38(Database issue), D473-9.

Chen, K. G., Mallon, B. S., McKay, R. D. G., & Robey, P. G. (2014). Human pluripotent stem cell culture: considerations for maintenance, expansion, and therapeutics. *Cell Stem Cell*, 14(1), 13–26.

DeBerardinis, R. J., Lum, J. J., Hatzivassiliou, G., & Thompson, C. B. (2008). The biology of cancer: metabolic reprogramming fuels cell growth and proliferation. *Cell Metabolism*, 7(1), 11–20.

Du, P., Kibbe, W. A., & Lin, S. M. (2008). lumi: a pipeline for processing Illumina microarray. *Bioinformatics* (Oxford, England), 24, 1547–1548.

Fan, Y., Hsiung, M., Cheng, C., & Tzanakakis, E. S. (2014). Facile Engineering of Xeno-Free Microcarriers for the Scalable Cultivation of Human Pluripotent Stem Cells in Stirred Suspension. *Tissue Engineering Part A,* 20(3–4), 588–599.

Folmes, C. D. L., Dzeja, P. P., Nelson, T. J., & Terzic, A. (2012). Metabolic plasticity in stem cell homeostasis and differentiation. *Cell Stem Cell*, 11(5), 596–606.

Gentleman, R. C., Carey, V. J., Bates, D. M., Bolstad, B., Dettling, M., Dudoit, S., … Zhang, J. (2004). Bioconductor: open software development for computational biology and bioinformatics. *Genome Biology*, 5(10), R80.

Hervy, M., Weber, J. L., Pecheul, M., Dolley-Sonneville, P., Henry, D., Zhou, Y., & Melkoumian, Z. (2014). Long Term Expansion of Bone Marrow-Derived hMSCs on Novel Synthetic Microcarriers in Xeno-Free, Defined Conditions. *PLoS ONE*, 9(3), e92120.

Inoue, H., & Yamanaka, S. (2011). The use of induced pluripotent stem cells in drug development. *Clinical Pharmacology and Therapeutics*, 89(5), 655–661.

Jin, S., Yao, H., Weber, J. L., Melkoumian, Z. K., & Ye, K. (2012). A synthetic, xeno-free peptide surface for expansion and directed differentiation of human induced pluripotent stem cells. *PloS One,* 7(11), e50880.

Kehoe, D. E., Jing, D., Lock, L. T., & Tzanakakis, E. S. (2010). Scalable stirred-suspension bioreactor culture of human pluripotent stem cells. *Tissue Engineering. Part A*, 16(2), 405–421.

Krawetz, R., Taiani, J. T., Liu, S., Meng, G., Li, X., Kallos, M. S., & Rancourt, D. E. (2010). Large-scale expansion of pluripotent human embryonic stem cells in stirred-suspension bioreactors. *Tissue Engineering. Part C, Methods*, 16, 573–582.

Kyriakopoulos, S., Polizzi, K. M., & Kontoravdi, C. (2013). Comparative analysis of amino acid metabolism and transport in CHO variants with different levels of productivity. *Journal of Biotechnology*, 168(4), 543–551.

Lambshead, J. W., Meagher, L., O´Brien, C., & Laslett, A. L. (2013). Defining synthetic surfaces for human pluripotent stem cell culture. *Cell Regeneration*, 2, 7.

Lei, Y., & Schaffer, D. V. (2013). A fully defined and scalable 3D culture system for human pluripotent stem cell expansion and differentiation. *Proceedings of the National Academy of Sciences,* 110(52), E5039-48.

Lin, S. M., Du, P., Huber, W., & Kibbe, W. A. (2008). Model-based variance-stabilizing transformation for Illumina microarray data. *Nucleic Acids Research*, 36(2), e11.

Melkoumian, Z., Weber, J. L., Weber, D. M., Fadeev, A. G., Zhou, Y., Dolley-Sonneville, P., … Brandenberger, R. (2010). Synthetic peptide-acrylate surfaces for long-term self-renewal and cardiomyocyte differentiation of human embryonic stem cells. *Nature Biotechnology*, 28, 606–610.

Müller, F.-J., Schuldt, B. M., Williams, R., Mason, D., Altun, G., Papapetrou, E. P., … Loring, J. F. (2011). A bioinformatic assay for pluripotency in human cells. *Nature Methods*, 8, 315–317.

Prigione, A., Fauler, B., Lurz, R., Lehrach, H., & Adjaye, J. (2010). The senescence-related mitochondrial/oxidative stress pathway is repressed in human induced pluripotent stem cells. *Stem Cells*, 28(4), 721–733.

Robinton, D. A., & Daley, G. Q. (2012). The promise of induced pluripotent stem cells in research and therapy. *Nature,* 481(7381):295-305.

Rodrigues, A. F., Formas-Oliveira, A. S., Bandeira, V. S., Alves, P. M., Hu, W. S., & Coroadinha, A. S. (2013). Metabolic pathways recruited in the production of a recombinant enveloped virus: mining targets for process and cell engineering. *Metabolic Engineering*, 20, 131–145.

Schmid, R., Baum, P., Ittrich, C., Fundel-Clemens, K., Huber, W., Brors, B., … Quast, K. (2010). Comparison of normalization methods for Illumina BeadChip HumanHT-12 v3. *BMC Genomics*, 11, 349.

Serra, M., Brito, C., Correia, C., & Alves, P. M. (2012). Process engineering of human pluripotent stem cells for clinical application. *Trends in Biotechnology*, 30(6), 350–359.

Serra, M., Brito, C., Leite, S. B., Gorjup, E., von Briesen, H., Carrondo, M. J. T., & Alves, P. M. (2009). Stirred bioreactors for the expansion of adult pancreatic stem cells. *Annals of Anatomy*, 191(1), 104–115.

Serra, M., Brito, C., Sousa, M. F. Q., Jensen, J., Tostões, R., Clemente, J., … Alves, P. M. (2010). Improving expansion of pluripotent human embryonic stem cells in perfused bioreactors through oxygen control. *Journal of Biotechnology*, 148(4), 208–215.

Serra, M., Correia, C., Malpique, R., Brito, C., Jensen, J., Bjorquist, P., … Alves, P. M. (2011). Microencapsulation technology: a powerful tool for integrating expansion and cryopreservation of human embryonic stem cells. *PloS One*, 6, e23212.

Simaria, A. S., Hassan, S., Varadaraju, H., Rowley, J., Warren, K., Vanek, P., & Farid, S. S. (2014).

Allogeneic cell therapy bioprocess economics and optimization: single-use cell expansion technologies. *Biotechnology and Bioengineering*, 111(1), 69–83.

Smith, J., Ladi, E., Mayer-Proschel, M., & Noble, M. (2000). Redox state is a central modulator of the balance between self-renewal and differentiation in a dividing glial precursor cell. *Proceedings of the National Academy of Sciences*, 97, 10032–10037.

Sun, Y., Yong, K. M. A., Villa-Diaz, L. G., Zhang, X., Chen, W., Philson, R., … Fu, J. (2014). Hippo/YAP-mediated rigidity-dependent motor neuron differentiation of human pluripotent stem cells. *Nature Materials*, 13, 599–604.

Varum, S., Rodrigues, A. S., Moura, M. B., Momcilovic, O., Easley, C. a, Ramalho-Santos, J., … Schatten, G. (2011). Energy metabolism in human pluripotent stem cells and their differentiated counterparts. *PloS One*, 6(6), e20914.

Zhang, J., Nuebel, E., Daley, G. Q., Koehler, C. M., & Teitell, M. A. (2012). Metabolic regulation in pluripotent stem cells during reprogramming and self-renewal. *Cell Stem Cell,* 11(5):589-95.

3

Human Mesenchymal Stem Cells Expansion in a Single-Use, Vertical-Wheel™ Bioreactor System

This chapter was adapted from:

Sousa MF*, **Silva MM***, Giroux D, Hashimura Y, Wesselschmidt R, Lee B, Roldão A, Carrondo JM, Alves PM, Serra M. (2015) Production of oncolytic adenovirus and human mesenchymal stem cells in a single-use, Vertical-Wheel bioreactor system: Impact of bioreactor design on performance of microcarrier-based cell culture processes. *Biotechnology Progress* 31(6):1600-12.

* Authors contributed equally

Abstract

Anchorage-dependent cell cultures are used for various cell therapies and tissue engineering applications. Most of these applications currently rely on planar technologies for the generation of biological products. However, as new cell therapy product candidates move from clinical trials towards potential commercialization, planar platforms have proven to be inadequate to meet large-scale manufacturing demand. Therefore, a new scalable platform for culturing anchorage-dependent cells at high cell volumetric concentrations is urgently needed. One promising solution is to grow cells on microcarriers suspended in single-use bioreactors.

Toward this goal, a novel bioreactor system utilizing an innovative Vertical-Wheel™ technology was evaluated for its potential to support scalable expansion bioprocess for human bone marrow-derived mesenchymal stem cells (hMSC). Key hydrodynamic parameters such as power input, mixing time, Kolmogorov length scale, and shear stress were estimated. The performance of Vertical-Wheel™ bioreactors (PBS-3 Air) was then evaluated for hMSC expansion and compared to traditional stirred-tank (ST) bioreactors. Although higher percentages of proliferative cells could be reached in the PBS-3 Air compared with ST bioreactors, no significant differences in the cell volumetric concentration and expansion factor were observed. Noteworthy, the hMSC population generated in the PBS-3 Air showed a significantly lower percentage of apoptotic cells as well as reduced levels of HLA-DR positive cells.

Overall, these results showed that process transfer from ST bioreactor to PBS-3 Air, and scale-up was successfully carried out for hMSC. Ultimately, the data herein generated demonstrate the potential of Vertical-Wheel™ bioreactors as a new scalable biomanufacturing platform for microcarrier-based stem cell cultures of complex biopharmaceuticals.

Table of Contents

1.Introduction

Traditionally, stirred tank (ST) bioreactors have been the most popular scalable platform for the production of biological therapeutics including monoclonal antibodies and other recombinant proteins (Matasci et al., 2008). Although ST bioreactors were initially limited to cell types growing in suspension, in 1967 Van Wezel pioneered the use of microcarriers in ST bioreactors to grow anchorage-dependent cells (van Wezel, 1967). Previous and ongoing clinical trials in cell therapies have used two-dimensional technologies such as plate stacking to produce challenging cell-based products, but it has become clear that these methods are insufficient for scaling up to clinical manufacturing. Therefore, a new scalable platform for the production of anchorage-dependent cells to high cell volumetric concentrations is still needed for the emerging cell therapy market (Rowley et al., 2012; Serra et al., 2012).

Recent findings indicate that microcarrier-based culture systems can increase therapeutic cell culture productivity in a cost-effective manner while ensuring culture homogeneity and strict process control (Simaria et al., 2014). However, developing and implementing microcarrier processes in conventional ST bioreactors presents major challenges and limitations. Keeping microcarriers suspended and uniformly distributed in a ST vessel is difficult due to the fluid mixing properties of the propeller-like impeller. A potentially greater issue arises during scale-up; the impeller must spin faster to mix larger volumes and will likely affect the cells growing on microcarrier surfaces, as they are much more sensitive to shear forces than cells cultured in suspension (Croughan et al., 1987, 1988).

Various types of single-use bioreactors have recently been developed with features designed to overcome these challenges. In particular, the Vertical-Wheel^{TM} bioreactor incorporates a vertically rotating wheel inside a U-shaped vessel, resulting in faster and more efficient mixing at very low shear rates

compared with ST bioreactor designs across a range of working volumes from 0.1–500 L (Hashimura et al. , 2012).

To investigate the potential applicability of Vertical-Wheel™ bioreactors (PBS-3 Air) on the microcarriers-based cell culture performance, human bone marrow-derived mesenchymal stem cells (hMSC) were used as cell source. The cell therapy market is highly interested in hMSC due to their immunosuppressive, immunoregulating, migrating, and trophic properties, as well as their proliferative capacity and potential to differentiate into several cell types such as osteocytes, chondrocytes, and adipocytes. They also show great potential in numerous clinical applications for a wide range of medical disorders such as, autologous and allogeneic therapies for diabetes mellitus, graft-versus-host disease, Crohn's Disease, myocardial infarction, orthopedic indications, and cancer (Wei et al., 2013).

In this study we evaluated (i) the growth performance of hMSC on microcarriers using ST bioreactor and PBS-3 Air, and (ii) the impact of bioreactor design on the yield and quality hMSC as cell-based product.

2. Material & Methods

2.1 Bioreactor configuration and hydrodynamics

2.1.1 Vessel Geometry and Impellers

The geometry of Vertical-Wheel™ bioreactors (PBS-3 Air) (PBS Biotech®, Camarillo) is significantly different from ST bioreactors (Table 3.1). The PBS-3 Air single-use vessel consists of four flat, vertical, baffle-less walls, and a U-shaped bottom (Figure 3.1A) whereas ST bioreactors are cylindrically shaped with wall baffles. The Vertical-Wheel impeller itself is very large, accounting for almost 85% of the width of the U-shaped bottom and rotates in a vertical plane about a stationary horizontal axle, whereas impellers in ST bioreactors rotate in a

horizontal plane. The Vertical-Wheel can be thought of as a combination of radial and axial flow impellers, with the radial component in a vertical plane and the axial component in the horizontal one. The vanes in the impeller responsible for the axial flow component are positioned to generate flow in opposite directions, one pumping from front-to-back and the other from back-to-front (Figure 3.1B). This opposition creates a cut-and-fold action that leads to very efficient and fast mixing. The PBS-3 Air used in these studies was powered by the buoyant energy of gas sparged from below the impeller whereas the ST bioreactor, equipped with axial flow three-pitched impeller 30° angled, was powered by top drive motor (Biostat Qplus from Sartorius Stedim Biotech, Gottingen, Germany). Aeration in ST bioreactors was promoted using the head-space of the bioreactor.

2.1.2 Mixing Time and Microcarrier Suspension

Mixing time was measured in PBS-3 Air using conductivity measurements and salt bolus additions. A conductivity probe was placed in the region of slowest mixing in the bioreactor, then a small volume of concentrated salt solution was added to the surface of the liquid and the conductivity signal recorded until equilibrium was reached, indicating complete mixing. The time for mixing to be 95% complete was measured from the conductivity vs. time plots, with these measurements carried out in triplicates and the results averaged.

In ST bioreactor, mixing time (t_m) was quantified by means of simple engineering correlation (Eq. 1) presented by Ruszkowski (Ruszkowski S., 1994) and many others:

$$\mathrm{t_m} = \mathrm{A}.\left(\frac{1}{N}\right).\left(\frac{1}{PN_{st}^{1/3}}\right).\left(\frac{d_{st}}{D_{st}}\right)^{-2} \qquad (1)$$

where A is a proportional factor, N is the stirring rate (s^{-1}), PN_{st} is the power number (dimensionless) for the impeller, d_{st} is impeller diameter (m), and D_{st} the vessel diameter (m). The A proportional factor used was 8.7 as estimated by

Kaiser and colleagues for identical ST bioreactors geometries used in our work (Kaiser et al., 2011). Power number (PN_{st}) for the three-blade pitched impeller was obtained from the same study and four-blade pitched impeller from Postmix Optimizaton and Solutions website (www.postmixing.com).

Microcarrier suspension experiments were performed using Synthemax® II microcarriers (Corning, USA) to determine the minimum agitation rates (N_{js}) that would fully suspend the microcarriers. This determination was made visually, with the criteria being the minimum agitation that kept all the microcarriers off the bottom of the vessel.

Table 3.1. Comparison of PBS-3 Air to traditional stirred-tank (ST) bioreactors

Characteristics	ST Bioreactors	Vertical-Wheel Bioreactor
Vessel Geometry	Cylindrical	U-shaped bottom and flat walls
Baffles	Baffles necessary for particle suspension and good mixing	Baffles not required
Impeller position and rotation	Vertical (or nearly vertical) shaft and rotates in the horizontal (or nearly horizontal) plane	Horizontal shaft and rotates in the vertical plane
Impeller power source	Rotating shaft and external motor	Buoyancy of gas introduced under the impeller and caught in circumferential air cups
Impeller type	Radial or axial flow impellers	Combination of axial and radial flow features
Vertical fluid circulation and particle suspension	Comes from axial flow component of impeller (especially in absence of baffles)	Comes from radial flow component of impeller interacting closely with vessel walls
Mixing power	From turbulent dissipation	From turbulent dissipation and also “cut-and-fold” action generated by axial vanes arranged to pump in opposite directions
Power input	Usually estimated from engineering correlations	Dependent on and calculated from sparged gas flow rate
Impeller zone mass	Typically 5% of bioreactor mass	22% - 33% of bioreactor mass, depending on scale

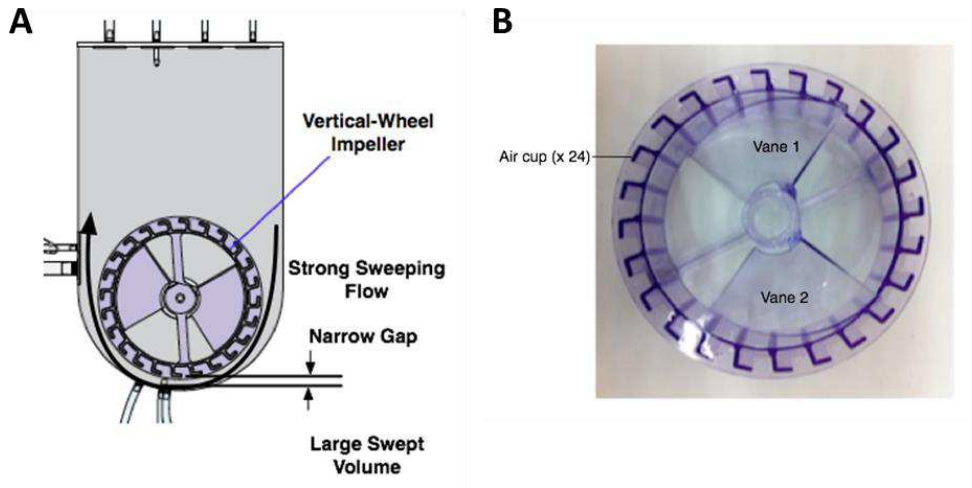

Figure 3.1. A) Geometry of PBS bioreactor single-use vessel with enclosed vertical-wheel, U-shape round bottom and flat sides in the front and back. **B)** Diagram of Vertical-Wheel impeller using AirDrive mixing mechanism.

2.1.2 Hydrodynamics Parameters

The estimation of shear stress (τ) (N/m^2) under stirred conditions as result of flow through Kolmogorov eddies was performed using Eq. 2, as described in the literature (Croughan et al., 1987, 1988; Cruz et al., 1998),

$$\tau = \left(\frac{\varepsilon}{\nu}\right)^{\frac{1}{2}} . \mu \qquad (2)$$

and the Kolmogorov length scale (KLS; λ), or eddy size (m) was estimated by Eq. 3:

$$\lambda = \sqrt[4]{\frac{\nu^3}{\varepsilon}} \qquad (3)$$

where (m^2.s^{-1}) is the kinematic viscosity, (m^2.s^{-3}) is the turbulent energy dissipation in the impeller zone and μ (N.s/m^2) is the viscosity of the fluid. For the microcarrier suspension studies using culture medium at 37°C, as well as the microcarrier cultures at the same temperature, the viscosity of the fluid was

assumed to be 0.0071 g/cm/sec. The kinematic viscosity used for the calculations was 0.007 cm^2/sec (Croughan et al., 1988).

The turbulent energy dissipation rate (EDR) for PBS-3 Air can be estimated by:

$$\varepsilon = \frac{P_{PBS}}{D_{PBS}^2 . W_{PBS} . \rho} \quad (4)$$

where P_{PBS} (W) is the power input and D_{PBS} (m) is the impeller (i.e., wheel) diameter for PBS-3 Air bioreactor, respectively, and ρ (kg/m^3) is the density of the medium (Croughan et al., 1988). A characteristic of PBS-3 Air geometry is that using D^3_{PBS} as an estimate of the impeller zone volume leads to a value greater than the actual culture volume of the present experiments. In present experiments, the impeller zone volume measurement was estimated by using D^2_{PBS} multiplied by impeller width (W_{PBS}, front-to-back). For the bioreactor used in this experiment, D_{PBS}=13.5 cm and W_{PBS}=5.5 cm. The density of the medium was assumed to be 1.003 g/ml. The power input to the PBS-3 Air impeller, P_{PBS} (W), is linearly dependent to the flow rate of the main sparged gas, similar to what is observed in a Pelton wheel (impulse type water turbine), and can be estimated by:

$$P_{PBS} = \rho . \frac{Q}{60} . g . D_{PBS} \quad (5)$$

where Q (m^3/min) is the volumetric flow rate of the main sparged gas and g is acceleration due to gravity (9.8 m/s^2). In Eq. 5 the mixing power in PBS-3 Air is equal to the power input minus any solid–solid friction drags between the shaft and the wheel. The friction drag was experimentally estimated and considered negligible. For this reason, the mixing power can be considered equal to the power input. The energy dissipation throughout a ST bioreactor volume is commonly determined using the following equation:

$$\varepsilon = \frac{PN_{ST} . \rho . N^3 . d_{ST}^5}{V} \quad (6)$$

where V the working volume (m^3) and d_{ST} the impeller diameter (m) of the ST bioreactor. In 1985, Placek and Tavlarides reported that the energy dissipation

near the impeller is much higher than estimated by equation above, in a ratio of approximately V/d^3_{ST} (Placek & Tavlarides, 1985). Assuming the impeller local power dissipation rate is the significant factor, the energy dissipation around the impeller can be estimated by:

$$\varepsilon = PN_{\mathrm{ST}}.\,\rho\,.N^3.d_{\mathrm{ST}}^2 \quad (7)$$

2.2 hMSC culture under static conditions

Human bone marrow-derived mesenchymal stem cells (hMSC) were obtained from STEMCELL™ Technologies (Cat. No. MSC-001F; STEMCELL™ Technologies, France). These hMSC were thawed and expanded to prepare working cell stocks following the manufacturer's instructions using the Mesencult-XF Kit (STEMCELL™ Technologies). Cryopreserved hMSC (passage 3 or 4) were thawed and plated at a cell density of 4×10^3 cell/cm^2 on tissue culture flasks of 175 or 225 cm^2 of available area for growth pre-coated with MesenCult™-SF attachment substrate using MesenCult™-XF medium (both from STEMCELL™ Technologies) supplemented with 2 mM L-glutamine (Life Technologies). Cells were cultured at 37°C in a humidified incubator at 5% CO_2. Fifty percent of culture medium was exchanged at day 5. At roughly 70% cell confluence, hMSC were detached from the flasks by rinsing with DPBS, adding TrypLE™ Select, and incubating the flask for 5 min at 37°C. Cells were removed, pooled, and counted using Trypan Blue exclusion method to determine number and viability.

2.3 hMSC culture under stirred conditions

In this study, two different bioreactor systems were used: PBS-3 Air and glass ST bioreactor. More specifically, hMSC cells were cultured in PBS-3 Air (PBS Biotech) and the Biostat Qplus bioreactor system equipped with three-blade segment impeller 30° angled (Sartorius Stedim Biotech). Data acquisition and process control were performed using Hello™ Software running on a Real-time OS

(PBS Biotech) and MFCS/Win (Sartorius Stedim Biotech) as described previously (Obom et al., 2014; Serra et al., 2010). In the following sections, we describe the operation parameters (Table 3.2) and methodology used for the expansion of hMSC. It is important to highlight that the selection of the operation parameters for ST bioreactors was based in previous data obtained by our group (Cunha et al., 2015; Fernandes et al., 2013; Silva et al., 2008). For the PBS-3 Air, the same operation parameters (e.g., pO_2, pH, cell inoculum concentration, microcarrier type and concentration, temperature) were used and the agitation rate used was estimated experimentally having as criteria the minimum agitation required for full suspension of the microcarriers (N_{S1}).

2.3.1 Expansion of hMSC in bioreactors

hMSC were inoculated in the PBS-3 Air (2.2 L) and Biostat Qplus ST bioreactor (0.25 L) at a concentration of 2.5×10^4 cell/mL using 16 g/L Synthemax II microcarriers (Corning) prepared according to the manufacturer's instructions. For each bioreactor system, hMSC were cultured for 14 days in MesenCult™-XF medium supplemented with 2 mM L-glutamine and 0.025% (v/v) antifoam C emulsion (Sigma- Aldrich). On day 6 of culture, additional empty Synthemax II microcarriers were added at a 2:1 ratio, increasing the final concentration to 48 g/L. Fifty percent of culture medium was replaced every 2.5 days, starting at day 5. Operation parameters of pH, temperature and pO_2 as well as the stirring rate and profile used in each bioreactor culture are indicated in Table 3.2. Sampling was performed daily and hMSC were characterized in terms of cell concentration, viability, morphology, proliferation capacity, and metabolism using the methodologies described below. The hMSC were harvested from the microcarriers using TrypLE™ Select solution according to the protocol described elsewhere (Cunha et al., 2015).

Table 3.2. Operational conditions used in Vertical-Wheel™ (PBS-3 Air) and stirred tank (ST) bioreactors for the culture of hMSC line.

Bioreactor	PBS-3 Air	ST
Temperature	37°C	
pH	7.2	
DO	20% air saturation	
Aeration	0.1 vvm	
Agitation	**0-7 h:** 15 rpm, 1 min; off 20 min **Day 1-6:** 15 rpm **Day 6-10**: 15 rpm, 5 min; off 1 h **Day 10-14:** 17 rpm	**0-6 h**: 40 rpm, 1 min; off 20 min **Day 1-6:** 40 rpm **Day 6-10:** 40 rpm, 5 min; off 1 h **Day 10-14:** 45 rpm

2.4 Analytical methods

2.4.1 Cell Growth and Microcarrier Colonization

Total cell concentration was determined using crystal violet staining. Cells were briefly disrupted using 0.1 M citric acid with 1% TritonX-100 at 37°C overnight and nuclei stained with 0.1% crystal violet as described elsewhere (Alves et al., 1996). Nuclei were counted in a Fuchs–Rosenthal hemocytometer chamber. Cell expansion in the bioreactors was characterized by assessing the specific growth rates, μ (day^{-1}), as previously described (Serra et al., 2010). Fold increase in cell concentration was evaluated based on the ratio X_{MAX}/X_0, where X_{MAX} is the peak cell concentration and X_0 is the cell concentration at inoculum. Cell viability and microcarrier colonization were assessed by staining cells with fluorescein diacetate (FDA, green, viable cells) and propidium iodide (PI, red, dead cells) as described by Serra and colleagues followed by visualization under a fluorescence microscope (Leica Microsystems GmbH, Germany) (Serra et al., 2010). The analysis of microcarrier colonization was performed by recording at least three representative images (with at least 300 microcarriers each) of cells on microcarriers. The percentage of colonized microcarriers was determined by dividing the number of colonized microcarriers with the total number of microcarriers (colonized and empty).

2.4.2 Metabolite Analysis

The consumption of glucose and glutamine as well as the production of lactate and ammonia were monitored throughout the culture period. Glucose, glutamine, and lactate concentrations were analyzed using an YSI 7100MBS (YSI Incorporated, USA) whereas the ammonia concentration was quantified enzymatically using a commercially available UV test (Roche, Switzerland). Specific metabolic rates, q_{met} (mol/day/cell) and apparent yield of lactate-to-glucose ($Y_{Lac/Glc}$) were determined as described in the literature (Serra et al., 2010).

2.5 hMSC characterization

2.5.1 Cell Apoptosis and Proliferation Assays

The percentage of apoptotic hMSC was evaluated using the Apoptosis Assay Kit NucView™ 488 (Biotium, Inc., USA), following the manufacturer's instructions. This kit contains the green fluorescent NucView 488 caspase-3 substrate, which detects intracellular caspase-3. The percentage of proliferating hMSC was determined using Click-iT EdU Flow Cytometry Assay Kit according to the manufacturer's recommendation (Life Technologies). All samples were analyzed in a CyFlow® space instrument (Partec GmbH, Germany). At least 10,000 events were registered *per* sample.

2.5.2 Cell Surface Marker Analysis by Flow Cytometry

Upon termination of each bioreactor culture, hMSC were dissociated from microcarriers using TrypLE™ Select solution and washed twice in DPBS. hMSC were incubated with primary antibodies for 1 h at 4°C, washed with DPBS and analyzed in a CyFlow® space instrument (Partec GmbH) as reported elsewhere (Serra, Brito, Costa, Sousa, & Alves, 2009). Ten thousand events were registered per analysis. Conjugated antibodies used: CD90-PE, CD73-PE, CD105-PE, CD166-PE, CD44-PE, CD45-PE, CD34-PE, HLA-DR, and isotype control antibodies (all from BD Pharmingen™).

2.5.3 Immunocytochemistry

hMSC immobilized on microcarriers were fixed in 4% (w/v) paraformaldehyde in DPBS for 20 min, then permeabilized for 20 min in 0.1% (w/v) Triton X-100 (Sigma-Aldrich) in DPBS. After 30 min of blocking with 0.2% (w/v) fish skin gelatin (Sigma- Aldrich) in DPBS, cells were incubated with phalloidin-FITC solution (1:100; Sigma-Aldrich) for 2 h at room temperature. Cells were washed three times in DPBS and then cell nuclei were counterstained with Hoechst 33342 (Sigma-Aldrich). The analysis of cytoskeleton organization was performed both qualitatively and quantitatively. After staining, fixed cells were visualized using fluorescence microscopy (Leica Microsystems GmbH). One hundred cells were analyzed from each condition and the percentage of cells showing actin fibers and/or granular actin was quantified.

2.5.4 Multilineage Differentiation Assays

hMSC multilineage differentiation assays were performed using the Stem-MACS™ AdipoDiff (Miltenyi Biotec, Germany), StemMACS™ OsteoDiff (Miltenyi Biotec) and StemPro® Chondrogenesis (Life Technologies) differentiation kits (Cunha et al., 2015).

2.5.5 Colony Forming Unit (CFU) Assay

After cell dissociation and separation from microcarriers, hMSCs were inoculated in 100 mm Petri dishes in 10 mL of DMEM supplemented with 10% (v/v) FBS (250 cells/Petri dish). Fifty percent of culture medium was replaced twice a week. After 15 days in culture, the number of CFUs was measured. Briefly, cells were washed twice with DPBS and fixed with methanol for 20–40 min at -20°C. After fixation, cells were dried under hood and then incubated with Giemsa solution (Sigma Aldrich) diluted 1:20 in H_2O for 30 min at room temperature. After staining, cells were washed twice with DPBS and dried under hood. The number of CFU was counted in each Petri dish. Colonies with less than 20 cells were not

considered. At least four replicates were carried out. The number of CFU is presented as mean ± standard error of all colonies in all Petri dishes.

2.6 Statistical Analysis

All values presented in this work are mean ± standard error of mean of two replicates (n=2). Student's t-tests (nonparametric test) were used to compare means. $p<0.05$ was chosen as the level of significance. All comparisons were made using two-tailed statistical tests.

3. Results & Discussion

3.1 Bioreactors configuration, hydrodynamics parameters, and operation

Although mixing and mass transfer in conventional ST bioreactors have been extensively characterized over the years (Chisti, 1993; Nienow, 1997), the performance of biological systems under specific environmental conditions is still difficult to understand and predict. This is especially true for complex systems such as microcarrier-based cell cultures; highly sensitive to shear stresses, making it difficult to fine-tune the necessary mixing power in bioreactors during process scale-up while maintaining microcarriers uniformly suspended, shear stresses below a damaging level, and providing sufficient mass transfer to achieve high cell volumetric concentration.

The aim of many of the novel mixing regimes designed into single-use bioreactors (SUB), such as the Vertical-Wheel^{TM} PBS bioreactor (PBS-3 Air), ST, wave motion and orbital shaken bioreactors, is to provide an environment that further enhances cellular productivity while maintaining mixing performance for optimal cell growth (van Eikenhorst et al., 2014). Löffelholz et al. showed that the size, geometry, and position of the Vertical-Wheel of PBS bioreactor leads to an

uniform distribution of the hydrodynamic forces (Löffelholz et al., 2010). Consequently, the maximum specific turbulent EDR (2×10^3 W/m^3) and maximum wall shear stress (1.7 N/m^2) calculated are within the range of values that animal cells can tolerate (Godoy-Silva et al., 2009; Godoy-Silva et al., 2009; Tramper et al., 1986; Vickroy et al., 2007). Furthermore, the power input generated by the Vertical-Wheel is significantly lower than a Rushton turbine, one of the types of impellers frequently used for the culture of animal cells in ST bioreactors. In a different study, Odeleye et al. showed that PBS-3 Air bioreactor exhibited a greater degree of fluid dynamic homogeneity and that the turbulent kinetics energy (TKE) generated at higher wheel speeds is lower when compared with Mobius™ CellReady 3 L ST bioreactor and wave motion Cultibag RM bioreactor from Sartorius (Odeleye et al., 2013). Vertical-Wheel bioreactors, together with orbital shaken technology bioreactors, are described as low shear stress bioreactors even under maximum agitation capacities (Löffelholz et al., 2010; Tissot et al., 2011).

In order to evaluate the suitability of PBS-3 Air for microcarrier applications, key hydrodynamic parameters were estimated, namely (i) specific power input (SPI), (ii) mixing time (t_m), (iii) KLS, and (iv) shear stress, and compared with the values determined for ST bioreactors (Table 3.3). To determine the N_{JS} in PBS-3 Air, suspension experiments with 16 and 48 g/L of Synthemax® II microcarriers were performed. From the N_{S1} values obtained, it was decided to run the culture of hMSC at 15/17 rpm, corresponding to a SPI of 0.3 W/m^3. These SPI values are within the range of those estimated for ST bioreactors.

The mixing studies were performed in the PBS-3 Air using conductivity measurements and salt bolus additions. In fact, the mixing characterization of one bioreactor is normally performed by investigating the fluid flows of an inert tracer inside the vessel aiming to establish numerical correlations to predict the time needed to reach homogeneity inside a ST. In the last decades, numerical

correlations have been established (Grenville K, Ruszkowski S, 1995; Ruszkowski et al., 1994) and have been shown to correlate well with the t_m predicted by CFD data (Kaiser et al., 2011). Based on such results and since no experimental data was generated to estimate the t_m in the ST bioreactor, it was decided to use a numerical correlation for this purpose. For both cultures, the t_m estimated for PBS-3 Air (18 s) was lower than for ST (56 s). The reason for this observation may lie on the greater degree of fluid dynamic homogeneity observed in PBS-3 Air when compared with ST as described by Odeleye et al. (Odeleye et al., 2013).

Table 3.3. Specific power input, mixing times and Kolmogorov length scales estimated for the experimental conditions used for culturing hMSC line in PBS 3L Vertical-Wheel™ (PBS-3 Air) and stirred tank (ST) bioreactors.

Bioreactor	**PBS-3 Air**	**ST**
Stirring rate (rpm)	17	40-45
Specific power input (W/m^3)	0.3	Average: 0.1-0.2 Impeller: 0.6-0.8
Mixing Time (sec)	18	56
Kolmogorov Length Scale (μm)	151	Average: 220-202 Impeller: 157-143
Shear stress rate (N/m^2)	0.021	Average: 0.008-0.010 Impeller: 0.019-0.024

With the objective of providing engineering correlations to guide the design of ST bioreactors for microcarrier cultures, Croughan et al. have established a relationship between KLS and cell growth inhibition and death rates (Croughan et al., 1987, 1988) identifying a critical threshold for KLS above which no harm to cells occurs. For cell culture on microcarriers, this threshold corresponds to approximately 130 μm (Croughan et al., 1988). The estimated KLS values for PBS-3 Air and average KLS in ST bioreactor are above that critical length: the lowest value estimate was 133 μm for PBS-3 Air (Table 3.3).

Shear stress is an essential parameter for the design and operation of ST bioreactors used for cultivations involving shear-sensitive cells. This is an

important engineering correlation since it is a function not only of the impeller speed or SPI but also of the density and rheological properties of culture medium. From the several descriptions available in the literature for microcarrier cultures, Croughan et al. reported shear stress levels detrimental for cell growth roughly an order-of-magnitude higher than those estimated in our study for the culture conditions used (Table 3.3) (Croughan et al., 1989).

Although different bioreactor scales of PBS-3 Air (2.2 L) and ST (0.25 L) bioreactors were used in this study, we believe that the results reported in the following sections can be directly compared. ST bioreactors have been used for decades and during this period, engineering/hydrodynamic parameters have been extensively explored and used to assist the transfer of processes from lab (e.g., 2 L) to manufacturing scale (e.g., >500 L). Importantly, in all these scaling-up processes, the main objective is to maintain constant as much hydrodynamic parameters as possible. Translating this concept to our study, the results obtained with a 0.2 L can be comparable to a 2 L scale as long as the hydrodynamic conditions are kept similar.

3.2 hMSC production

The impact of bioreactor design on the growth, metabolism, and quality of hMSC derived from bone marrow was evaluated based on the following parameters: seeding efficiency, microcarrier colonization, growth rate, expansion factors, actin organization, apoptosis, metabolite consumption/production, and hMSC phenotype.

An intermittent agitation scheme was used with the aim of promoting cell attachment during the first hours after inoculation (Table 3.2). Using this strategy, more than 95% of seeded hMSC attached to microcarriers 12 h after inoculation in both types of bioreactor cultures. Despite these similar seeding efficiencies, a

higher percentage of colonized beads were attained in the PBS-3 Air (68% ± 6%) when compared with ST bioreactor (48% ± 16%) (Figure 3.2A-B).

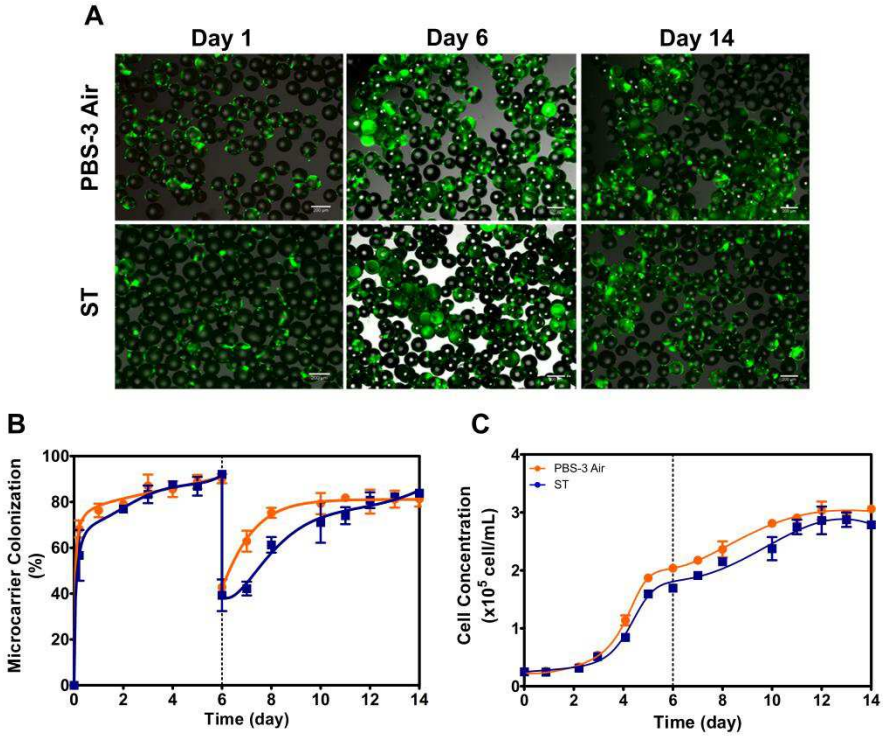

Figure 3.2. hMSC expansion in PBS-3 Air and ST bioreactors. A) Representative images of hMSC at day 1 of culture (green: live cells stained with FDA; red: dead cells stained with PI; scale bars: 200 mm). **B)** Percentage of colonized microcarriers and **C)** cell growth curves, expressed in terms of cell concentration per volume of medium, in PBS-3 Air (orange circles) and ST (blue circles) bioreactors. Data are mean ± standard deviation of two replicates.

These results might be a direct consequence of the more efficient and gentle mixing characteristics of PBS-3 Air (Table 3.3). At day 6, empty microcarriers were added to the cultures to provide additional area available for cell growth, as described previously (Hervy et al., 2014). In both bioreactor systems, hMSC were able to migrate to empty microcarriers and proliferate (Figure 3.2B-C and Figure 3.3A). Again, the percentage of colonized microcarriers was higher in the PBS-3 Air

from day 7 to day 12 (Figure 3.2B), confirming that cell migration was more efficient in this system. The more homogenous microcarrier colonization and better migration efficiency observed in the PBS-3 Air bioreactor resulted in higher percentages of proliferative cells and were significantly different at days 3 and 9 of culture when compared with ST bioreactors (Figure 3.3A). However, the differences observed in cell volumetric concentrations between PBS-3 Air and ST bioreactors throughout culture time (Figure 3.2C) were not statistically significant; in both bioreactor systems hMSC displayed similar maximum growth rates (0.012 h^{-1} in PBS-3 Air vs. 0.010 h^{-1} in ST bioreactor) and expansion factors (12 and 11, respectively). The maximum cell concentration achieved in both bioreactor systems (3×10^5 cell/mL) were lower than other reports in the literature (Caruso et al., 2014; Dos Santos et al., 2014; Goh et al., 2013).

The difference in the cell growth profile may reflect the distinct cell origins (hMSC were isolated from the bone marrow of different donors), and the different culture conditions such as the microcarrier type, medium formulation, culture system, and operation mode. It is important to highlight that in our study, hMSC were cultured under well-defined conditions using synthetic microcarriers and xeno- and serum-free culture medium, which facilitates process transfer to a GMP- compliant environment. Further studies should be carried out in the future to test hMSC derived from different tissue origins and isolated from different donors in order to confirm the robustness of the PBS-3 Air bioreactor process implemented in this study and integrate biological variability.

Actin organization is believed to play a pivotal role in hMSC phenotype (Mammoto & Ingber, 2009) and proliferation capacity (Sart et al., 2013). Bioreactor design did not impact the actin organization since the hMSC displaying organized actin fibers were observed in both culture systems at days 6 and 14 (Figure 3.3B-C). The percentage of apoptotic cells was also assessed at these time-points. Although no differences were observed at day 6, a significantly higher

percentage of apoptotic cells were observed in ST at day 14 (Figure 3.3D). These results might be explained by the lower shear stress and more efficient mixing environment of PBS-3 Air bioreactors (Table 3.3).

The consumption of glucose and glutamine as well as the production of lactate and ammonia were monitored throughout the culture period (Figure 3.3E). Results show that bioreactor design did not impact cell metabolism since similar consumption and production rates were observed. The yield Lac/Glc ($Y_{LAC/GLC}$) was approximately 2 for both bioreactor types, which is in accordance with results described in the literature for various types of stem cell during the self- renewal process (Zhang et al., 2012). Measurements of glucose and glutamine concentrations showed that there was no complete depletion of these nutrients during culture period (Figure 3.4). Moreover, the accumulation of lactate and ammonia was always below the growth-inhibitory concentrations (<8 and <1 mM, respectively) (Schop et al., 2010).

It is well known that the cellular and immunophenotype of hMSC depend not only on the isolation protocol but also on the culture conditions (Bocelli-Tyndall et al., 2015; Sotiropoulou et al., 2006). Our results showed that both bioreactor types were able to maintain the hMSC cellular phenotype; hMSC were negative for hematopoietic CD34 and CD45 markers and displayed high levels of CD44, CD73, CD105, CD90, and CD166 mesenchymal stem markers (Figures 3.5A-B). According to the International Society for Cellular Therapy, hMSC are also considered HLA-DR-negative with no/reduced (below 5%) expression of HLA-DR surface molecules (Dominici et al., 2006). Importantly, in our work, we demonstrated that the percentage of HLA-DR positive cells was significantly reduced when hMSC were cultured in PBS-3 Air bioreactor (from 22% at the inoculum time to 3% at day 14) than the cells expanded in ST bioreactors (30% at day 14) (Figure 3.5B), suggesting that it might be the consequence of the different

cell culture conditions provided by the different bioreactor configurations/hydrodynamics.

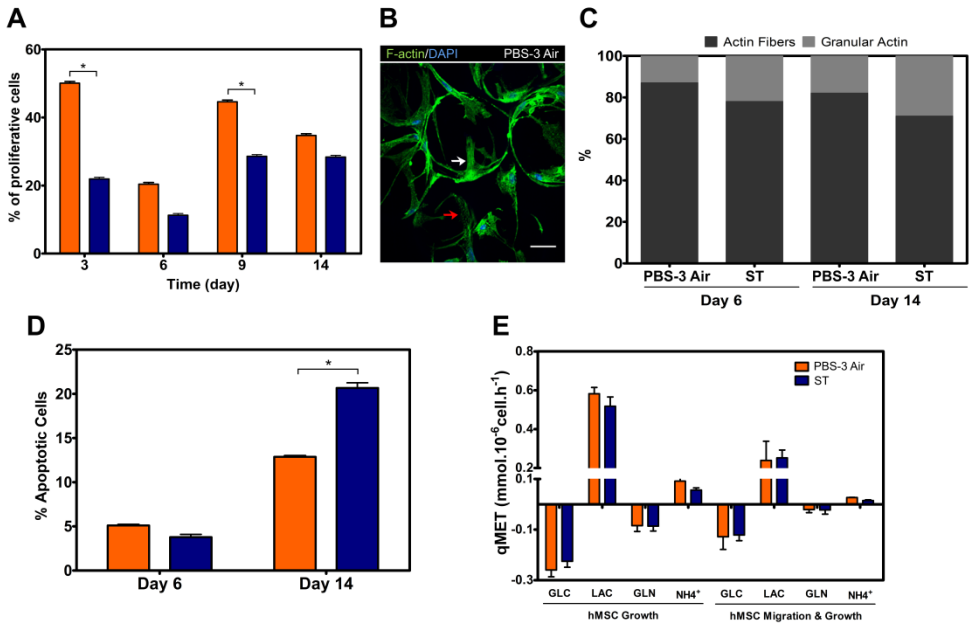

Figure 3.3. Characterization of hMSC during expansion in PBS-3 Air and ST bioreactors. A) Percentage of proliferative cells evaluated at days 3, 6, 9, and 14 of culture in PBS-3 Air (orange bars) and ST (blue bars) using Click-iT EdU flow cytometry assay kit. **B)** Representative image of actin organization of hMSC attached to microcarriers in PBS-3 Air at day 6, assessed by cell staining with phalloidin FITC (green; nuclei stained in blue); white arrows show cortical actin and red arrows show globular actin (scale bar: 50 mm). **C)** Percentage of hMSC with actin fibers (dark gray bars) or granular actin (light gray bars) organization estimated by microscopic evaluation. **D)** Percentage of apoptotic cells assessed by NucView^{TM} dye and flow cytometry at days 6 and 14. Data are mean6standard deviation of two measurements. **E)** Specific rates of glucose (GLC) and glutamine (GLN) consumption and lactate (LAC) and ammonia (NH_4^+) production for hMSC growth and hMSC migration and growth phases in PBS-3 Air (orange bars) and ST (blue bars) bioreactors. Data of hMSC growth phase are mean6standard deviation of mean of two independent experiments; data of hMSC growth and migration phase are mean6standard deviation of two replicates. Asterisks indicate significant difference (*P<0.05).

Finally, in both bioreactor strategies, expanded hMSC were able to reattach on plastic surfaces and presented the ability to form colony forming units (CFU), showing similar number of colonies (83 ± 9 in PBS-3 Air and 83 ± 5 in ST). The

multipotent differentiation potential of hMSC was similar in both PBS-3 Air and ST since they could successfully differentiate into adipocytes, osteocytes, and chondrocytes (Figure 3.5C). No spontaneous differentiation was observed (data not shown). In future studies it will also be important to evaluate whether the gene expression profile and the paracrine activity of hMSC are affected by the expansion process using different bioreactor systems. It has been described in the literature that the cell culture system (planar technologies vs. microcarrier-based stirred systems) and operation conditions (e.g., hypoxia) greatly impacts and regulates the secretion of bioactive molecules such as growth factors, immune modulating and anti- inflammatory molecules, and anti-cancer factors (Hupfeld et al., 2014; Madrigal et al., 2014).

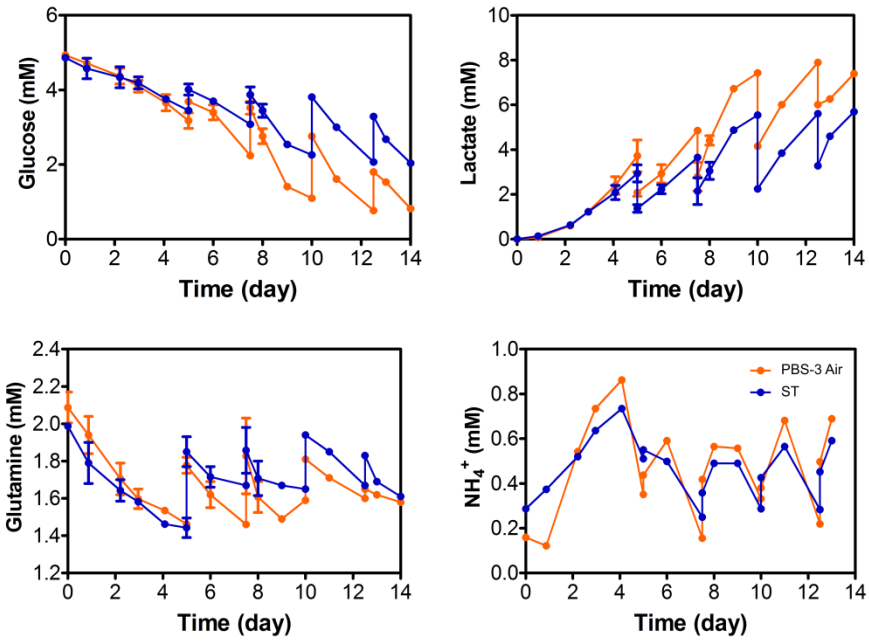

Figure 3.4. Metabolite concentration profiles during hMSC expansion in both bioreactors. Concentration profiles of Glucose, Lactate, Glutamine and Ammonia (NH_4^+) during hMSC growth and migration.

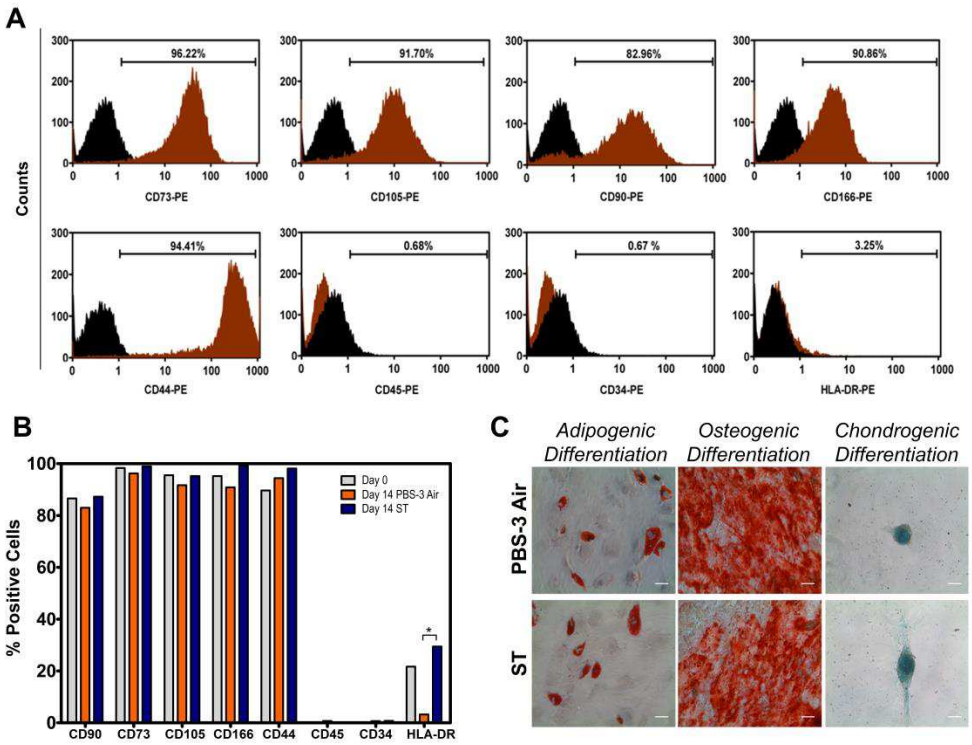

Figure 3.5. Quality control assays of hMSC expanded in PBS-3 Air and ST bioreactors. A-B) Flow cytometry analysis of percentages of hMSC markers CD90, CD73, CD105, CD166, CD44, and non-hMSC markers CD45, CD34, as well as HLA-DR at day 0 (gray bars) and day 14 after expansion in PBS-3 Air (orange bars) and ST (blue bars) bioreactor. Representative histo- grams from flow cytometry analysis of hMSC after expansion in PBS-3 Air are included in (A). **C)** Multilineage differentiation potential of hMSC expanded in each bioreactor; cell differentiation was induced for up to 21 days then assessed by staining for adipogenesis (Oil Red-O), osteogenesis (Alizarin red), and chondrogenesis (Alcian blue); (Scale bar: 100 mm). Asterisks indicate significant difference (*P<0.05).

4. Conclusions

This study demonstrates the applicability of Vertical-Wheel^{TM} bioreactor for microcarrier-based hMSC expansion processes. Hydrodynamic studies and calculations were performed in this bioreactor, allowing for the estimation of key

hydrodynamic parameters such as power input, mixing time, and Kolmogorov length scale. Higher percentage of proliferative cells was observed in PBS-3 Air when compared with ST bioreactor. However, this does not translate into significant differences in cell volumetric concentration, expansion factor, or metabolic performance. Both bioreactor system types investigated here were able to maintain the hMSC phenotype and multipotent differentiation potential. Noteworthy, the hMSC population generated in the PBS-3 Air showed a significantly lower percentage of apoptotic cells as well as reduced levels of HLA-DR positive cells when compared with the cells produced in the ST bioreactors, which may be an important finding for the clinical application of these cells. Further studies are required to understand the effect of bioreactor hydrodynamics and culture conditions in modulating HLA-DR surface expression of hMSC.

Overall, these results show that process transfer from ST bioreactor to PBS-3 Air and scale-up of hMSC expansion was successfully carried out. Regarding a new 3-dimensional manufacturing platform for cell therapy process development, PBS-3 Air bioreactors offer benefits over ST systems. The low shear stress mixing environment of Vertical-Wheel bioreactors address the key scalability limitation of existing platforms and thus they are positioned to become a potential boon for the needs of emerging cell therapy applications.

5. Author contribution & Acknowledgments

Marta M. Silva participated on the experimental setup, design and performed the experiments of hMSC cultures, analyzed the data and wrote the chapter. Key hydrodynamic parameters presented in this chapter were estimated by Marcos F. Sousa, António Roldão and Daniel Giroux.

6. References

Alves, P. M., Moreira, J. L., Rodrigues, J. M., Aunins, J. G., & Carrondo, M. J. (1996). Two-dimensional versus three-dimensional culture systems: Effects on growth and productivity of BHK cells. *Biotechnology and Bioengineering*, 52(3), 429–432.

Bocelli-Tyndall, C., Trella, E., Frachet, A., Zajac, P., Pfaff, D., Geurts, J., … Tyndall, A. (2015). FGF2 induces RANKL gene expression as well as IL1β regulated MHC class II in human bone marrow-derived mesenchymal progenitor stromal cells. *Annals of the Rheumatic Diseases*, 74(1), 260–266.

Caruso, S. R., Orellana, M. D., Mizukami, A., Fernandes, T. R., Fontes, A. M., Suazo, C. A. T., … Swiech, K. (2014). Growth and functional harvesting of human mesenchymal stromal cells cultured on a microcarrier-based system. *Biotechnology Progress*, 30(4), 889–895.

Chisti, Y. (1993). Animal cell culture in stirred bioreactors: Observations on scale-up. *Bioprocess Engineering*, 9(5), 191–196.

Croughan, M. S., Hamel, J. F., & Wang, D. I. (1987). Hydrodynamic effects on animal cells grown in microcarrier cultures. *Biotechnology and Bioengineering*, 29(1), 130–141.

Croughan, M. S., Hamel, J. F., & Wang, D. I. (1988). Effects of microcarrier concentration in animal cell culture. *Biotechnology and Bioengineering*, 32(8), 975–982.

Croughan, M. S., Sayre, E. S., & Wang, D. I. (1989). Viscous reduction of turbulent damage in animal cell culture. *Biotechnology and Bioengineering*, 33(7), 862–872.

Cruz, P. E., Cunha, A., Peixoto, C. C., Clemente, J., Moreira, J. L., & Carrondo, M. J. T. (1998). Optimization of the production of virus-like particles in insect cells. *Biotechnology and Bioengineering*, 60(4), 408–418.

Cunha, B., Aguiar, T., Silva, M. M., Silva, R. J. S., Sousa, M. F. Q., Pineda, E., … Alves, P. M. (2015). Exploring continuous and integrated strategies for the up- and downstream processing of human mesenchymal stem cells. *Journal of Biotechnology*, 213, 97-108.

Cunha, B., Peixoto, C., Silva, M., Carrondo, M., Serra, M., & Alves, P. M. (2015). Filtration methodologies for the clarification and concentration of human mesenchymal stem cells. *Journal of Membrane Science*, 478, 117–129.

Dominici, M., Le Blanc, K., Mueller, I., Slaper-Cortenbach, I., Marini, F., Krause, D., … Horwitz, E. (2006). Minimal criteria for defining multipotent mesenchymal stromal cells. The International Society for Cellular Therapy position statement. *Cytotherapy*, 8(4), 315–317.

Dos Santos, F., Campbell, A., Fernandes-Platzgummer, A., Andrade, P. Z., Gimble, J. M., Wen, Y., … Cabral, J. M. S. (2014). A xenogeneic-free bioreactor system for the clinical-scale expansion of human mesenchymal stem/stromal cells. *Biotechnology and Bioengineering*, 111(6), 1116–1127.

Fernandes, P., Peixoto, C., Santiago, V. M., Kremer, E. J., Coroadinha, A. S., & Alves, P. M. (2013). Bioprocess development for canine adenovirus type 2 vectors. *Gene Therapy*, 20(4), 353–360.

Godoy-Silva, R., Chalmers, J. J., Casnocha, S. A., Bass, L. A., & Ma, N. (2009). Physiological responses of CHO cells to repetitive hydrodynamic stress. *Biotechnology and Bioengineering*, 103(6), 1103–1117.

Godoy-Silva, R., Mollet, M., & Chalmers, J. J. (2009). Evaluation of the effect of chronic hydrodynamical stresses on cultures of suspensed CHO-6E6 cells. *Biotechnology and Bioengineering,* 102(4), 1119–1130.

Goh, T. K.-P., Zhang, Z.-Y., Chen, A. K.-L., Reuveny, S., Choolani, M., Chan, J. K. Y., & Oh, S. K.-W. (2013). Microcarrier culture for efficient expansion and osteogenic differentiation of human fetal mesenchymal stem cells. *BioResearch Open Access*, 2(2), 84–97.

Grenville K, Ruszkowski S, G. E. (1995). Blending of miscible liquids in the turbulent and transional regimes. In 15th NAMF Mixing Conference, Canada.

Hashimura Y, Giroux D, and L. B. (2012). Designing the Ideal Bioreactor with Single-Use Technology. BioProcess International, 10(5), 36–29.

Hervy, M., Weber, J. L., Pecheul, M., Dolley-Sonneville, P., Henry, D., Zhou, Y., & Melkoumian, Z. (2014). Long Term Expansion of Bone Marrow-Derived hMSCs on Novel Synthetic Microcarriers in Xeno-Free, Defined Conditions. *PLoS ONE*, 9(3), e92120.

Hupfeld, J., Gorr, I. H., Schwald, C., Beaucamp, N., Wiechmann, K., Kuentzer, K., … Wegmeyer, H. (2014). Modulation of mesenchymal stromal cell characteristics by microcarrier culture in bioreactors. *Biotechnology and Bioengineering*, 111(11), 2290–2302.

Kaiser, S., Löffelholz, C., Werner, S., & Eibl, D. (2011). CFD for Characterizing Standard and Single-use Stirred Cell Culture Bioreactors. In I. V. Minin & O. V. Minin (Eds.), Computational Fluid Dynamics Technologies and Applications (pp. 97–122). InTech.

Löffelholz C, Kaiser S., Werner S., E. D. (2010). Single-Use Technology in Biopharmaceutical Manufacture. (R. Eibl & D. Eibl, Eds.). Hoboken, NJ, USA: John Wiley & Sons, Inc.

Madrigal, M., Rao, K. S., & Riordan, N. H. (2014). A review of therapeutic effects of mesenchymal stem cell secretions and induction of secretory modification by different culture methods. *Journal of Translational Medicine*, 12(1), 260.

Mammoto, A., & Ingber, D. E. (2009). Cytoskeletal control of growth and cell fate switching. *Current Opinion in Cell Biology*, 21(6), 864–870.

Matasci, M., Hacker, D. L., Baldi, L., & Wurm, F. M. (2008). Recombinant therapeutic protein production in cultivated mammalian cells: current status and future prospects. Drug Discovery Today. *Technologies*, 5(2–3), e37-42.

Nienow, A. W. (1997). On impeller circulation and mixing effectiveness in the turbulent flow regime. *Chemical Engineering Science*, 52(15), 2557–2565.

Obom, K. M., Cummings, P. J., Ciafardoni, J. A., Hashimura, Y., & Giroux, D. (2014). Cultivation of mammalian cells using a single-use pneumatic bioreactor system. *Journal of Visualized Experiments: JoVE,* (92), e52008.

Odeleye, A., Lye, G. J., & Micheletti, M. (2013). Engineering characterisation of single-use bioreactor technology for mammalian cell culture applications. *BMC Proceedings*, 7(Suppl 6), P91.

Placek, J., & Tavlarides, L. L. (1985). Turbulent flow in stirred tanks. Part I: Turbulent flow in the turbine impeller region. *AIChE Journal*, 31(7), 1113–1120.

Rowley, J., Abraham, E., Campbell, A., Brandwein, H., & Oh, S. (2012). Meeting lot-size challenges of manufacturing adherent cells for therapy. *BioProcess Int*., 10, 16–22.

Ruszkowski, & S. (1994). Rational method for measuring blending performance and comparison of different impeller types. In In Proc. 8th Europ. Mixing Conf., I Chem E, Rugby, UK (pp. 283–291).

Sart, S., Errachid, A., Schneider, Y.-J., & Agathos, S. N. (2013). Modulation of mesenchymal stem cell actin organization on conventional microcarriers for proliferation and differentiation in stirred bioreactors. *Journal of Tissue Engineering and Regenerative Medicine*, 7(7), 537–551.

Schop, D., van Dijkhuizen-Radersma, R., Borgart, E., Janssen, F. W., Rozemuller, H., Prins, H.-J., & de Bruijn, J. D. (2010). Expansion of human mesenchymal stromal cells on microcarriers: growth and metabolism. *Journal of Tissue Engineering and Regenerative Medicine*, 4(2), 131–140.

Serra, M., Brito, C., Correia, C., & Alves, P. M. (2012). Process engineering of human pluripotent stem cells for clinical application. *Trends in Biotechnology*, 30(6), 350–359.

Serra, M., Brito, C., Costa, E. M., Sousa, M. F. Q., & Alves, P. M. (2009). Integrating human stem cell expansion and neuronal differentiation in bioreactors. *BMC Biotechnology*, 9, 82.

Serra, M., Brito, C., Sousa, M. F. Q., Jensen, J., Tostões, R., Clemente, J., … Alves, P. M. (2010). Improving expansion of pluripotent human embryonic stem cells in perfused bioreactors through oxygen control. *Journal of Biotechnology*, 148(4), 208–215.

Silva, A. C., Delgado, I., Sousa, M. F. Q., Carrondo, M. J. T., & Alves, P. M. (2008). Scalable culture systems using different cell lines for the production of Peste des Petits ruminants vaccine. *Vaccine,* 26(26), 3305–3311.

Simaria, A. S., Hassan, S., Varadaraju, H., Rowley, J., Warren, K., Vanek, P., & Farid, S. S. (2014). Allogeneic cell therapy bioprocess economics and optimization: single-use cell expansion technologies. *Biotechnology and Bioengineering*, 111(1), 69–83.

Sotiropoulou, P. A., Perez, S. A., Salagianni, M., Baxevanis, C. N., & Papamichail, M. (2006). Characterization of the optimal culture conditions for clinical scale production of human mesenchymal stem cells. *Stem Cells*, 24(2), 462–471.

Tissot, S., Reclari, M., Quinodoz, S., Dreyer, M., Monteil, D. T., Baldi, L., … Wurm, F. M. (2011). Hydrodynamic stress in orbitally shaken bioreactors. *BMC Proceedings*, 5 Suppl 8, P39.

Tramper JB, Williams J, Joustrad and D, V. J. (1986). Shear sensitivity of insect cells in suspension. EMT J, 8, 33–36.

van Eikenhorst, G., Thomassen, Y. E., van der Pol, L. A., & Bakker, W. A. M. (2014). Assessment of mass transfer and mixing in rigid lab-scale disposable bioreactors at low power input levels. *Biotechnology Progress*, 30(6), 1269–1276.

van Wezel, A. L. (1967). Growth of cell-strains and primary cells on micro-carriers in homogeneous culture. Nature, 216(5110), 64–65.

Vickroy, B., Lorenz, K., & Kelly, W. (2007). Modeling shear damage to suspended CHO cells during cross-flow filtration. *Biotechnology Progress*, 23(1), 194–199.

Wei, X., Yang, X., Han, Z., Qu, F., Shao, L., & Shi, Y. (2013). Mesenchymal stem cells: a new trend for cell therapy. *Acta Pharmacologica Sinica*, 34(6), 747–754.

Zhang, J., Nuebel, E., Daley, G. Q., Koehler, C. M., & Teitell, M. A. (2012). Metabolic regulation in pluripotent stem cells during reprogramming and self-renewal. *Cell Stem Cell*.

4

Unveiling CCBE1 role as a modulator of human pluripotent stem cells cardiomyocyte differentiation

This chapter was adapted from:

Silva MM, Vicente P, Terrasso AP, Inácio JM, Gomes-Alves P, Serra M, Belo JA, Alves PM (2018) Unveiling CCBE1 role as a modulator of human pluripotent stem cells cardiomyocyte differentiation. *submitted*

Abstract

Chronic heart failure represents a major cause of mortality worldwide and is still an unmet clinical need arising from the loss of viable and functional cardiac muscle. There is a need to identify key molecules and signaling pathways acting on the coronary vasculature system towards regenerative therapies. Human induced pluripotent stem cells (hiPSC) are an attractive cell source to understand the regulatory networks involved in cardiac commitment and cardiomyocyte (CM) differentiation. Particularly, CCBE1 (collagen and calcium-EGF biding domain 1) gene was identified in heart precursors of first and second heart field, and proepicardium in mouse embryos from day (E)7.0 to (E)9.5. Noteworthy, mutations in CCBE1 have been associated with Hennekam syndrome, characterized by abnormal lymphatic system and congenital heart defects. This strongly argues that CCBE1 may have a determinant role during heart morphogenesis/specification and could contribute to regenerate cardiac tissue upon heart injury. Within this context, our main aim was to examine the CCBE1 functional role in cardiac commitment and CM development by taking advantage of gene editing tools for loss-of-function studies.

A modified hiPSC line with CRISPR interference technology (CRISPRi), harboring a doxycycline-inducible deactivated Cas9, was used to selectively knockdown (KD) the CCBE1 expression. The CCBE1 KD led to a reduction on the expression of cardiac troponin marker *TNNT2* and on the ratios of *MYH7:MYH6* and *TNNI3:TNNI1*, and to an immature-related ultrastructure, suggesting that CCBE1 may modulate the CM phenotype. On the other hand, the EC differentiation was not impaired by CCBE1 KD. Therefore, CCBE1 might have a key role on CM maturation. This work would provide novel insights towards the development of CCBE1-mediated therapeutic strategies for cardiac regenerative medicine.

Table of Contents

1.Introduction

Chronic heart failure (CHF) arising from the loss of viable and functional cardiac muscle represents a major cause of mortality worldwide. Coronary artery (CA) anomalies are one of the major cause of myocardial infarction (MI). A variable incidence has been reported, ranging from 0.21 to 5.79% of the general population (Pérez-Pomares et al., 2016). Despite this prevalence and clinical relevance of CA anomalies, the cellular and molecular mechanisms beyond their impact on adult pathophysiology are still unknown. Hence, there is a need to identify the key molecules and signaling pathways acting on the coronary vasculature system development towards regenerative therapies.

Vascular Endothelial Growth Factor-C (VEGF-C) was firstly described as a master regulator of lymphangiogenesis (Joukov et al., 1997), but has also been indicated as a key molecule for the coronary vasculature development (Chen et al., 2014a; Chen et al., 2014b). The proliferation and migration of lymphatic endothelial cells (LEC) is driven by the activation of VEGF receptor 3 (VEGFR-3) through VEGF-C. Moreover, the correct processing of pro-VEGF-C into an active molecule relied on the formation of an extracellular activation complex, comprising the collagen and calcium binding EGF domains 1 (CCBE1) protein and the protease A disintegrin and metallopeptidase with thrombospondin type 1 motif 3 (ADAMTS3) (Bos et al., 2011; Bui et al., 2016; Jeltsch et al., 2014). CCBE1 protein is characterized by two EGF domains and two collagen repeats at N- and C-terminals, respectively. In humans, mutations in *CCBE1* gene were identified in patients with Hennekam syndrome, an autosomal recessive disorder, displaying diverse pathological features like lymphedema, lymphangiectasia and heart defects (Alders et al., 2009; 2012). Moreover, two different studies reported the expression of CCBE1 in heart precursors of first heart field and second heart field, and proepicardium in mouse embryos from day E7.0 to E9.5, as well as in the

bilateral cardiogenic mesoderm in chicken embryos (Facucho-Oliveira et al., 2011; Furtado et al., 2014). Recently, the regulation of VEGF-C signaling by CCBE1 was also demonstrated in mouse models, where coronary vascular defects were observed in *CCBE1* and *Vegfc* mutants (Sharma *et al.*, 2017, Bonet *et al.* 2018). These data suggest that CCBE1 may have a determinant role during heart morphogenesis/specification.

Human induced pluripotent stem cells (hiPSC) are an attractive cell source to investigate regulatory networks involved in cardiovascular development. Furthermore, by combining genome-engineering strategies and hiPSC technologies it is possible to generate human cellular disease models in a precise and controlled manner (Hendriks et al., 2016). CRISPR-Cas9 technology has emerging as versatile gene editing/regulation tool using a nuclease/nuclease-deficient Cas9, which retains the ability to target specific sequences and cleaving (Cas9) or not (dCas9) the DNA. Nowadays, this system has a tremendous impact in basic or clinical research settings (Adli, 2018).

The current study was designed to explore the hypothesis that CCBE1 is a modulator of hiPSC cardiac commitment by combining hiPSC cardiac differentiation and CRISPR interference genomic editing technology for temporal control of CCBE1 loss-of-function phenotype.

2. Material & Methods

2.1 Human iPSC lines

hiPSCs lines were used, a wild-type genetic background C (hereafter designated as WTC) and a modified and inducible CRISPRi Gen1C (hereafter referred to as CRISPRi) that express the deactivated Cas9 (dCas9) fused with the repressor KRAB domain from the inducible TetO promoter (TRE3G). mCherry reporter gene is under the control of the same inducible promoter (at

downstream of dCas9-KRAB, separated by p2A). These hiPSC were generated by Mandegar MA and colleagues (Mandegar et al., 2016) and provided by The J. David Gladstone Institutes.

2.2 Culture of hiPSC

2.2.1 hiPSC expansion

hiPSC lines were routinely propagated in static culture systems (6-well plates) coated with growth factor reduced Matrigel® (BD Biosciences) in mTeSR1™ media (STEMCELL Technologies), according to the protocol described by Mandegar MA et al. (Mandegar et al., 2016). Cells were maintained under humidified atmosphere with 5% CO_2 at 37°C.

2.2.2 hiPSC cardiomyocyte differentiation

hiPSC were differentiated into CM in monolayer culture systems, according to protocol recently published by our group (Correia et al., 2018). Briefly, hiPSC were harvested and dissociated as single cells using Accutase (STEMCELL Technologies) and seeded at a density of 7-9 × 10^4 cell/cm^2 in Matrigel-coated 6 well plate or µ-Slide 4 well formats. Two days after cell seeding, the differentiation was induced by replacing the mTeSR1™ (STEMCELL Technologies) by RPMI supplemented with 2% B27 minus insulin (Invitrogen), 12 µM CHIR99021 (Biogen Cientifica S.L), 80 ng/mL Activin A (PeproTech) and 50 µg/mL Ascorbic acid (Sigma-Aldrich) as shown in Figure 4.1A. At day 1 of differentiation, the media was replaced by RPMI supplemented with 2% B27 minus insulin, 5 µM IWR-1 (Sigma-Aldrich) and 50 µg/mL ascorbic acid. At day 3, cells were incubated with RPMI supplemented with 2% B27 minus insulin and 5 µM IWR-1. From day 6 until day 15, the medium was exchanged 3 times per week with the RPMI supplemented with 2% B27 minus insulin. Cells were maintained under humidified atmosphere with 5% CO_2 at 37°C.

2.2.3 hiPSC endothelial differentiation

hiPSC were differentiated into endothelial cells according to the protocol described elsewhere (Giacomelli et al., 2017) (Figure 4.5). Cells were seeded at 1.25×10^4 cell/cm^2 in Matrigel-coated 6 well plate format 24 hours before the differentiation process start. At day 0 of differentiation, the medium was replaced by APEL-Li (STEMCELL Technologies) supplemented with Activin A (20 ng/ mL), BMP4 (20 ng/mL) and CHIR99021 (1.5 µM). The medium was replaced every 3 days by APEL-Li supplemented with VEGF (50 ng/mL) until day 10 of differentiation. Cells were maintained under humidified atmosphere with 5% CO_2 at 37°C. All supplements were supplied by Peprotech.

2.3 CCBE1 knockdown: gRNA design, cell electroporation and selection

For CCBE1 knockdown, four gRNAs were designed to target near the transcription start site (TSS) of CCBE1 (150 bp upstream and downstream). All gRNAs were phosphorylated, annealed and cloned into the pgRNA-CKB was a gift from Bruce Conklin (Addgene plasmid # 73501) at BsmBI restriction site. All the cloning steps were performed as described elsewhere (Mandegar et al., 2016). gRNA oligo sequences are listed in Table 4.1.

The pgRNA-CKB expression vector, containing mKate2 as reporter gene and blasticidin as antibiotic selection marker (mKate2-T2A-Bsd), was transfected into CRISPRi cells using the NeoTransfection System (Thermo Fisher Scientific) according to manufacturer's instructions, using the following conditions: 1) 1400 V, 20 ms, 2 pulses; 2) 1100 V, 30ms, 1 pulse. CRISPRi cells (2×10^6 cells) were transfected with 5 µg of vector carrying a CCBE1-specific gRNA generating the CRISPRi-CCBE1 KD cell line or with empty pgRNA-CKB vector to generate the CRISPRi-Ctrl cell line (control condition).

Table 4.1. **List of gRNA oligo sequences**. Each gRNA indicates the binding relative to the transcription start site (TSS) of CCBE1 gene, and whether they target the template (T) and non-template (NT) strand. Forward and reverse primers for cloning into the pgRNACKB gRNA-expression vector are listed from 5' to 3'. Legend: KD – knockdown.

gRNA Name (Targeting Strand)	**Oligo Sequences** 5' – Forward Primer – 3' 5' – Reverse Primer – 3'
CCBE1 g-145 (NT)	TTGGAAGGGGGTACCTGCGGTGTC AAACGACACCGCAGGTACCCCCTT
CCBE1 g-82 (NT)	TTGGCAGGGGTCCGGAATATTATG AAACCATAATATTCCGGACCCCTG
CCBE1 g+22 (T)	TTGGAGCAGGACGCTTGGTCCGGA AAACTCCGGACCAAGCGTCCTGCT
CCBE1 g+37 (NT)	TTGGTCCCAGCGCCGAGCTCCGTC AAACGACGGAGCTCGGCGCTGGGA

Twenty-four hours post transfection, blasticidin selection (10 µg/mL) was applied in mTeSR1 supplemented with Y-27632 (10 µM). Stable colonies were pooled and passaged five times to enrich for cells with integration into sites of active transcription. The percentage of nucleofected cells was evaluated by mKate2 expression using the inverted fluorescence microscope (Leica Microsystems GmbH).

CRISPRi mediated gene knockdown studies (using CCBE1 g+37) were performed by supplementing the media with doxycycline (Dox; 2 µM). To allow the CCBE1 expression, cells were cultured in the absence of Dox. The gene knockdown efficiency was examined by RT-qPCR.

2.4 hiPSC Characterization

243.1 Cell proliferation

The percentage of proliferating cells was determined using Click-iT EdU Flow Cytometry Assay Kit according to the manufacturer's recommendation (Life Technologies). All samples were analyzed in a CyFlow® space instrument (Partec GmbH, Germany). At least 10,000 events were registered *per* sample.

2.3.2 Immunocytochemistry

The detection of cardiomyocyte marker cardiac troponin T (cTnT) in both iPSC cultures (CRISPRi-Ctrl and CRISPRi-CCBE1 KD) was performed as described elsewhere (Serra et al., 2011). Preparations were visualized in a point scan confocal microscope (SP5, Leica).

2.3.3 Flow Cytometry

Cells along expansion and differentiation were collected and dissociated as single cells using Accutase for undifferentiated cells and TrypLE™ Select (Gibco Life Technologies) for differentiated cells.

For membrane markers detection, cells were detached, washed with PBS containing 2% (v/v) FBS (washing buffer), and then incubated for 1 hour at 4°C with the primary/conjugated antibody. After two washing steps cells were incubated with the suitable secondary antibody for 30 min at 4°C. After this time, cells were washed twice in washing buffer.

For intracellular markers detection, the washing, fixation and antibody incubation steps were performed using Inside Stain Kit, according to the manufacturer's instructions and the protocol described elsewhere (Correia et al., 2018). Samples were analyzed in a CyFlow® space instrument (Partec GmbH, Germany). At least 10,000 events were registered per sample. Data was examined using FlowJo software. Primary and secondary antibodies used are listed in Table 4.2.

2.3.3 mRNA Extraction and RT-qPCR

Cell pellets were collected and washed with PBS, snap-freezed with liquid nitrogen and stored at -80°C until mRNA extraction.

mRNA was extracted using a High Pure RNA isolation Kit (Roche) according to manufacturer's instructions and quantified in the NanoDrop 2000c (Thermo Fisher).

Table 4.2. List of all antibodies and appropriate dilution used for immunocytochemistry and flow cytometry.

	Antibody	Origin	Supplier	Catalog No.	Dillution (Application)
Primary	Oct-3/4	Mouse	Santa Cruz	sc-5279	1:10 (FC)
	TRA-1-60	Mouse	Santa Cruz	sc-21705	1:10 (FC)
	TroponinT	Mouse	Thermo Scientific	MS-295-P1	1:200 (FC,IC)
Secondary	Alexa 488, anti-mouse IgG1	Goat	Life Technologies	A-21121	1:200 (FC, IC)
	Alexa 488, anti-mouse IgM	Goat	Life Technologies	A-21042	1:200 (FC, IC)
Conjugated	SSEA1-FITC	Mouse	BD Biosciences	560127	1:10 (FC)
	VCAM-1 (CD106) PE	Mouse	BD Biosciences	555647	1:5 (FC)
	SIRPα/β (CD172) PE	Mouse	BioLegend	323805/323806	1:5 (FC)
Isotype	FITC Mouse IgM		BD Biosciences	553474	1:400 (FC)
	Mouse IgG1		Santa Cruz	sc-2877	1:2.5 (FC)
	Mouse IgGk1-PE		Santa Cruz	sc-2878	1:5 (FC)

Note: FC, flow cytometry; IC, immunocytochemistry.

cDNA synthesis was carried out using the Transcriptor High Fidelity cDNA Synthesis Kit (Roche). RT-qPCR reactions were performed using the LightCycler 480 Instrument II 384-well block (Roche) and the program cycles as follow: pre-incubation for 10 minutes at 95°C; 45 cycles of amplification with denaturation at 95°C for 15 seconds, and annealing at 60°C for 1 minute; extension at 72°C for 5 minutes. The primers and probes used in this work are listed in Table 4.3. The Cycle threshold (Ct) was determined using LightCycler 480 Software version 1.5 (Roche). The results were analyzed as described elsewhere (Livak & Schmittgen 2001), using the $2^{-\Delta\Delta Ct}$ method for relative gene expression analysis. The gene expression data was normalized using two housekeeping genes, RPLP0 and GADPH, and represented relative to a control sample (set at 1).

Table 4.3. List of all Primers used in RT-qPCR (purchased from Life Technologies).

Gene	Reference	Gene	Reference
CCBE1	Hs99999905_m1	*MYL2*	Hs00166405_m1
Nanog	Hs02387400_g1	*MYL7*	Hs00221909_m1
POU5F1	Hs00999632_g1	*MYH6*	Hs01101425_m1
T	Hs00610080_m1	*MYH7*	Hs01110632_m1
KDR	Hs00911700_m1	*TNNI1*	Hs00913333_m1
MESP1	Hs00251489_m1	*TNNI3*	Hs00165957_m1
GATA4	Hs00171403_m1	*PECAM-1*	Hs01065279_m1
Nkx2.5	Hs00231763_m1	*CDH5 (VE-cadherin)*	Hs00901463_m1
VCAM-1	Hs01003372_m1	*RPLP0*	Hs99999902_m1
TNNT2	Hs00165960_m1	*GAPDH*	Hs99999905_m1

2.3.4 Transmission electron microscopy (TEM)

Monolayers of differentiated CRISPRi-Ctrl and CRISPRi-CCBE1 KD cultures (day 15 of differentiation) were fixed in 2% (v/v) paraformaldehyde and 2% (v/v) glutaraldehyde in 0.1 M phosphate buffer (pH 7.4) for 1 h and subsequently washed four times in 0.1 M phosphate buffer before fixation with osmium tetroxide (1% (v/v) in 0.1 M phosphate buffer) for 30 min on ice in the dark under agitation. After two washes with 0.1 M phosphate buffer and two washes with water, samples were incubated with tannic acid (1% (w/v) in water) for 20 min, on ice. After five washes with water, the samples were contrasted with aqueous uranyl acetate (0.5% (w/v), 1 h, on ice, in the dark), washed three times in distilled water and dehydrated in a graded series of ethanol (30%, 50%, 75%, 90%, 100% (v/v)). Finally, samples were embedded in epon resin. Ultrathin sections of cell monolayers were cut on a Leica UC6 ultramicrotome using a diamond knife. Sections were collected on formvar-coated slot grids, stained with lead citrate, and analyzed on a FEI Morgagni 268 at 80 kV. Images were taken with an Olympus MegaView III using the iTEM software.

2.4 Statistical Analysis

Statistical parameters including the exact value of n, precision measures (mean ± SEM) and statistical significance are reported in the Figures and the Figure Legends. Statistical analysis was performed by unpaired Multiple t tests using 0.5 % False Discovery Rate (FDR) approach to compare CRISPRi-CCBE1 KD with CRISPRi-Ctrl at different time points of differentiation. For all graphs, data are represented as mean ± SEM. Results with $p < 0.05$ were considered statistically significant. GraphPad PRISM software was used for graphing and statistical analyses (www.graphpad.com/scientific-software/prism/).

3. Results

3.1 CCBE1 expression is transiently upregulated at early stages of cardiac differentiation

To investigate the CCBE1 functional role in cardiovascular development, a modified and inducible hiPSC line, harboring the deactivated Cas9 (dCas9 fused with a repressor domain) under the control of an inducible promoter (TetO) recently developed by Mandegar and colleagues, was used (Mandegar et al., 2016). Firstly, a phenotypic comparison between this modified hiPSC line (CRISPRi) with the wild type hiPSC line (WTC), holding the same genetic background, was performed to their their pluripotent phenotype and ability to differentiate into cardiomyocytes (CM). The hiPSC pluripotency was assessed at gene and protein expression levels. High percentage of cells expressing stemness markers, such as TRA-1-60, TRA-1-81 and SSEA-4, and very low percentage of positive cells for SSEA-1 (early differentiation marker) were detected in both cell lines by flow cytometry (Figure 4.1B). Indeed, both cells expressed Oct-4 and Nanog pluripotency markers (Figure 4.1C). Nonetheless, the modified CRISPRi cell line expressed higher levels of Nanog compared with WTC line (Figure 4.1C). At the

different stages of CM differentiation, both cells were able to express stage-specific markers: *Brachyury (T)* at day 1, indicating the differentiation of mesendoderm cells; *MESP1* at day 2 and 3, representing the differentiation of cardiac mesoderm cells; *GATA4* from day 5 onwards, suggesting the cardiac progenitors specification; and *TNNT2* from day 6 onwards, indicating the CM differentiation (Figure 4.1D).

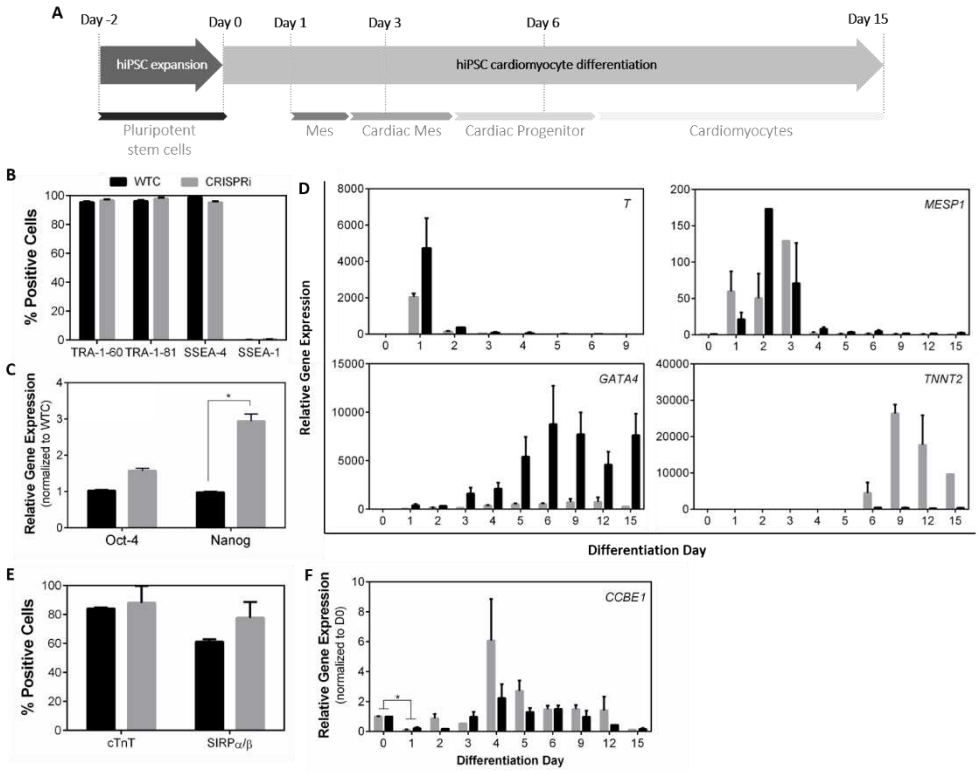

Figure 4.1. Pluripotency and cardiomyocyte differentiation of CRISPRi and WTC hiPSC lines – CCBE1 expression profile. A) Schematic representation of the differentiation protocol using growth factors and small molecules for Wnt signaling modulation as recently published (Correia et al., 2018). Legend: Mes - mesendoderm; Cardiac Mes - cardiac mesoderm. **B)** Flow cytometry analysis of stemness markers (TRA-1-60, TRA-1-80, SSEA-4) and SSEA-1 in both CRISPRi-hiPSC and WTC-hiPSC lines along the expansion process. **C)** Gene expression of stemness markers Oct-4 and Nanog relative to WTC line. Gene expression was quantified using the ΔΔCt method relatively to day 0 of differentiation of each cell line (housekeeping: RPLP0). **D)** Relative expression of *Brachyury (T)*, *MESP1*, *GATA4* and *TNNT2* genes in WTC and CRISPRi lines along the differentiation into cardiomyocytes. **E)** Flow cytometry analysis of cardiac markers, SIRPα/β and cardiac

troponin T (cTnT) in both CRISPRi-hiPSC and WTC-hiPSC lines at the last day of differentiation. **F)** CCBE1 gene expression along cardiomyocyte differentiation in both WTC and CRISPRi lines. Gene expression was quantified using the ΔΔCt method relatively to day 0 of differentiation of each cell line (housekeeping: RPLP0 and GAPDH). Data are presented as mean ± SEM of 3 independent experiments. * $p < 0.05$, Unpaired t-test with Welch's correction.

Lower expression of *GATA4* concomitantly with higher expression of *TNNT2* in CRISPRi line compared with WTC, was not translated into higher percentage of cardiac troponin T (cTnT)-positive cells at the end of the differentiation (Figure 4.1D-E). Comparable percentage of differentiated cells expressing cardiac markers was observed in WTC and CRISPRi cell lines: 84.2 ± 0.5% and 88.2 ± 6.8% for cTnT and 61.3 ± 1.1% and 77.8 ± 7.7% for SIRPα/β (Figure 4.1E). Finally, CCBE1 expression profile was also evaluated along this differentiation protocol in both cell lines: an initial downregulation from day 0 to day 2, followed by an increased expression from day 3 until day 9, and being downregulated at day 15 (Figure 4.1F). Then, this modified CRISPRi cell line was used to pursue the CCBE1 loss-of-function studies.

3.2 Efficient CCBE1 knockdown in hiPSC cell line

To determine the CCBE1 role in CM development, CCBE1 knockdown (KD) was performed in the modified CRISPRi cell line used in the previous section. For this, two cell lines were generated by nucleofection of CRISPRi cells: i) CRISPRi-CCBE1 KD, using pgRNA-CKB vector harboring the CCBE1-targeting gRNA (g+37), and ii) CRISPRi-Ctrl, using empty pgRNA-CKB vector, as a control culture (Figure 4.2A). Higher electroporation efficiencies (60 ± 4% using the pgRNA containing the gRNA4 and 52 ± 2% using the empty pgRNA) were attained using higher voltage (1400 V, Figure 4.2B). To select the electroporated cells, 15 days of blasticidin treatment was performed. At day 15, higher than 90 % of mKate2^{+} cells were observed for CRISPRi- Ctrl and CRISPRi-CCBE1 KD (Figure 4.2C). Subsequence

passages under blasticidin selection were performed to further increase the percentage of cells containing the pgRNA-CKB vector (data not shown).

The regulation the CCBE1 expression relied on the addition of doxycycline (Dox) to induce the expression of dCas9-KRAB that will bind to CCBE1-targeting gRNA (at 37 bp after the transcription start site of this gene) blocking CCBE1 expression (Figure 4.2A). The selected gRNA4 enabled CCBE1 expression interference, by knocking down CCBE1 expression in 80 % after 8 days of Dox addition (Figure 4.2D).

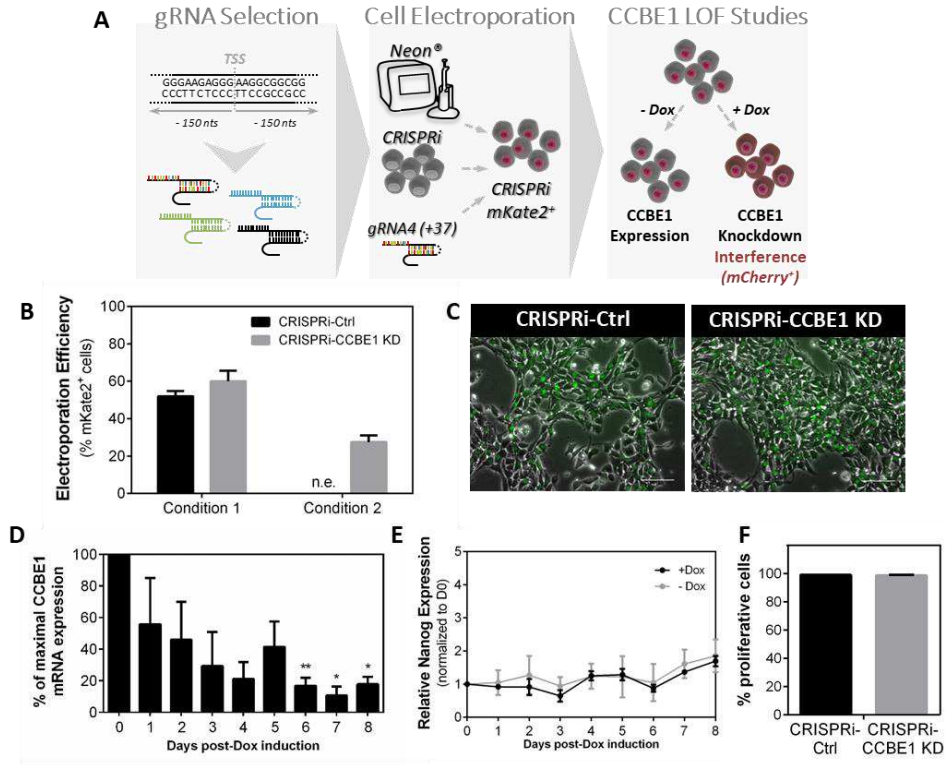

Figure 4.2. CRISPRi technology for CCBE1 knockdown. A) Schematic representation of guideRNAs design (+/-150 nts from the transcription start site (TSS)) and selection (higher score); CRISPRi hiPSC electroporation with the selected gRNA; and CCBE1 loss-of-function (LOF) studies by doxycycline (Dox) induction. **B)** Electroporation efficiency of CRISPRi hiPSC line with CCBE1-targeting gRNA (CRISPRi-CCBE1 KD) and empty pgRNA plasmid as control condition (CRISPRi-Ctrl) assessed by mKate2 expression. n.e., not evaluated. **C)** Detection of mKate2 reporter on cell nuclei of efficiently electroporated cells after 15 days post-

blasticidin selection. Scale bar, 100 µm. **D)** CCBE1 was knocked down by 80 % in polyclonal CRISPRi-CCBE1 KD after 8 days of doxycycline induction. **E)** Nanog expression in the presence or absence of doxycycline in CRISPRi-CCBE1 KD culture. **F)** Percentage of proliferative cells (EdU^+ cells) after 8 days under doxycycline induction in both cultures. Data are presented as mean ± SEM of three independent experiments. * $p< 0.05$, ** $p< 0.01$, Unpaired t-test with Welch's correction.

CCBE1 KD did not affected the expression of stemness markers, namely Nanog (Figure 4.2E) neither the hiPSC proliferative capacity, showing similar percentage of EdU-positive cells after 8 days of Dox induction in both cultures (Figure 4.2F).

3.3 CCBE1 knockdown impacts on cardiomyocyte differentiation

To study the impact of CCBE1 knockdown (KD) during CM differentiation, both generated CRISPRi-Ctrl and CRISPRi-CCBE1 KD cell lines were differentiated under Dox induction. These cells were previously expanded for 7 days with Dox to guarantee that CCBE1 was efficiently knocked down (at least 80 %) at the beginning of the differentiation (Figure 4.3A-B). Both cell lines were differentiated into CM under Dox induction until day 3 of differentiation to prevent the fluctuation on CCBE1 expression from day 1 to day 3 (Figure 4.3B). CCBE1 KD did not result in phenotypic differences compared with CRISPRi-Ctrl, namely at the expression level of early and progenitor stage-specific genes like *Brachyury (T)*, *MESP1*, *GATA4* and *Nkx2-5* (Figure 4.3B), and the proliferative capacity at day 6 of differentiation was maintained (Figure 4.3C). After CM differentiation (day 15), significant reduction on *TNNT2* expression was detected in CRISPRi-CCBE1 KD than in CRISPRi-Ctrl cultures (Figure 4.3B). Despite this observation at gene expression level, the percentage of cardiac troponin T-positive cells at the end of the differentiation (day 15) was not affected, resulting in a CM population with higher than 95 % $cTnT^+$ cells (Figure 4.3D) in both conditions with similar beating rates (Figure 4.3E) and number of CM (data not shown). Corroborating these data, very

low percentage of proliferative cells (EdU^+ cells) were also detected at day 15 in both cell lines (Figure 4.3C).

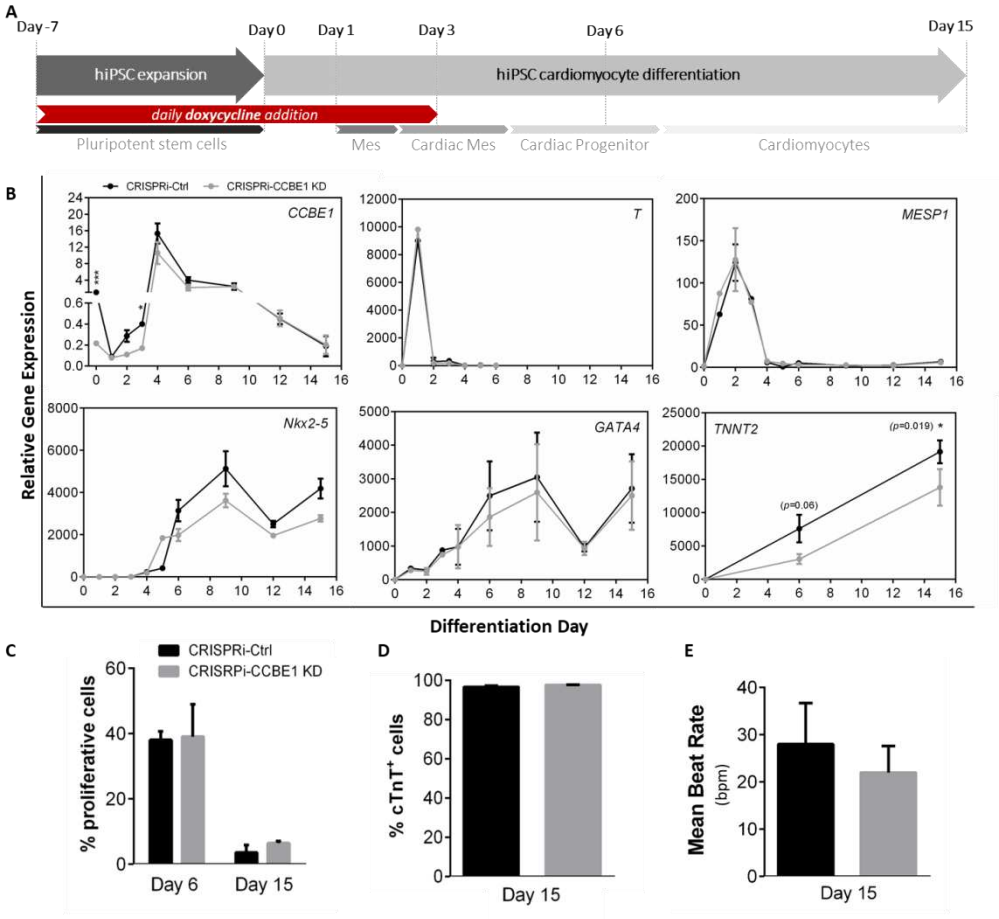

Figure 4.3. CCBE1 knockdown during cardiomyocyte differentiation. A) Schematic representation of doxycycline supplementation mode (2 µM from Day -7 until Day 3 of differentiation) along cardiomyocyte (CM) differentiation using both control (CRISPRi-Ctrl) and CRISPRi-CCBE1 KD lines. **B)** RT-PCR analyses of the following genes in control (CRISPRi-Ctrl) and CRISPRi-CCBE1 KD cultures along CM differentiation: *CCBE1*, *T*, *MESP1*, *Nkx2-5*, *GATA4 and TNNT2*. Gene expression was quantified using the ΔΔCt method relatively to CRISPRi-Ctrl culture at day 0 (housekeeping: RPLP0 and GAPDH). **C)** Percentage of proliferative cells (EdU^+ cells) in CRISPRi-Ctrl and CRISPRi-CCBE1 KD cultures at day 6 and 15. **D)** Percentages of cTnT-positive cells at day 15 of differentiated cultures. **E)** Mean Beat Rate (beats per minute) in both cultures at day 15. Data presented as mean ± SEM of three independent experiments. * $p< 0.05$, *** $p< 0.001$ Multiple t-test (FDR 0.05).

To further investigate the effect of CCBE1 KD on CM differentiation, the expression of other cardiac genes in both CRISPRi-CCBE1 KD and CRISPRi-Ctrl was evaluated at days 6 and 15. The expression ratios of cardiac troponin I isoforms *(TNNI1*:*TNNI3*) and α- and β-cardiac myosin heavy chain (*MYH7*:*MYH6*) were lower in CRISPRi-CCBE1 KD than in control condition at day 15 (Figure 4.4A). On the other hand, lower expression ratio of cardiac light chain genes (*MYL2:MYL7*) was detected in CCBE1 KD at day 6, though no impact of CCBE1 KD was observed at day 15 (Figure 4.4A). These data suggested a more immature cardiac phenotype in CRISPRi-CCBE1 KD cultures. Moreover, cardiac troponin T immunostaining suggested randomly aligned fibers in CM derived from CRISPRi-CCBE1 KD hiPSC when compared to control culture (Figure 4.4C). These evidences were corroborated by TEM analyses, where the CRISPRi-CCBE1 KD cultures displayed a poorly organized contractile machinery, characterized by low myofibril density and orientation, variable Z-disc alignment and few mitochondria close to the myofibrils (Figure 4.4D-E). Whereas control cultures presented high density of aligned myofibrils composed by sarcomeres with organized Z-disks, A- and I-bands, and mitochondria with prominent cristae close to the myofibrils (Figure 4.4D-E). Indeed, significant lower sarcomere length (1.58 ± 0.13 *versus* 1.72 ± 0.17) and alignment (higher standard deviation of the sarcomeres 'angle, 4.29 ± 3.49 *versus* 2.68 ± 2.40) was observed in CCBE1 KD cultures compared with CRISPRi-Ctrl (Figure 4.4F-G). Similar results were obtained by Dox induction throughout the differentiation process (daily Dox addition from day -7 to day 15) (data not shown).

3.4 CCBE1 knockdown has no impact on endothelial expression markers

CCBE1 implication on vascular development was also evaluated by differentiating CRISPRi-Ctrl and CRISPRi-CCBE1 KD cell lines into endothelial cells.

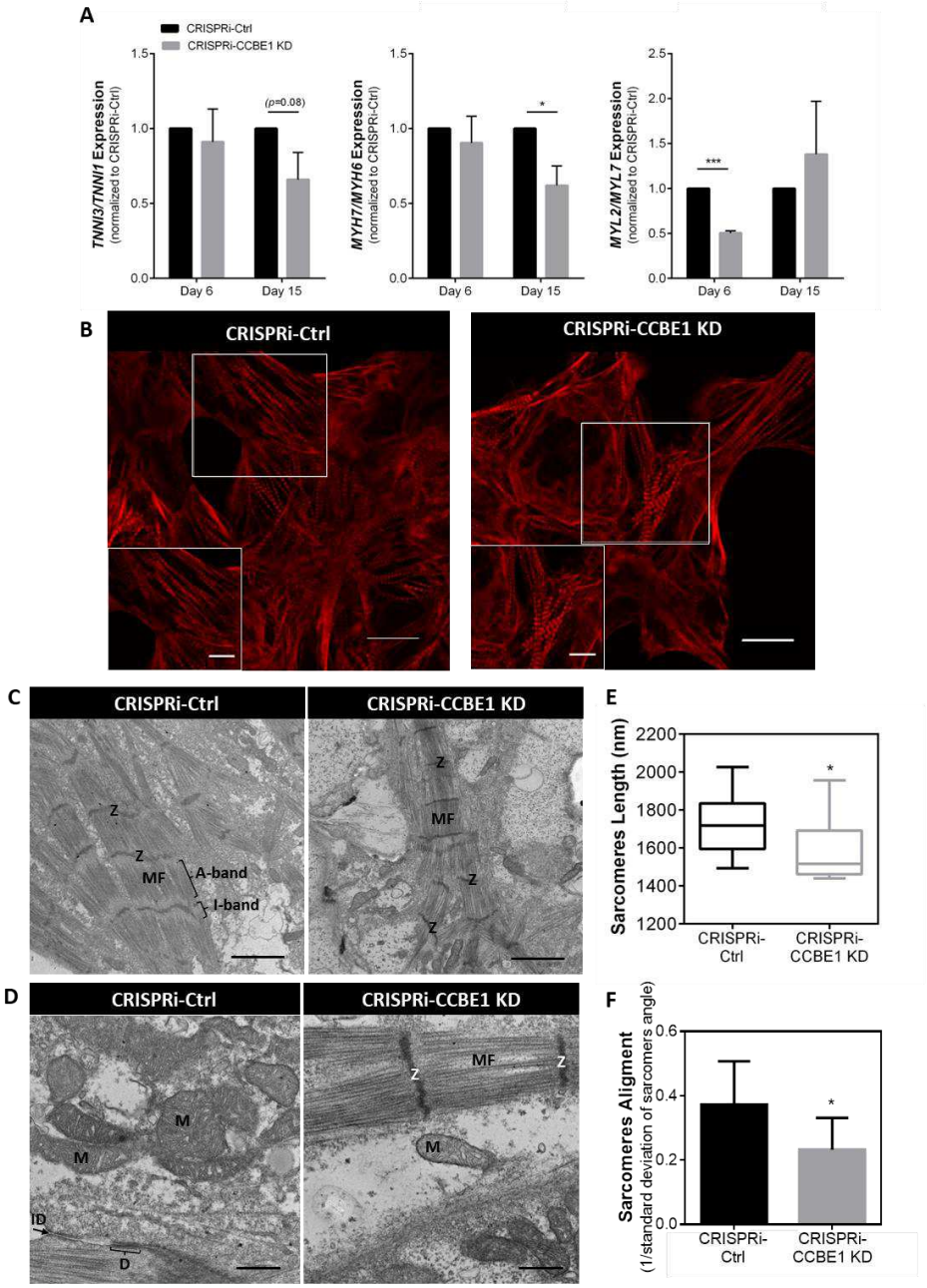

Figure 4.4. Impact of CCBE1 knockdown on cardiomyocyte differentiation/maturation. A) Ratios of relative expression of *TNNI3*:*TNNI1*, *MYH7*:*MYH6 and MYL2*:*MYL7* in both cultures at day 6 and 15. Gene expression was quantified using the ΔΔCt method relatively to CRISPRi-Ctrl culture at day 6 (housekeeping: *RPLP0* and *GAPDH*). Data are presented as

mean ± SEM of three independent experiments. * $p< 0.05$, *** $p< 0.001$, Multiple t-test (FDR 0.05). **B)** Representative images of cTnT staining at day 15 in both cultures. Scale bar, 50 µm and 10 µm in insight. **C-D)** Representative TEM images of CM from both cultures at day 15. Myofbrils (MF), Z-disks (Z), sarcomeric bands: A- and I-bands in panel **D**, intercalated disks (ID) and desmosomes (arrows) connecting adjacent CMs, and Mitochondria (M) in panel **E** are highlighted. Scale bars= 2µm (**C**), 500nm (**D**). **E-F)** Sarcomeres length (nm) and sarcomeres alignment (determined by the standard deviation of the sarcomere angle in each taken image) in both conditions was assessed from TEM images using Fiji Image J software. * $p< 0.05$, *** $p< 0.001$, Unpaired t test with Welch's correction.

As mentioned in previous section, both cells were expanded for 7 days under Dox induction before endothelial differentiation for CCBE1 KD (Figure 4.5A). CRISPRi-CCBE1 KD and CRISPRi-Ctrl cultures were differentiated in the presence of Dox throughout the differentiation protocol, showing a monolayer of cells with endothelial-like cell morphology at the end of differentiation (day 10 in Figure 4.5B). The normal CCBE1 expression profile along endothelial specification (Figure 4.5C) is completely different in comparison to CM differentiation (Figure 4.1F), where an upregulation of CCBE1 expression was observed at day 4, achieving even higher expression until the last day of differentiation (day 10) (Figure 4.5C). Despite the effective CCBE1 KD throughout the endothelial differentiation process, no significant changes on endothelial-related genes expression, such as *KDR*, *PCAM1*, *CDH5 (VE-cadherin)* and *VCAM-1*, were detected in CRISPRi-CCBE1 KD (Figure 4.5C). Indeed, no differences were observed on the percentage of VE-cadherin-positive cells at the last day of differentiation in CRISPRi-CCBE1 KD compared with CRISPRi-Ctrl (23.5 ± 0.3% and 29.2 ± 2.8%) assessed by flow cytometry, and these values are comparable with the ones reported in the literature (Giacomelli et al. 2017).

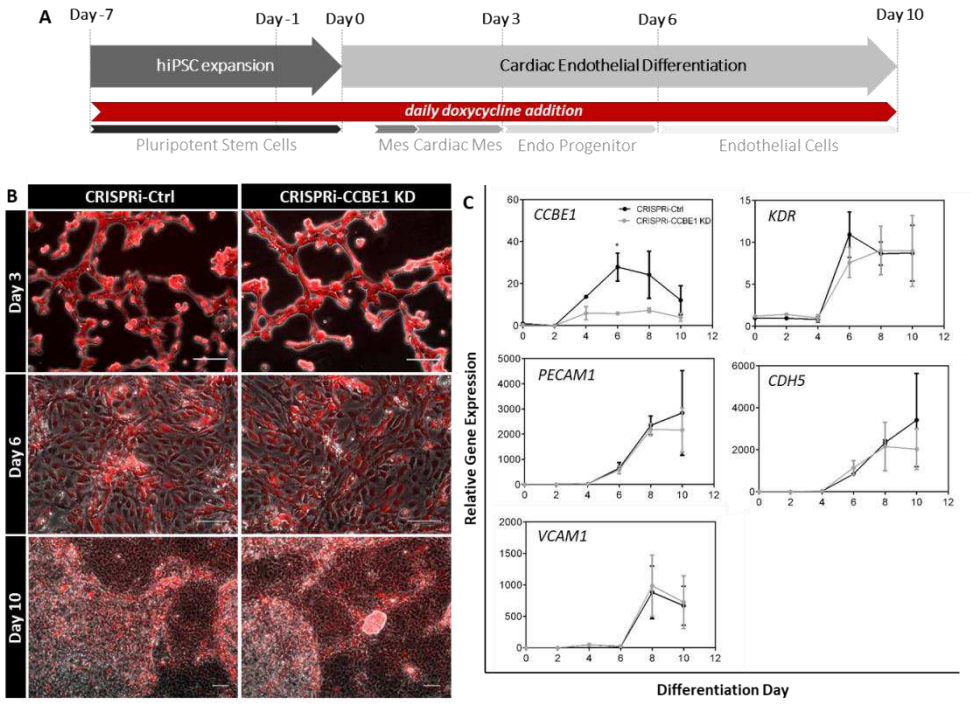

Figure 4.5. Effect of CCBE1 knockdown on cardiac endothelial differentiation. A) Schematic representation of cardiac endothelial differentiation with doxycycline induction (from day -7 until day 10). **B)** Detection of mCherry^{+} cells (cytoplasmic staining) and mKate2^{+} cells (nuclear staining) in both CRISPRi cells at day 3, 6 and 10. Scale bar, 100 µm. **C)** RT-PCR analyses of *CCBE1*, *KDR*, *PECAM1, CDH5 (VE-cadherin)* and *VCAM1,* genes in CRISPRi-Ctrl and CRISPRi-CCBE1 KD cultures along cardiac endothelial differentiation. Gene expression was quantified using the ΔΔCt method relatively to CRISPRi-Ctrl culture at day 0 (housekeeping: RPLP0 and GAPDH). Data are presented as mean ± SEM of two independent experiments. * $p< 0.05$, Multiple t-test (FDR 0.05).

4. Discussion

The implementation of protocols to obtain individual cell types of the heart has been hampered by the limited knowledge on regulatory mechanisms, signaling pathways or key molecules involved on cardiac specification. CCBE1 has been suggested as a therapeutic molecule on lymphatic and vascular development. Its expression was detected on specific cardiac embryonic tissues

using mouse and chicken models, indicating that CCBE1 may play a role during cardiac development (Facucho-Oliveira et al., 2011; Furtado et al., 2014).

In this work, we performed for the first time the regulation of CCBE1 expression on a human induced pluripotent stem cell (hiPSC) line, using CRISPR interference gene editing technology, to unveil the role of CCEBE1 along cardiac commitment.

The combination of hiPSC culture and CRISPR-Ca9 technology has been widely employed on biomedical research (Hendriks et al., 2016; Hockemeyer & Jaenisch, 2016). CRISPR-Cas9 technology has also been explored for gene expression control, using a deactivated Cas9 fused with a repressor (KRAB) or activator (VP64) to inactivate or activate the target gene expression in a precise and efficient manner (Dominguez et al., 2016; Qi et al., 2013). Two different studies were conducted in human pluripotent stem cells providing gene editing platforms to control gene expression (Kearns et al., 2014; Mandegar et al., 2016). In particular, Mandegar and colleagues reported an inducible and versatile tool to repress the expression of cardiac genes at cardiac progenitors and CM stages (Mandegar et al., 2016), which was employed herein for CCBE1 knockdown (KD) along CM and endothelial cells differentiation.

The transfection efficient of guideRNAs into hiPSC for gene repression in the CRISPR system is absolutely critical. Here, high electroporation efficiencies (up to 60 %) were attained using an electroporator at high voltage (1400 V), comparing with reported literature. These efficiencies are hiPSC line- and electroporation condition (voltage and pulse number)-dependent, ranging from 17 % to 64 % (Li et al., 2016).

CCBE1 knockdown (KD) was successfully achieved in hiPSC (CRISPRi cell line) by 80 %. Similar percentages of KD were reported for other cardiac-related disease-causing genes, such as *MYBPC3* and *HERG* (90 % and 60 %, respectively), using the same gene editing tool (Mandegar et al., 2016). We showed that CCBE1

KD had no impact on hiPSC stemness, neither on cardiac progenitor specification or endothelial cell differentiation. Noteworthy, CCBE1 KD had implications on CM differentiation at transcriptional level, with a downregulation of *TNNT2* and lower ratios on cardiac troponin I genes (*TNNI3:TNNI1*) and cardiac myosin heavy chain genes (*MYH7:MYH6*). In humans, *TNNT2* mutations have been associated with cardiomyopathies, where the sarcomeres are severely affected (Luedde et al., 2010). These changes at structural level, namely on the sarcomeres length and alignment, were also observed in the CM derived from CRISPRi-CCBE1 KD cell line, indicating a more immature state of CM. The assessment of electrophysiological characteristics, such as action potential and calcium signaling, in differentiated cultured would also be valuable readouts to further delineate the impact of CCBE1 on CM functional maturation. Nonetheless, these evidences suggest a potential role of CCBE1 on CM maturation, acting as a modulator of CM phenotype through the regulation of other cardiac genes. Until now, there are thirteen putative CCBE1-interacting partners identified based on reported literature, five of them are cardiac-related transcription factors, namely MEF2C, GATA4, TBX5, HAND2 and MYOCD (Ingenuity Pathway Analysis) (Nam et al., 2013). The validation of such interactions along CM differentiation in CRISPRi-CCBE1 KD cells by combining the gene editing tools employed herein and proteomic-based approaches, would provide novel hints on CCBE1 modulatory signaling pathways in cardiac setting.

Lower percentages of Dox-responsive cells along differentiation processes might affect the feasibility of this system, namely in CM differentiation only 50-80 % of CM are responsive to Dox induction. Nonetheless, these observations were not detected on CM differentiation, since no CCBE1 expression is observed on CM. Though, in endothelial differentiation no clear differences on gene KD were observed throughout the culture, which was maintained at low levels (65±10 % of CCBE1 KD).

Together, our data suggest a putative role of CCBE1 as a modulator of CM differentiation. This work opens new avenues for the identification of CCBE1-modulated proteins/pathways in cardiac commitment, which may contribute for novel and more efficacious cardiac regenerative therapies.

5. Author contribution & Acknowledgments

Marta M. Silva participated on the experimental setup and design, performed the majority of the experiments, analyzed the data and wrote the chapter. The author acknowledges A.L Sousa and E.M. Tranfield from the Electron Microscopy Facility at the Instituto Gulbenkian de Ciência for the technical support in TEM.

6. References

Adli, M. (2018). The CRISPR tool kit for genome editing and beyond. *Nature Communications.*

Alders, M., Hogan, B. M., Gjini, E., Salehi, F., Al-Gazali, L., Hennekam, E. A., … Hennekam, R. C. (2009). Mutations in CCBE1 cause generalized lymph vessel dysplasia in humans. *Nature Genetics,* 41(12), 1272–1274.

Alders, M., Mendola, A., Adès, L., Al Gazali, L., Bellini, C., Dallapiccola, B., … Hennekam, R. C. (2013). Evaluation of Clinical Manifestations in Patients with Severe Lymphedema with and without CCBE1 Mutations. *Molecular Syndromology,* 4(3):107-13.

Bos, F. L., Caunt, M., Peterson-Maduro, J., Planas-Paz, L., Kowalski, J., Karpanen, T., … Schulte-Merker, S. (2011). CCBE1 is essential for mammalian lymphatic vascular development and enhances the lymphangiogenic effect of vascular endothelial growth factor-C in vivo. *Circulation Research*, 109(5), 486–491.

Bonet, F. *et al.* (2018). CCBE1 is Required for Proper Coronary Vessels Development and Coronary Artery Stems Formation in Mice. *Under Revisions.*

Bui, H. M., Enis, D., Robciuc, M. R., Nurmi, H. J., Cohen, J., Chen, M., … Kahn, M. L. (2016). Proteolytic activation defines distinct lymphangiogenic mechanisms for VEGFC and VEGFD. *Journal of Clinical Investigation*, 126(6), 2167–2180.

Chen, H. I., Poduri, A., Numi, H., Kivela, R., Saharinen, P., McKay, A. S., … Red-Horse, K. (2014a). VEGF-C and aortic cardiomyocytes guide coronary artery stem development. *Journal of Clinical Investigation*, 124(11), 4899–4914.

Chen, H. I., Sharma, B., Akerberg, B. N., Numi, H. J., Kivela, R., Saharinen, P., … Red-Horse, K. (2014b). The sinus venosus contributes to coronary vasculature through VEGFC-stimulated angiogenesis. *Development*, 141(23), 4500–4512.

Correia, C., Koshkin, A., Duarte, P., Hu, D., Carido, M., Sebastião, M. J., … Serra, M. (2018). 3D aggregate culture improves metabolic maturation of human pluripotent stem cell derived cardiomyocytes. *Biotechnology and Bioengineering*, 115(3), 630–644.

Dominguez, A. A., Lim, W. A., & Qi, L. S. (2016). Beyond editing: Repurposing CRISPR-Cas9 for precision genome regulation and interrogation. *Nature Reviews Molecular Cell Biology*, 17(1), 5–15.

Facucho-Oliveira, J., Bento, M., & Belo, J.-A. (2011). Ccbe1 expression marks the cardiac and lymphatic progenitor lineages during early stages of mouse development. *The International Journal of Developmental Biology*, 55(10–12), 1007–1014.

Furtado, J., Bento, M., Correia, E., Inácio, J. M., & Belo, J. A. (2014). Expression and Function of Ccbe1 in the Chick Early Cardiogenic Regions Are Required for Correct Heart Development. *PLoS ONE*, 9(12), e115481.

Giacomelli, E., Bellin, M., Orlova, V. V., & Mummery, C. L. (2017). Co-Differentiation of Human Pluripotent Stem Cells-Derived Cardiomyocytes and Endothelial Cells from Cardiac Mesoderm Provides a Three-Dimensional Model of Cardiac Microtissue. *In Current Protocols in Human Genetics* (p. 21.9.1-21.9.22). Hoboken, NJ, USA: John Wiley & Sons, Inc.

Hendriks, W. T., Warren, C. R., & Cowan, C. A. (2016). Genome Editing in Human Pluripotent Stem Cells: Approaches, Pitfalls, and Solutions. *Cell Stem Cell*, 18(1), 53–65.

Hockemeyer, D., & Jaenisch, R. (2016). Induced pluripotent stem cells meet genome editing. *Cell Stem Cell*, 18(5), 573–586.

Jeltsch, M., Jha, S. K., Tvorogov, D., Anisimov, A., Leppänen, V.-M., Holopainen, T., … Alitalo, K. (2014). CCBE1 enhances lymphangiogenesis via A disintegrin and metalloprotease with thrombospondin motifs-3-mediated vascular endothelial growth factor-C activation. *Circulation*, 129(19), 1962–1971.

Joukov, V., Sorsa, T., Kumar, V., Jeltsch, M., Claesson-Welsh, L., Cao, Y., … Alitalo, K. (1997). Proteolytic processing regulates receptor specificity and activity of VEGF-C. *The EMBO Journal,* 16(13), 3898–3911.

Kearns, N. A., Genga, R. M. J., Enuameh, M. S., Garber, M., Wolfe, S. A., & Maehr, R. (2014). Cas9 effector-mediated regulation of transcription and differentiation in human pluripotent stem cells. *Development,* 141(1), 219–223.

Li, H. L., Gee, P., Ishida, K., & Hotta, A. (2016). Efficient genomic correction methods in human iPS cells using CRISPR-Cas9 system. *Methods*, 101, 27–35.

Luedde, M., Ehlermann, P., Weichenhan, D., Will, R., Zeller, R., Rupp, S., … Frey, N. (2010). Severe familial left ventricular non-compaction cardiomyopathy due to a novel troponin T (TNNT2) mutation. *Cardiovascular Research*, 86(3), 452–460.

Mandegar, M. A., Huebsch, N., Frolov, E. B., Shin, E., Truong, A., Olvera, M. P., … Conklin, B. R. (2016). CRISPR Interference Efficiently Induces Specific and Reversible Gene Silencing in Human iPSCs. *Cell Stem Cell,* 18(4), 541–553.

Pérez-Pomares, J. M., de la Pompa, J. L., Franco, D., Henderson, D., Ho, S. Y., Houyel, L., … Basso, C. (2016). Congenital coronary artery anomalies: a bridge from embryology to anatomy and pathophysiology—a position statement of the development, anatomy, and pathology ESC Working Group. *Cardiovascular Research*, 109(2), 204–216.

Qi, L. S., Larson, M. H., Gilbert, L. A., Doudna, J. A., Weissman, J. S., Arkin, A. P., & Lim, W. A. (2013). Repurposing CRISPR as an RNA-Guided Platform for Sequence-Specific Control of Gene Expression. *Cell*, 152(5), 1173–1183.

Serra, M., Correia, C., Malpique, R., Brito, C., Jensen, J., Bjorquist, P., … Alves, P. M. (2011). Microencapsulation technology: a powerful tool for integrating expansion and cryopreservation of human embryonic stem cells. *PloS One*, 6, e23212.

Sharma, B., Ho, L., Ford, G. H., Chen, H. I., Goldstone, A. B., Woo, Y. J., … Red-Horse, K. (2017). Alternative Progenitor Cells Compensate to Rebuild the Coronary Vasculature in Elabela - and Apj - Deficient Hearts. *Developmental Cell*, 42(6), 655–666.e3.

Takeuchi, J. K., Lou, X., Alexander, J. M., Sugizaki, H., Delgado-Olguín, P., Holloway, A. K., … Bruneau, B. G. (2011). Chromatin remodelling complex dosage modulates transcription factor function in heart development. *Nature Communications*, 2, 187.

5

Full-length human CCBE1 production and purification: leveraging bioprocess development for high quality glycosylation attributes and functionality

This chapter was adapted from:

Silva MM, Gomes-Alves P, Rosa S, Simão D, Inácio JM, Peixoto, C, Serra M, Belo JA, Alves PM (2018) Full-length human CCBE1 production and purification: leveraging bioprocess development for high quality glycosylation attributes and functionality. *J Biotechnol.* 10;285:6-14.

Abstract

Collagen and calcium-binding EGF domain-1 (CCBE1) is a secreted protein critical for lymphatic/cardiac vascular development and regeneration. However, the low efficient production of the recombinant full-length CCBE1 (rCCBE1) has been a setback for functional studies and therapeutic applications using this protein.

The main goal of this work was to implement a robust bioprocess for efficient production of glycosylated rCCBE1. Different bioprocess strategies were combined with proteomic tools for process/product characterization, evaluating the impact of process parameters on cell performance, rCCBE1 production and quality.

We have shown that rCCBE1 volumetric yield was positively correlated with higher cell density at transfection (HDT), and under these conditions the secreted protein presented a mature glycosylated profile (complex N-glycans). Mild hypothermia was also applied to HDT condition that resulted in enhanced cell viability; however an enrichment of immature rCCBE1 variants was detected. Mass spectrometry-based tools allowed the identification of rCCBE1 peptides confirming protein identity in the affinity chromatography purified product. rCCBE1 biological activity was validated by *in vitro* angiogenesis assay, where enhanced vessel formation was observed.

Herein, we report a step forward in the production and characterization of human glycosylated rCCBE1, amenable for *in vitro* and *in vivo* studies to explore its regenerative therapeutic potential.

Table of Contents

1.Introduction

Collagen and calcium-binding EGF domain-1 (CCBE1) protein is involved in the formation of lymphatic vessels and venous sprouting (Hogan et al., 2009). CCBE1 gene encodes a 44 kDa extracellular matrix (ECM) protein, containing a calcium-binding epidermal growth factor (EGF)-like and a EGF domains at N-terminal and at C-terminal two collagen-like repeats (Jeltsch et al., 2014). CCBE1 protein also presents post-translational modifications: two glycosylated sites and chondroitin sulfate in the C-terminal domain (Bui et al., 2016). Mutations in CCBE1 gene have been associated with Hennekam syndrome, characterized by an abnormal lymphatic system and congenital heart defects (Alders et al., 2009). Besides its role in lymphatic vessels formation (Jeltsch et al., 2014; Roukens et al., 2015), CCBE1 has also been reported as an important protein in heart development (precursor cells' migration and proliferation)(Furtado et al. 2014; Facucho-Oliveira et al. 2011), as a tumor suppressor gene in ovarian cells (Barton et al., 2010) and as a new predictor of poor prognosis in post-operative gastrointestinal stromal tumor patients (Tian et al., 2016).

Most of the recently published work on VEGF-C activation regulated by CCBE1 reports low efficiency in the expression of the full-length recombinant CCBE1 in mammalian cell lines, namely HEK-293T (Bui et al., 2016; Jeltsch et al., 2014) or HEK-293E6 (Roukens et al., 2015). Still, high productivities were obtained for the truncated protein CCBE1ΔCol (containing only the N-terminal domain)(Bui et al., 2016), but both domains are important for *in vitro* and *in vivo* VEGF-C processing (Jha et al., 2017).

Mammalian cells are often preferred over prokaryotic systems for recombinant protein (rProtein) production, as they can introduce proper protein folding, post-translational modifications (e.g. glycosylation) and product assembly, which are essential for the synthesis of biologically active therapeutic proteins.

Additionally, faster approaches to produce rProteins are sometimes preferred to the stable transfection strategies, achieving high protein quantity in shorter periods (Baldi et al., 2007). However, the reported CCBE1 production yields were similar using transient or stable expression systems (Bui et al., 2016; Jeltsch et al., 2014; Roukens et al., 2015). On the other hand, the CCBE1 purification has also been a critical issue. Most of the downstream strategies for protein purification applied to "easy-to-express" proteins has shown high efficacy, but further optimizations are needed for the purification of "difficult-to-express" proteins (Hussain et al., 2017).

In the present study, we demonstrate the importance of a controlled bioprocess (upstream and downstream) to achieve higher rCCBE1 yield, recovery and quality. The impact of bioprocess parameters on CCBE1 quality, namely the glycosylation profile, was also evaluated through advanced high sensitivity mass spectrometry (MS)-based tools.

2. Material & Methods

2.1 Cell culture

HEK293-EBNA1-6E cell line (National Research Council, Biotechnological Research Institute, Montreal, Canada) was routinely passaged twice a week (0.3×10^6 cell/mL at inoculum) and maintained in F17 medium, supplemented with 4 mM L-GlutaMAX^{TM}, 0.1% (v/v) pluronic F68 and 25 mg/L G418 (all from Thermo Fisher Scientific). Cells were cultivated in 125 mL to 2 L shake flasks (Corning Inc) under orbital shaking (stirring rate: 120 rpm) at 37°C in a humidified atmosphere of 5% CO_2 in the air. Cell concentration and viability were determined with a Fuchs-Rosenthal counting chamber (Marienfeld) using the Trypan Blue (Thermo Fisher Scientific) exclusion method.

2.2 Expression vector

Human CCBE1 cDNA (gene ID 147372) synthetically synthesized with a C-terminal 6xHis tag was amplified and cloned into pTT5 vector (Zhang et al., 2009) using In-Fusion PCR cloning (Takara) at *HindIII* restriction site. The expression plasmid was purified using Genopure Plasmid Maxi Kit (Roche Applied Science) according to the manufacturer's protocol.

2.3 Recombinant CCBE1 protein production

2.3.1 Standard Transfection protocol (STD)

Cells were transfected at 1.5×10^6 cell/mL with pTT5-hCCBE1 plasmid using polyethyleneimine (PEI, Polysciences) cationic polymer at a ratio of 1:2 prepared in 10% (v/v) of the total volume. Briefly, the PEI was slowly added in a dropwise manner to the DNA plasmid-medium mix, incubated 8 min at room temperature (RT) and the mix was added to the culture. Lipofectamine 2000 (Thermo Fisher Scientific) was also selected as an alternative transfection reagent and used according to the manufacturer's protocol. Seven hours post-transfection, all transfected cultures were supplemented with 1% (v/v) of Ultra Low IgG Fetal Bovine Serum (Thermo Fisher Scientific). Shake flasks or stirred-tank bioreactors (STB) were used. In both systems, cells were inoculated at 1 × 106 cell/mL 24 hours prior to transfection. In STB, cells were inoculated on Biostat Qplus bioreactor system equipped with six-blade Rushton impeller (Sartorius Stedim Biotech) under defined culture conditions. Partial pressure of oxygen (pO_2) was set to 40% air saturation and controlled by sequentially varying the stirring rate (90-280 rpm) and oxygen percentage in gas inlet; pH was set to 7.4 and controlled by CO_2 and base addition ($NaHCO_3$); and temperature at 37°C. Data acquisition and process control were performed using MFCS/Win (Sartorius Stedim Biotech). Samples were collected daily for analysis as described in the protein

characterization sections. Cells and supernatant were harvested, centrifuged at 300 x g and stored at - 80°C until further analysis.

2.3.2 High-Cell Density Transfection protocol (HDT)

Cells were inoculated in shake flasks at 1 × 10^6 cell/mL 24 hours prior to transfection. Cells were concentrated by centrifugation to 20 × 10^6 cell/mL and transfected with pTT5-hCCBE1 plasmid using PEI as described elsewhere without the addition of valproic acid 3 h after transfection (Backliwal et al., 2008). Samples were collected and stored as described above. Glucose supplementation (24 mM) was performed at 2 dpt (days post transfection) (hereafter referred to as 37°C|GLC).

2.3.3 Mild Hypothermia condition

Culture condition was based on a biphasic temperature culture protocol as described elsewhere (Lin et al., 2015). Briefly, cells were transfected accordingly to both transfection protocols described above and maintained at 37°C. Twenty-four hours after transfection, cells were transferred to a different incubator with lower temperature (33°C) until the last day of culture. Samples were collected and stored as described above. Glucose supplementation (24 mM) was performed at 2 dpt (hereafter referred to as 33°C|GLC).

2.3.4 Metabolic Profiling

In all conditions, the cell metabolic profile was evaluated daily. Glucose and lactate concentrations were measured using the YSI 7100 MBS system (YSI Life Sciences).

2.4 Recombinant CCBE1 protein purification

Purification of secreted rCCBE1 was carried out on ÄKTA explorer 100 system (GE Healthcare) using two different chromatography strategies: affinity and anion exchange. Cell supernatant was harvested at 3 dpt, clarified by centrifugation at

2.000 × g for 10 min at room temperature (RT) and filtered through 0.22 µm membrane filters (polyethersulfone) before further purification.

In chromatographic approach I (AEX+IMAC), anion exchange column (Resource Q, GE Healthcare) followed by HisTrap Fast Flow column were used for rCCBE1 purification from STD 37°C condition at 5 dpt. The Resource Q was equilibrated with 20 mM sodium phosphate buffer, pH 7.4, containing 50 mM NaCl, and eluted using 20 column volumes (120 mL) in a linear gradient with 20 mM sodium phosphate buffer, 1 M NaCl, pH 7.4. The protein sample was 3x diluted, 7x concentrated and 8x diafiltrated using Pellicon cassette 50 cm^2 10 kDa (Merck Millipore) into the phosphate buffer. The concentrated sample was further purified using HisTrap column as previous described.

In chromatographic approach II (IMAC), the secreted rCCBE1 from HDT 37°C condition at 3 dpt was purified using HisTrap Fast Flow column (GE Healthcare). The sample was loaded onto the pre-equilibrated HisTrap column with phosphate buffer (20 mM sodium phosphate buffer, 20 mM imidazole pH 7.4), and then washed using the same buffer. The elution was performed using 3-step elution method with 100, 300 and 500 mM of imidazole.

Final purified sample was 6x diluted, 7x concentrated and 8x diafiltrated with the storage buffer (25 mMTris/0.15 M NaCl/2 mM $CaCl_2$, pH 7.4), using the previous cassette device. Glycerol (10% (v/v)) was added to the final sample, aliquoted and stored at -80°C. Purified protein samples were characterized by SDS-PAGE, Western blot and nanoLC-mass spectrometry.

2.5 Recombinant CCBE1 protein characterization

2.5.1 Immunocytochemistry

The intracellular detection of rCCBE1 in HEK-293E6 was performed at different time points of the culture (1, 3 and 5 dpt). One million of cells were harvested and inoculated in a poly-D-lysine-coated coverslip (P1524; Sigma-

Aldrich). Twenty four hours after seeding, cells were fixed in 4 % (w/v) paraformaldehyde in DPBS for 10 min, and then the blocking and permeabilization was performed for 30 min in 0.2% (v/v) fish skin gelatin (Sigma-Aldrich) and 0.1% (w/v) TX-100 (Sigma-Aldrich) in DPBS. After the incubation with primary antibody at RT for 2 hours and three washing steps with PBS, cells were incubated with secondary antibodies at RT for 1 hour in the dark and finally cell nuclei were counterstained with 4,6-diamidino-2-phenylindole (DAPI, Thermo Fisher Scientific).

Primary antibodies used were: anti-CCBE1 (ab101967; Abcam), anti-CANX (SICGEN; AB0037-200) and anti-GM-130 (610822; BD Transduction Laboratories™). Secondary antibodies used were: donkey anti-goat IgG-AlexaFluor647, goat anti-mouse IgG-AlexaFluor488 and goat anti-rabbit IgG-AlexaFluor549 (all from Thermo Fisher Scientific). Samples were visualized using point scan confocal (SP5, Leica) microscopy and processed using FIJI software (Schindelin et al., 2012).

2.5.2 SDS-PAGE & Western Blot

For cellular protein extraction, 1-2 million of cells were lysed in 0.2 mL lysis buffer containing 50 mM Tris, 5 mM EDTA, 150 mM NaCl, 1% (w/v) Triton X-100 and protease inhibitor cocktail (Roche Applied Science). The obtained extracts were clarified by centrifugation at 15.000 x g for 15 min at 4°C. Total protein concentration was determined using BCA Protein Assay Kit (Pierce), according to the manufacturer's instructions. Proteins from cell extracts and precipitated supernatants (200 µL precipitated in 80% (v/v) of ethanol) were resolved on a 1 mm NuPAGE® Novex BisTris gel (Invitrogen) under reducing conditions and transferred with iBlot system (Invitrogen), according to the manufacturer's instructions. Membranes were blocked by incubation for 1 hour with blocking solution (0.1% (v/v) Tween 20 and 5% (w/v) dry milk in PBS), and incubated

overnight with primary antibody at 4°C (1:1000 of rabbit anti-CCBE1 (Abcam; ab101967), 1:2000 of mouse anti-polyHistidine (Sigma-Aldrich; H1029) or 1:1000 of mouse anti-alfa tubulin (clone DM1A, Sigma-Aldrich)). After the washing steps with 0.1% (v/v) Tween 20 in PBS, membranes were incubated with secondary antibody at RT for 2 hours according to the manufacturer´s instructions (anti-rabbit HRP or anti-mouse HRP, Ge Healthcare Europe GmbH). Chemiluminescence detection was performed with ECL reagent (GE Healthcare). rCCBE1 protein concentration was determined by densitometry analysis of the Western blot for CCBE1 antibody using FIJI software (Schindelin et al., 2012).

2.5.3 Glycosylation pattern

Two hundred µL of culture supernatant of each condition was collected and clarified by centrifugation (1.000 x g for 8 min) to be further digested with peptide-N-glycosidase F (PNGase F) and Endoglycosidase H (Endo H). For PNGase F and Endo H digestion, samples were precipitated overnight at -20°C in 80% (v/v) Ethanol. The deglycosylation with PNGase F (Glyko® N-glycanase, Prozyme) was performed according to the manufacturer's instructions. In Endo H digestion, precipitated proteins were solubilized in denaturation buffer (0.5% SDS and 1% β-mercaptoethanol) for 10 min at 100°C. After the samples cooling, 2.5 mU Endo H and the corresponding buffers were added. Incubations were performed in 50 µl reaction mixtures, at 37°C, for 18 hours and the reactions were stopped by precipitation with 80% ethanol at -20°C. Proteins were separated by SDS-PAGE and analyzed by Western blot with the anti-CCBE1 antibody, as described above.

2.5.4 LC-MS/MS and Functional annotation

Cell extracts: cultures of HDT 37°C (3 dpt) and STD 37°C (5 dpt) were collected for cellular protein extraction as described in SDS-PAGE & Western Blot section**.** Two µg of each sample were used for information-dependent acquisition (IDA) analysis by NanoLC-MS using TripleTOF 6600 (ABSciex, Framingham, MA,

USA). External calibration was performed using beta-galactosidase digest (ABSciex). The 40 most intense precursor ions from the MS spectra were selected for MS/MS analysis. Data were acquired with the Analyst software TF 1.7 (ABSciex). The raw MS and MS/MS data were analyzed using Protein Pilot Software v. 5.0 (ABSciex) for protein identification. The search was performed against the protein sequences provided by the sponsor and against Swissprot protein Homo sapiens database. Protein identification was considered with an unused score greater than 1.3 (95% confidence). Analysis of the proteome list of each sample was performed using Venny 2.1 (http://bioinfogp.cnb.csic.es/tools/venny/). The identification of significantly enriched gene ontology biological processes (GO-BP) on each analyzed sample was performed using DAVID Bioinformatics Resource 6.8 (Huang, Sherman, & Lempicki, 2008), considering a *p*-value < 0.05 as statistically significant. Qualitative proteomic analysis was performed in two technical replicates.

Purified sample: 2 µg of purified sample (using Chromatography A described before) from HDT method was analyzed as described above for cell extracts. Qualitative proteomic analysis was performed in two technical replicates.

2.5.5 *In vitro* angiogenesis tube formation assay

Human Umbilical Vein Endothelial Cells (HUVECs) were seeded onto Matrigel-coated 96 well plates at 55000 cell/cm^2. Cells were incubated with different culture media: EBM-2 (positive control), rCCBE1 storage buffer (negative control) and 20 µg/mL of purified rCCBE1 (HDT 37°C 3 dpt, approach II of DSP). Tube formation after incubating for 4h, 9h and 21h was monitored and the analysis was performed using Angiogenesis Analyzer FIJI Plugin.

3. Results

3.1 Upstream bioprocess strategies for rCCBE1 expression

3.1.1 The effect of DNA concentration and transfection reagent on rCCBE1 production

The full-length human recombinant CCBE1 protein (rCCBE1) was expressed using two different transfection reagents (lipofectamine and PEI) in combination with different DNA concentrations aiming at increasing protein production (Figure 5.1). Higher cell growth and viability were observed at low DNA concentration (1 µg/mL) combined with both transfection reagents (Figure 5.1A-B). Secreted rCCBE1 was not detected along the culture when using 5 µg DNA/mL combined with lipofectamine, which might be due to low cell concentration at low viability (data not shown). Comparable rCCBE1 secretion profiles were observed at 1 µg DNA/mL using both transfection reagents, with the highest amount being detected at 5 dpt (Figure 5.1C). One µg DNA/mL and PEI were used for all the following experiments of rCCBE1 production (hereafter referred to as STD protocol). This selection was based on its impact on cell viability and transfection reagent cost effectiveness (PEI *vs* lipo) when transferring to large-scale bioprocesses.

From the results obtained in the western blot regarding the intracellular/secreted amounts of rCCBE1, some retention was observed during the first days of culture (1-3 dpt). As it is known, polypeptide processing and secretion might be a limiting cellular bottleneck to produce “difficult-to-express” protein (Le Fourn et al., 2014). Hence, we investigated rCCBE1 localization by looking into the endoplasmic reticulum (ER) and Golgi secretory pathways. Our data confirmed that rCCBE1 was retained at the ER level, as evidenced by co-

localization of CCBE1 and ER marker CANX1, but not with the GM-130 Golgi marker (Figure 5.1D).

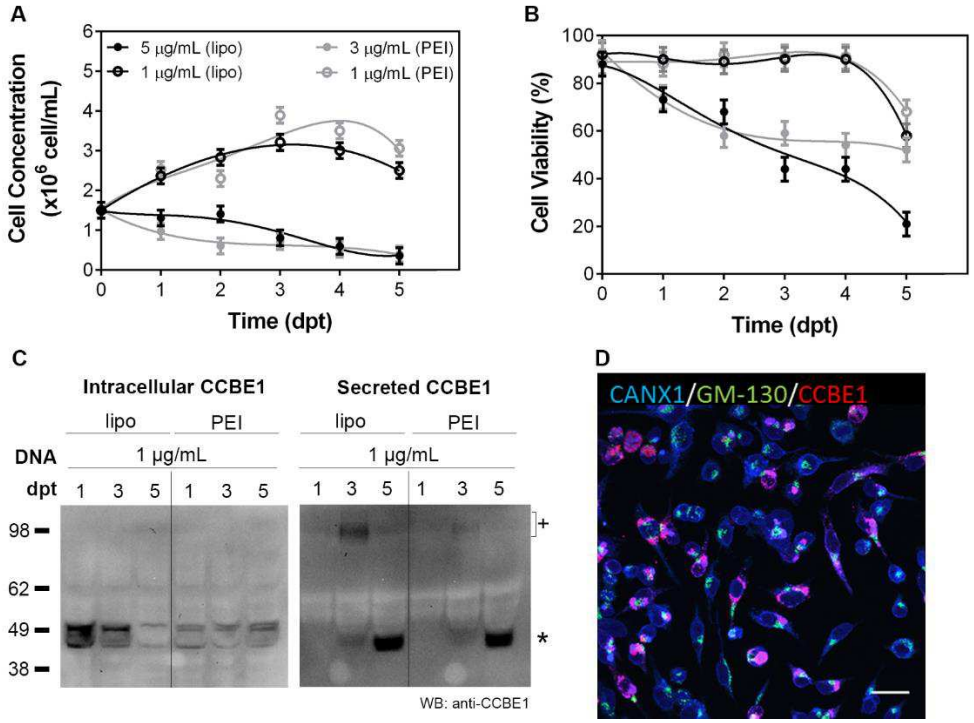

Figure 5.1. The effect of DNA concentration and transfection reagent type on rCCBE1 production. Cell growth **(A)** and viability **(B)** profiles for HEK-293E6 transfected with 1, 3 and 5 µg DNA/mL in stirred cultures using lipofectamine (Lipo) or PEI. Data represent mean ± standard error of 3 independent experiments. *Curves fit with third order polynomial (cubic).* **C)** Detection of intracellular and secreted CCBE1 along culture time in all conditions. Asterisk (*) denotes the 49 kDa CCBE1 and plus sign (+) denotes the higher MW (70-100 kDa) CCBE1. **D)** Confocal immunofluorescence image of CANX1, GM-130 and recombinant CCBE1 of HEK-293E6 transfected with 1 DNA/mL at 1 dpt. Scale bar: 25 µm

3.1.2 High-cell density transfection and mild hypothermia impact on rCCBE1 production and secretion

Aiming to improve rCCBE1 production and secretion, two different bioprocess strategies were further exploited: high-cell density transfection (HDT; 20 × 10^6 cell/mL) and mild hypothermia (33°C). The impact of such process

parameters (cell concentration and temperature) on rCCBE1 production and quality as well as on the proteome of producing cells was evaluated (Figure 5.2). Higher cell concentrations were obtained in HDT condition when compared to STD, while similar cell viability profiles were observed in both conditions until 3 dpt (Figure 5.2A-B). Higher production yields of secreted rCCBE1, considering both 70-100 kDa and 49 kDa forms, were detected in HDT condition at 37°C than in STD condition at the same temperature (14±5.6-fold improvement in volumetric yields compared to STD condition) (Figure 5.2C). The temperature shift to 33°C maintained higher cell viability but has no impact on rCCBE1 yield when compared to 37°C in both STD and HDT conditions (Figure 5.2A-C). These results showed that HDT protocol at 37°C allowed an improved rCCBE1 production and secretion compared with other tested conditions.

In this condition, a significant enrichment of biological processes (GO-BP) related with cellular metabolism, cell cycle/DNA metabolism and RNA processing/gene expression was observed when compared to STD at 37°C by proteomic analysis (Figure 5.2D). Proteins involved in 2-oxoglutarate and isocitrate metabolic processes were identified in both conditions but a higher number of proteins (with statistical significance) related with these GO-terms were observed in HDT condition. Also, proteins related to fatty acid beta-oxidation using acyl-CoA dehydrogenase were only identified in HDT condition (Cellular Metabolism plot in Figure 5.2D). Higher number of nucleotide metabolic/biosynthesis processes-related GO-BP terms were also significantly enriched in HDT condition (e.g. purine nucleotide metabolic process and nucleoside triphosphate biosynthesis process) (Cellular Metabolism plot in Figure 5.2D). The observed enrichment of GO-BP terms related to DNA repair and recombination as well as in mRNA polyadenylation and regulation of translation in such condition (Cell Cycle and RNA Metabolism/Gene Expression plots in Figure 5.2D), which might be related to the higher cell proliferation observed. A detailed

comparative analysis of the proteomic data regarding the protein folding and transport GO-BP terms in both conditions was also carried out.

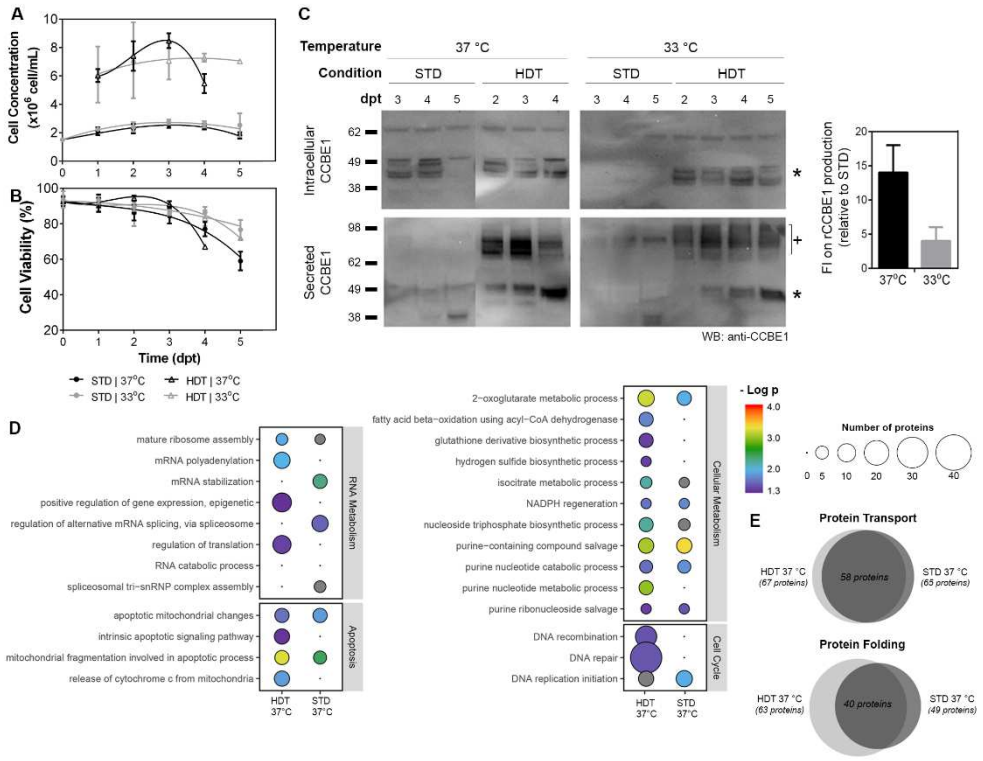

Figure 5.2. The impact of high-cell density transfection and mild hypothermia on rCCBE1 production and whole cell proteome. Cell growth **(A)** and viability **(B)** of HEK-293E6 in all conditions. Data represent mean ± standard error of 3 independent experiments. *Curves fit with third order polynomial (cubic).* **C)** Detection of intracellular and secreted rCCBE1 along culture time. Asterisk (*) denotes the 49 kDa CCBE1 and plus sign (+) denotes the higher MW (70-100 kDa) CCBE1. Fold improvement (FI) on rCCBE1 production in HDT conditions at 3 dpt relative to STD at each temperature. **D)** Gene ontology (GO) enrichment analysis for cell extracts from HDT 37°C, STD 37°C and STD 33°C cultures. Differentially enriched GO biological process (GO-BP) terms are presented. Logarithmized *p*-values and protein counts are graphically represented by colors and spheres, respectively. Non-significant GO-BP terms are represented as gray colored spheres. Detailed composition and statistical parameters of these GO terms are reported in Supplementary Table S5.1, S5.2, S5.3 **E)** The coverage and overlap of protein folding and transport-related proteins in all samples are represented in the Venn diagrams. Legend: HDT 37°C - transfected cells at high-cell density cultured at 37°C (3 dpt); STD 37°C - transfected cells at 1.5×10^6 cell/mL cultured at 37°C (5 dpt).

Heat shock protein family members acting as chaperones (e.g. Hsp40 member B1) were identified at 37°C in both STD and HDT (Figure 5.2E and Supplementary Table S5.1). High number of proteins related to protein transport was identified in HDT (63 proteins), 23 proteins were exclusively present in this condition (Figure 5.2E and Supplementary Table S5.2).

3.1.3 Impact of feeding strategy on rCCBE1 production

Cells transfected in HDT condition at 37°C rapidly consumed the glucose present in culture media (depletion in 2-3 dpt) with lactate accumulation (supplementary Figure S5.1A-B). Therefore, a feeding strategy was implemented by adding a pulse of glucose (24 mM Glc) at 2 dpt (Figure S5.1B). This supplementation resulted in improved cell viability and rCCBE1 volumetric yield (secreted rCCBE1), which increased 4-fold at 37°C after 7 dpt (Figure 5.3B-C). In mild-hypothermic conditions, the effect of glucose supplementation was also evaluated, where a 3-fold increase was observed in secreted rCCBE1 yield, but with no effect on cell viability (Figure 5.3B-C).

Besides the increased rCCBE1 yield in supplemented cultures at 7 dpt, a negative impact on glycosylation profile of the secreted protein was observed. In batch HDT culture at 37°C at 3 dpt, the secreted rCCBE1 was only digested by peptide-N-glycosidase F (PNGase F), indicating the presence of N-linked complex glycans (Figure 5.3D). However, at 4 dpt, this protein was also digested by Endoglycosidase H (Endo H), suggesting the secretion of both mature and immature glycosylated rCCBE1. Nonetheless, this effect was also observed for supplemented conditions at both temperatures. Interestingly, complex glycosylation profile of secreted rCCBE1 was mainly observed in cultures with high cell viabilities (> 90 %, at 3 dpt), whereas time points with lower cell viability presented high-mannose glycoprotein enrichment (4 dpt onwards). As described before, the higher molecular weight form of secreted rCCBE1 (70-100 kDa)

resulted from a post-translational modification (chondroitin sulfate proteoglycan, data not shown). Here, in supplemented conditions the inverse correlation between the amounts of each CCBE1 form during time might be related to the chondroitin sulfated rCCBE1 stability in culture (Figure 5.3E). Despite the similar volumetric yield at 7dpt in different temperature cultures, a higher specific yield of rCCBE1 of both forms of rCCBE1 was observed for HDT 37°C (Figure 3F).

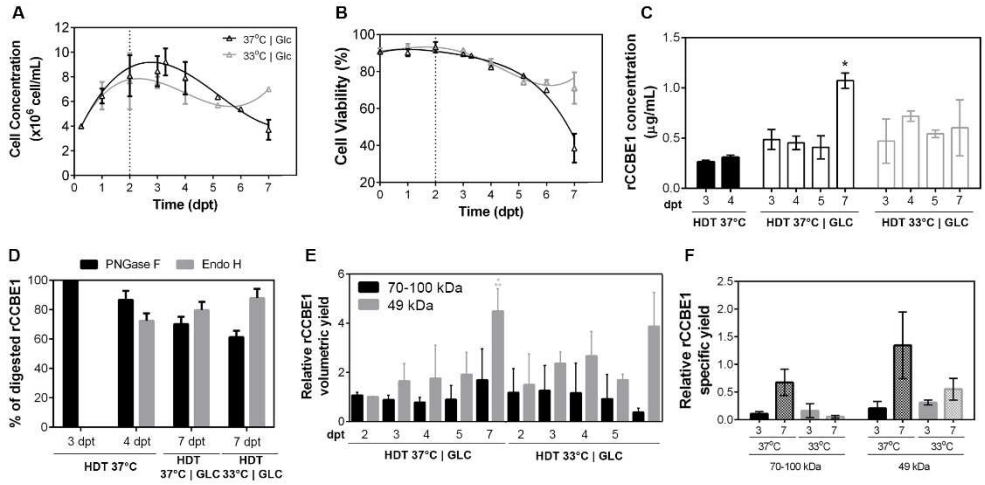

Figure 5.3. Feeding strategy effect on rCCBE1 production and quality. Cell growth **(A)** and viability **(B)** profiles along culture of HDT at both temperatures with glucose supplementation. Dashed line represents Glc supplementation time. Data represent mean ± standard error of 3 independent experiments. *Curves fit with third order polynomial (cubic).* **C)** Secreted rCCBE1 concentration in supplemented and non-supplemented conditions along culture. Western blot for CCBE1 antibody analysis by densitometry using FIJI software. Absolute quantification was determined through an inactive commercially available purified recombinant CCBE1. Error bars denote mean ± standard error of at least 2 independent experiments. * $p < 0.05$ when compared to HDT 37°C at 3 dpt using *t-test* analysis. **D)** The percentage of digested rCCBE1 (secreted) with PNGase F or Endo H in supplemented and non-supplemented conditions at both temperatures. **E)** Relative rCCBE1 volumetric yield along time (normalized to 2 dpt 37°C) at both temperatures after glucose supplementation. Black bars represent the 70-100 kDa detected CCBE1 and gray bars represent the 49 kDa detected CCBE1. Western blot for CCBE1 was analyzed by densitometry using the ImageJ software. Error bars denote mean ± standard error of 3 independent experiments. Two-way ANOVA analysis of 49 kDa CCBE1 form, ** $p < 0.01$ when compared to 2 dpt 37°C and + $p < 0.05$ when compared to 3 and 4 dpt 37°C. **F)** Relative rCCBE1 specific yield at 3 and 7 dpt (values presented in panel E) were normalized

to the number of cells at the indicated dpt) at both temperatures after glucose supplementation. Legend: 37°C and 37°C|Glc - non-supplemented culture at 37°C and glucose supplemented culture at 37°C, respectively; 33°C and 33°C|Glc - non-supplemented culture at 33°C and glucose supplemented culture at 33°C, respectively.

3.2 Downstream process (DSP) strategies for rCCBE1 purification

Two chromatographic approaches were evaluated to optimize rCCBE1 purification (Figure 5.4A) using the secreted rCCBE1 produced from both STD and HDT conditions. The purification of rCCBE1 from STD condition (5 dpt) was performed using two chromatographic columns; an anion exchanger (AEX) column was firstly exploited to eliminate most of the impurities, followed by a diafiltration step and HisTrap column (IMAC) (approach I in Figure 5.4A). Low percentage of contaminants were detected in the elution fractions at 100 mM and 300 mM imidazole concentrations; however, both forms of secreted rCCBE1 (70-100 kDa and the 49 kDa) were eluted at 100 mM and 300 mM imidazole steps (STD in Figure 5.4B-C). Only 40 % of rCCBE1 (both forms) was recovered after IMAC (considering the 300 mM imidazole fractions), which can be associated with the lower ratio of rCCBE1 and contaminants in the bulk, decreasing its affinity to the column. This was overcome with the enhanced upstream strategies showing higher rCCBE1 production yield, where a single column (approach II) was needed to purify this protein with higher recovery yields (>95% of full-length rCCBE1) (Figure 5.4C). Still, only 50% of the 70-100 kDa rCCBE1 form was recovered at 300 mM imidazole, being also eluted in the flow-through, washing and in 100 mM imidazole fraction (HDT in Figure 5.4C).

3.3 Characterization of rCCBE1 protein

Characterization of the purified rCCBE1 (using the DSP approach II) through MS-based tools was performed. CCBE1 protein was identified in the final purified product after trypsin or trypsin and PNGase F digestion, but higher sequence

coverage was attained with double digestion, an evidence of rCCBE1 glycosylation (29.1 % versus 26.9 %).

A

Chromatography Approach	Transfection Protocol	DSP Volume (mL)	DSP Temp (°C)	DSP 1x PI addition	DSP rCCBE1 detection[3]
I (AEX+IMAC)	STD	200[1] - 500[2]	4 - 8	yes	yes
II (IMAC)	HDT	150[1]		no	

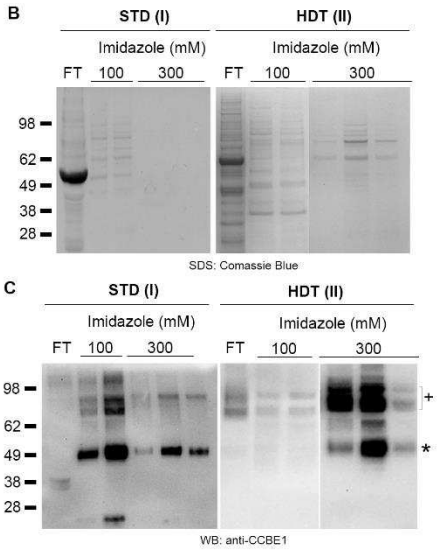

Figure 5.4. DSP strategies to purify rCCBE1. A) The chromatographic approaches (I and II) explored to purify the secreted rCCBE1 protein using clarified supernatant from STD or HDT protocols cultured at 37°C. Flow-through (FT) and eluted fractions (with 100 and 300 mM of imidazole) from IMAC using STD supernatant post-AEX chromatography (approach I) and HDT supernatant (approach II) were analyzed by **B)** SDS-PAGE under reducing conditions and comassie staining, and **C)** Western blot using anti-CCBE1 antibody. Asterisk (*) denotes the 49 kDa CCBE1 and plus sign (+) denotes the higher MW (70-100 kDa) CCBE1. Legend: IMAC - Immobilized Metal Ion Affinity Chromatography; AEX - Anion Exchange Chromatography; PI – protease inhibitors; [1] Culture in shake flasks; [2] Culture in stirred-tank bioreactors; [3] rCCBE1 detection by western blot after all purification steps.

Also, several host-cell proteins were identified as impurities of the final product (515 proteins identified), in agreement with SDS-PAGE profile detected (300 mM imidazole fractions HDT panel in Figure 5.4B). The extracted ion chromatograms (XIC) of LC-MS/MS data were plotted using the list of identified CCBE1 peptides (Figure 5.5A). Some represented XIC have multiple peaks to the same m/z value, which can be due to individual analyte components with the same m/z (different sequences with modifications or different charge states), which were subjected to further peak validation. Particularly, the peptide 218-IALLPNNAADLGK-231 was represented by 3 different peaks (68.058, 77.309 and 87.570 min); however, only the peak at 68.058 min was matched to its specific m/z, doubly charged $[M+2H]^{2+}$ ion at m/z 655.37 (Figure 5.5A-B). As shown in Figure 5.5C, b2, b3, y2, y4, y6-10 and y12 ions were observed within the fragment ion mass tolerance range and confirmed the peptide identity (>95 % confidence). All other peptides were also identified with a confidence greater than 95 %.

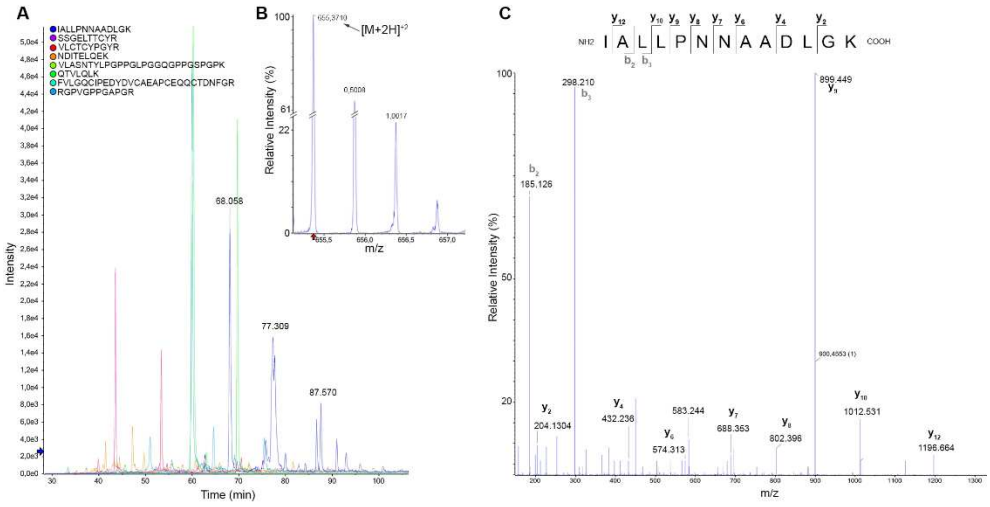

Figure 5.5. Proteomic characterization of the purified CCBE1. A) Extracted Ion Chromatogram (XIC) of nano-LC-MS/MS data (TripleTOF) using the list of identified CCBE1 peptides. **B)** MS spectrum of [M+2H]+2 ions of the peptide IALLPNNAADLGK (monoisotopic m/z 655.4). **C)** A peptide sequence (IALLPNNAADLGK) example of CCBE1 protein produced

by trypsin proteolysis. Cleavage at the peptide backbone in the MS/MS would result in the predicted fragment ion masses shown (b- and y-type ions). Fragmentation pattern (MS/MS spectrum) acquired for the peptide sequence (IALLPNNAADLGK).

To further demonstrate the reported ability of CCBE1 to stimulate the formation of lymphatic vessels and coronary vasculature (Sharma et al., 2017), the *in vitro* tube formation assay (HUVECs) was performed using the purified rCCBE1 (HDT 37°C at 3 dpt using the DSP approach II). The results indicated that the presence of rCCBE1 might have an impact on the tube formation capacity, showing an increase on the total length of formed branches in supplemented condition after 9h of treatment when compared to positive and negative controls (Figure 5.6).

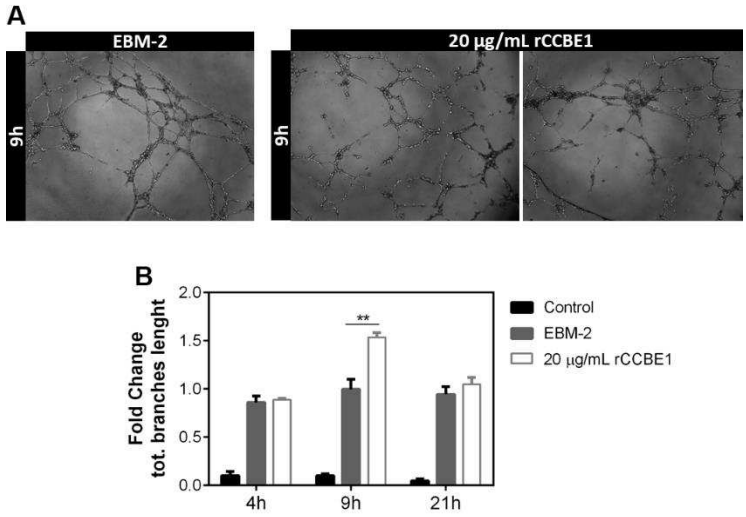

Figure 5.6. The angiogenesis potential of purified rCCBE1. **(A)** Representative images of tube-like structures using HUVECs and **(B)** fold change in total branches length in CCBE1 supplemented when compared with EBM-2 condition (positive control) and rCCBE1 storage buffer (negative control) at 4, 9 and 21 h was measured using an ImageJ plugin (Angiogenesis Analysis). ** $p < 0.01$, Two-way ANOVA.

4. Discussion

Several studies using CCBE1 for *in vitro* experiments have reported low productivities of the full-length rCCBE1 (1-5 nM) (Bui et al., 2016; Jeltsch et al., 2014; Roukens et al., 2015). In this work, we exploited different approaches to efficiently produce and purify the full-length rCCBE1 protein and further characterizing it by biochemical and functional assays and using MS-based tools. These analytical tools were also used for in-process control allowing a better understanding of the impact of key process parameters on the rCCBE1 productivity and proteome of the producer cells. The bioprocess strategies devised herein allowed a 3-fold improvement in full-length rCCBE1 yield (HDT at 37°C at 3 dpt) when compared to the literature (Bui et al., 2016).

The detection of secreted rCCBE1 only at 5 days post transfection (dpt) suggests a tight regulation of the secretion cell machinery along the production, as the normal required time for the detection of transiently produced proteins is 2 or 3 days. The saturation of the folding machinery might have contributed to the protein retention in the ER for further degradation (Schröder, 2008). Thus, we employed alternative bioprocessing strategies to maximize the rCCBE1 production and secretion yields: high-cell density transfection (HDT) and mild-hypothermia. Increased productivities attained in HDT condition at 37°C were also reported for other biopharmaceuticals in mammalian cell lines (Backliwal et al., 2008; Rajendra et al., 2015). This alteration in transfection procedure allowed the detection of secreted rCCBE1 at 2 dpt with higher volumetric and specific rCCBE1 yield in comparison to standard culture, which might be related to higher transfection efficiency. A culture temperature shift from 37°C (during proliferation stage) to 28-33°C (during stationary phase) is a well-known bioprocess strategy to reduce cellular metabolism while increasing recombinant protein productivity (Sunley & Butler, 2010; Wulhfard et al., 2008). In our work, we observed higher cell viability

along culture when shifting the temperature to 33°C, as observed for suspension-adapted CHO-K1 cells (Kumar et al., 2008), but with no effect on productivities.

The investigation of the transcriptome, proteome and/or metabolome has provided novel insights on cellular phenotype so as to facilitate bioprocess optimization, ensuring product quality and potency (Kildegaard et al., 2013). Here, the characterization of the whole cell proteome allowed the identification of enriched biological processes (GO-BP) in each culture condition explored. In HDT condition, the increased productivity might also overload the secretion machinery to continuously produce higher amount of recombinant protein. This phenomenon would consequently induce an oxidative stress at the ER and Golgi in the producer cell. This mechanism has been extensively studied as well as its impact on protein folding and glycosylation (Chong et al., 2017; Hussain et al., 2014), which also represents a critical bottleneck in the bioprocessing of recombinant proteins. The whole proteome analysis allowed the identification of stress-related proteins only in HDT condition, suggesting that the increased rCCBE1 production might induce an oxidative stress in the ER.

rCCBE1 glycosylation pattern can be severely affected by the culture conditions. The glucose starvation has a negative impact on product glycosylation (monoclonal antibodies or glycosylated proteins), since there is a preferential use of the energy metabolism substrate to generate glycosylation precursors (Liu et al., 2014). This might explain the decreased formation of complex-type glycans at 7 dpt (glucose and lactate starvation) in comparison to 3 dpt. A negative effect of mild hypothermia condition was also observed in our study, with the presence of under-processed glycan structures in secreted rCCBE1 produced at 33°C (Sou et al., 2015). In sum, here we show that the secreted rCCBE1 must be collected at high cell viabilities (> 90 %) to guarantee that the extracellular protein is correctly processed with proper glycosylation profile (complex-type glycans), since the

attached glycans may have an important role for structural and functional properties of secreted proteins (Krištić & Lauc, 2017).

CCBE1 DSP studies previously reported were based on affinity chromatography strategies (Strep-Tactin™) (Jeltsch et al., 2014; Tian et al., 2016), but with no available data on the purification yield and rCCBE1 purity. Different chromatographic approaches explored in our study were adapted according to the complexity of the bulk product. In STD condition, the use of an extra column (anion exchange chromatography) was required to eliminate most of the impurities (FBS-derived) followed by the IMAC. The most efficient strategies for rCCBE1 production and purifications (HDT 37°C and chromatographic Approach II) allowed a 25-fold improvement in rCCBE1 production and recovery compared with STD 37°C and chromatographic Approach I. Despite the increased rCCBE1 recovery using such strategy (> 95% *vs* 40%), a higher number of impurities were detected and identified by nano-LC-MS/MS (516 *vs* 127). The produced and purified protein (from chromatographic Approach II) also showed an enhanced capacity for tube formation *in vitro*.

Overall, this work provides valuable bioprocess insights to produce and purify a "difficult-to-express" protein and demonstrates the importance of a tightly controlled bioprocess to attain higher rCCBE1 yield, recovery and quality. High cell density at transfection had a positive impact on rCCBE1 yield, whereas the product secretion and quality were negatively affected by glucose starvation and culture temperature. Also, prolonged production processes contributed to a decreased in product quality (mixture of high-mannose and complex-type glycosylation profiles). MS-based tools explored herein, such as for in-process control and detailed final product characterization, are important to further understand CCBE1 structure and host cell metabolism/pathways. In conclusion, we demonstrated that the herein produced and purified secreted rCCBE1 is correctly processed with proper glycosylation profile (complex-type glycans) and

angiogenesis potential suitable for further validation of CCBE1 role, e.g. along cardiovascular development, in both *in vitro* and *in vivo* studies.

5. Author contribution & Acknowledgments

Marta M. Silva participated on the experimental setup and design, performed the experiments, analyzed the data and wrote the chapter.

6. References

Alders, M., Hogan, B. M., Gjini, E., Salehi, F., Al-Gazali, L., Hennekam, E. A., … Hennekam, R. C. (2009). Mutations in CCBE1 cause generalized lymph vessel dysplasia in humans. *Nature Genetics*, 41(12), 1272–1274.

Backliwal, G., Hildinger, M., Chenuet, S., Wulhfard, S., De Jesus, M., & Wurm, F. M. (2008). Rational vector design and multi-pathway modulation of HEK 293E cells yield recombinant antibody titers exceeding 1 g/l by transient transfection under serum-free conditions. *Nucleic Acids Research*, 36(15), e96.

Baldi, L., Hacker, D. L., Adam, M., & Wurm, F. M. (2007). Recombinant protein production by large-scale transient gene expression in mammalian cells: state of the art and future perspectives. *Biotechnology Letters*, 29(5), 677–684.

Barton, C. A., Gloss, B. S., Qu, W., Statham, A. L., Hacker, N. F., Sutherland, R. L., … O'Brien, P. M. (2010). Collagen and calcium-binding EGF domains 1 is frequently inactivated in ovarian cancer by aberrant promoter hypermethylation and modulates cell migration and survival. *British Journal of Cancer*, 102(1), 87–96.

Bui, H. M., Enis, D., Robciuc, M. R., Nurmi, H. J., Cohen, J., Chen, M., … Kahn, M. L. (2016). Proteolytic activation defines distinct lymphangiogenic mechanisms for VEGFC and VEGFD. *Journal of Clinical Investigation*, 126(6), 2167–2180.

Chong, W. C., Shastri, M. D., & Eri, R. (2017). Endoplasmic Reticulum Stress and Oxidative Stress: A Vicious Nexus Implicated in Bowel Disease Pathophysiology. *International Journal of Molecular Sciences*, 18(4), 771.

Facucho-Oliveira, J., Bento, M., & Belo, J.-A. (2011). Ccbe1 expression marks the cardiac and lymphatic progenitor lineages during early stages of mouse development. *The International Journal of Developmental Biology*, 55(10–12), 1007–1014.

Furtado, J., Bento, M., Correia, E., Inácio, J. M., & Belo, J. A. (2014). Expression and Function of Ccbe1 in the Chick Early Cardiogenic Regions Are Required for Correct Heart Development. *PLoS ONE,* 9(12), e115481.

Hogan, B. M., Bos, F. L., Bussmann, J., Witte, M., Chi, N. C., Duckers, H. J., & Schulte-Merker, S. (2009). Ccbe1 is required for embryonic lymphangiogenesis and venous sprouting. *Nature Genetics*, 41(4), 396–398.

Huang, D. W., Sherman, B. T., & Lempicki, R. A. (2008). Systematic and integrative analysis of large gene lists using DAVID bioinformatics resources. *Nature Protocols,* 4(1), 44–57.

Hussain, H., Maldonado-Agurto R., Dickson A.J. (2014). The endoplasmic reticulum and unfolded protein response in the control of mammalian recombinant protein production. *Biotechnology Letters*, 36(8), pp 1581–1593.

Hussain, H., Fisher, D. I., Abbot, W. M., Roth, R. G., & Dickson, A. J. (2017). Use of a Protein Engineering Strategy to Overcome Limitations in the Production of 'Difficult to Express' Recombinant Proteins. *Biotechnology and Bioengineering*, 114(10), 2348–2359.

Jeltsch, M., Jha, S. K., Tvorogov, D., Anisimov, A., Leppänen, V.-M., Holopainen, T., … Alitalo, K. (2014). CCBE1 enhances lymphangiogenesis via A disintegrin and metalloprotease with thrombospondin motifs-3-mediated vascular endothelial growth factor-C activation. *Circulation*, 129(19), 1962–1971.

Jha, S. K., Rauniyar, K., Karpanen, T., Leppänen, V.-M., Brouillard, P., Vikkula, M., … Jeltsch, M. (2017). Efficient activation of the lymphangiogenic growth factor VEGF-C requires the C-terminal domain of VEGF-C and the N-terminal domain of CCBE1. *Scientific Reports*, 7(1), 4916.

Kildegaard, H. F., Baycin-Hizal, D., Lewis, N. E., & Betenbaugh, M. J. (2013). The emerging CHO systems biology era: harnessing the 'omics revolution for biotechnology. *Current Opinion in Biotechnology*, 24(6), 1102–1107.

Krištić, J., & Lauc, G. (2017). Ubiquitous Importance of Protein Glycosylation. In G. Lauc & M. Wuhrer (Eds.), *Methods Mol Biol*. (pp. 1–12).

Kumar, N., Gammell, P., Meleady, P., Henry, M., & Clynes, M. (2008). Differential protein expression following low tKumar, N., Gammell, P., Meleady, P., Henry, M., & Clynes, M. (2008). Differential protein expression following low temperature culture of suspension CHO-K1 cells. *BMC Biotechnology*, 8(1), 42.

Le Fourn, V., Girod, P., Buceta, M., Regamey, A., & Mermod, N. (2014). CHO cell engineering to prevent polypeptide aggregation and improve therapeutic protein secretion. *Metabolic Engineering*, 21, 91–102.

Lin, C. Y., Huang, Z., Wen, W., Wu, A., Wang, C., & Niu, L. (2015). Enhancing protein expression in HEK-293 cells by lowering culture temperature. *PLoS ONE*, 10(4), 1–19.

Liu, B., Spearman, M., Doering, J., Lattová, E., Perreault, H., & Butler, M. (2014). The availability of glucose to CHO cells affects the intracellular lipid-linked oligosaccharide distribution, site occupancy and the N-glycosylation profile of a monoclonal antibody. *Journal of Biotechnology*, 170, 17–27.

Rajendra, Y., Kiseljak, D., Baldi, L., Wurm, F. M., & Hacker, D. L. (2015). Transcriptional and post-transcriptional limitations of high-yielding, PEI-mediated transient transfection with CHO and HEK-293E cells. *Biotechnology Progress*, 31(2), 541–549.

Roukens, M. G., Peterson-Maduro, J., Padberg, Y., Jeltsch, M., Leppanen, V.-M., Bos, F. L., … Schulte, D. (2015). Functional Dissection of the CCBE1 Protein: A Crucial Requirement for the Collagen Repeat Domain. *Circulation Research*, 116(10), 1660–1669.

Schindelin, J., Arganda-Carreras, I., Frise, E., Kaynig, V., Longair, M., Pietzsch, T., … Cardona, A. (2012). Fiji: an open-source platform for biological-image analysis. *Nature Methods*, 9(7), 676–682.

Schröder, M. (2008). Engineering eukaryotic protein factories. *Biotechnology Letters,* 30(2), 187–196.

Sharma, B., Ho, L., Ford, G. H., Chen, H. I., Goldstone, A. B., Woo, Y. J., … Red-Horse, K. (2017). Alternative Progenitor Cells Compensate to Rebuild the Coronary Vasculature in Elabela - and Apj - Deficient Hearts. *Developmental Cell*, 42(6), 655–666.e3.

Sou, S. N., Sellick, C., Lee, K., Mason, A., Kyriakopoulos, S., Polizzi, K. M., & Kontoravdi, C. (2015). How does mild hypothermia affect monoclonal antibody glycosylation? *Biotechnology and Bioengineering*, 112(6), 1165–1176.

Stein, A., & Bailey, S. M. (2013). Redox biology of hydrogen sulfide: Implications for physiology, pathophysiology, and pharmacology. *Redox Biology*, 1(1), 32–39.

Sunley, K., & Butler, M. (2010). Strategies for the enhancement of recombinant protein production from mammalian cells by growth arrest. *Biotechnology Advances,* 28(3), 385–394.

Templeton, N., Dean, J., Reddy, P., & Young, J. D. (2013). Peak antibody production is associated with increased oxidative metabolism in an industrially relevant fed-batch CHO cell culture. *Biotechnology and Bioengineering*, 110(7), 2013–2024.

Tian, G.-A., Zhu, C.-C., Zhang, X.-X., Zhu, L., Yang, X.-M., Jiang, S.-H., … Zhang, Z.-G. (2016). CCBE1 promotes GIST development through enhancing angiogenesis and mediating resistance to imatinib. *Scientific Reports*, 6, 31071.

Wulhfard, S., Bouchet, S., Cevey, J., Jesus, M. De, Hacker, D. L., & Wurm, F. M. (2008). Mild Hypothermia Improves Transient Gene Expression Yields Several Fold in Chinese Hamster Ovary Cells. *Biotechnology Progress*, (2):458-65.

Zhang, J., Liu, X., Bell, A., To, R., Baral, T. N., Azizi, A., … Durocher, Y. (2009). Transient expression and purification of chimeric heavy chain antibodies. *Protein Expression and Purification*, 65(1), 77–82.

7. Supplementary files

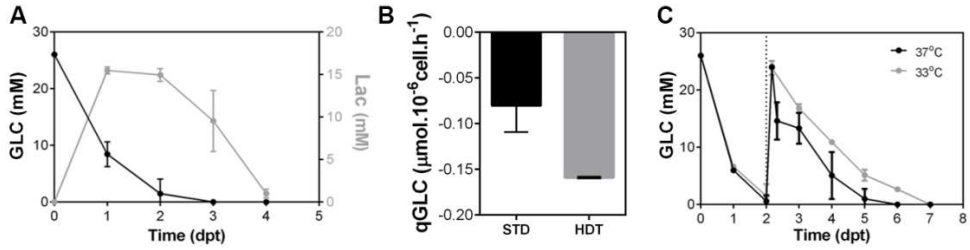

Figure S1. Metabolites concentration in non-supplemented and supplemented HDT cultures. A) Glucose and lactate concentration in non-supplemented culture along time. **B)** Glucose consumption rate in STD and HDT cultures at 37°C. **C)** Glucose concentration in glucose supplemented culture along time at 37°C and 33°C. Dashed line represents glucose supplementation (24 mM) time point. Error bars denote mean ± standard error of 3 independent experiments.

Table S5.1. List of identified proteins involved in protein folding, in each condition (HDT 37°C and STD 37°C) at the last days of culture**.**

Protein Folding			
HDT 37 ºC (#67)		**STD 37 ºC (#65)**	
P30405	P27797	Q9Y230	P25685
Q9Y230	P25685	Q96DA6	Q13451
Q96DA6	Q13451	P30405	Q14165
Q32P28	Q14165	O15212	Q99832
O15212	Q99832	Q9NZL4	P13667
Q9NZL4	P13667	P61604	P07900
Q8WUA2	P07900	P11142	P62873
P61604	P14625	Q9UHV9	P14625
P11142	O95757	Q9H3N1	O95757
Q9UHV9	Q8WVJ2	Q9Y266	Q8WVJ2
Q9H3N1	P62879	Q9HAV0	O95817
P50502	P48643	Q16543	P48643
Q9Y266	P50990	Q8IVD9	P50990
Q16543	P50991	Q9HAV7	P50991
Q9HAV7	P26885	P49588	P26885
P49588	Q9Y3C6	P78371	O75347
P78371	O75347	P17987	P30101
P17987	P08754	P49257	P27824
Q8NBS9	P30101	Q8NBS9	Q9BTW9
Q99471	P27824	Q99471	O60925
O60884	Q9BTW9	O60884	P30040
Q08752	O60925	Q08752	Q12931
P38646	P30040	P38646	P49368
P14314	Q12931	P14314	P62937
P08238	P49368	P08238	Q15084
P10599	P62937	P10599	Q99615
Q9UBS4	Q15084	Q9UBS4	Q99614
Q9NQP4	Q99615	Q9NQP4	Q14697
Q9BS26	Q99614	Q9BS26	Q96HE7
P19784	Q14697	P40227	O75190
O00170	Q96HE7	Q02790	O43447
P40227	P61758	P62942	
Q02790	O43447	P27797	
P62942		Q14696	

Table S5.2. List of identified proteins involved in protein transport, in each condition (HDT 37°C and STD 37°C) at the last days of culture**.**

Transport Proteins			
HDT 37 ºC (#63)		**STD 37 ºC (#49)**	
Q8NC96	Q96A65	Q9NZZ3	P61619
Q13765	Q15833	Q8NC96	P35579
Q12907	O43823	Q13765	Q53FT3
Q9BVK6	Q96FZ7	Q12907	P51148
Q8WUD1	P61020	Q8WUD1	**P20339**
Q3ZCQ8	O94979	Q96FZ7	O75396
Q9Y4E1	Q86UP2	P61020	P50395
P49321	**O43264**	Q86UP2	Q9P2E9
P18085	P14625	P49321	P57737
P61106	O14828	P18085	P61923
O15498	O14579	P61106	P62330
O15027	P62834	P50897	P48444
Q9NV70	Q9NP79	O15027	O95721
O95352	Q9UP83	P14625	P84085
Q9H6Z4	**Q8N1B4**	Q99598	P0CG08
Q7Z7H5	Q9NP72	Q5JRA6	
Q9Y3E0	Q9UMR2	O14828	**endosomal transport**
O43707	O60826	O43707	**tranfficking ER-Golgi**
P84077	P51149	P84077	**vesicular trafficking to membrane**
P20290	Q9Y5L4	O14579	**Rab proteins**
Q9UL25	P51148	P62834	
Q8WUM4	Q641Q2	O00161	
O75165	O75396	Q9NP79	
Q8TEX9	P50395	P20290	
Q9H0U4	P57737	P49257	
Q53FT3	Q8IYI6	Q8WUM4	
Q08752	P62330	Q8TEX9	
P35579	P48444	Q9NP72	
P61619	P0CG08	Q9UMR2	
P61923		P51149	
P84085		Q9Y5L4	
P31150		P61019	
Q8NI22		Q9H0U4	
Q9NZZ3		Q08752	

6

Discussion

Table of contents

1. Discussion

Most of the available therapies for heart failure treatment are non-curative and hold no regenerative potential, focusing on ameliorating patients' symptoms. Promising alternatives based on stem cells' potential have been explored and assessed in several ongoing clinical trials. Nonetheless, their efficacy to promote heart regeneration and repair injury remains elusive and controversial. The biological complexity of stem cells has limited the translation of implemented protocols at laboratory-scale towards reliable, standardized and cost-effective platforms of cell therapy products (Chamuleau et al., 2018; Lipsitz et al., 2016).

The work developed in this thesis aimed at the implementation of strategies with potential for cardiac regeneration, as the: (A) development of robust and scalable approaches for stem cell therapy products manufacturing and (B) interrogation of CCBE1 functional role on cardiac commitment, as potential therapeutic factor. The major achievements obtained for **Chapters 2-5** are summarized in Figure 6.1.

1.1 Stem cell manufacturing challenges for cardiac therapies

Defining the optimal cell source for cell-based cardiac therapies is a critical step due to the wide range of features that each cell type presents. This selection relies on different aspects: cell availability, cell potency (differentiation into specific cardiac derivatives or secretion of therapeutic factors), associated clinical risks, stage of heart failure and type of therapy (autologous *versus* allogeneic). Moreover, the manufacturing of complex biological products, as stem cells, still faces several technical challenges. Manufacturers have to take into consideration critical factors, from acquisition of starting material until product shipping, for the production of therapeutic cells at high quality, quantity and low cost of goods (Lipsitz et al., 2016).

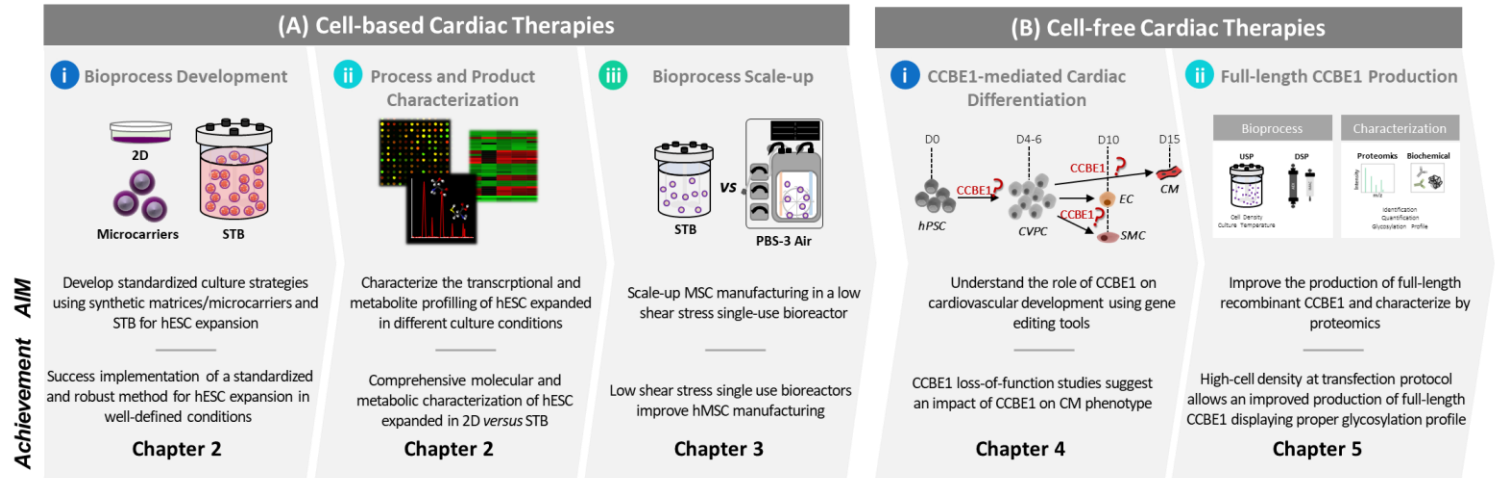

Figure 6.1 Schematic representation of thesis' aims and major achievements of each chapter (2-5) towards cardiovascular regeneration and repair therapies. 2D- two-dimensional culture; STB- stirred-tank bioreactors; PBS-3 Air- Vertical-Wheel™ bioreactor (PBS Biotech®); hESC- human embryonic stem cells; hMSC- human mesenchymal stem cells; CVPC- cardiovascular progenitor cells; CM- cardiomyocytes; EC- endothelial cells; SMC- smooth muscle cells; USP- upstream bioprocess; DSP- downstream bioprocess.

For translating stem cell manufacturing protocols into industrial and clinical settings, it is essential to implement robust, scalable, GMP-compliant and cost-effective processes. Thus, in **Chapter 2** and **Chapter 3**, we implemented scalable and controllable manufacturing processes for hESC and hMSC expansion, respectively. Both cells present key features with potential for heart failure treatment (revised in Hashimoto et al., 2018; Quevedo et al., 2009). hMSC hold a direct clinical potential upon transplantation in injured tissue; however, hESC will need to be first differentiated into cardiac derivatives as final therapeutic products for replacement therapies.

In bioprocess optimization, there are three main parameters to be considered, which directly influence the cell characteristics (quality attributes): (i) culture media and matrices, (ii) physicochemical parameters and (iii) bioreactor design. Firstly, in **Chapter 2**, we evaluated the impact of different culture and process parameters on hESC expansion yields and phenotype. Our strategy relied on the expansion of hESC on xeno-free microcarriers (Synthemax II) in stirred culture conditions. This work showed, for the first time, the effectiveness of these xeno-free microcarriers to sustain high expansion yields of hESC (2×10^6 cell/mL), while maintaining cell pluripotency. Since then, other studies have shown the expansion of hiPSC using this strategy with similar cell growth profiles (Badenes et al., 2016; Kropp et al., 2017). Alternatively, the expansion of hPSC as cell aggregates was also described to support high cell yields ($2.85\text{-}4.7 \times 10^6$ cell/mL) (Abecasis et al., 2017; Kropp et al., 2016). Both strategies have contributed to major progresses in hPSC cultivation in stirred cultures. Even though, differences in nutrients and gas diffusion into the cell aggregate center may lead to phenotype heterogeneity. These differences would have implications on the product safety and efficacy, suggesting the microcarrier-based cultures as more controllable expansion systems. Nonetheless, the selected culture strategy will depend on the final application of the cell product and their own characteristics/requirements.

Our group and others have reported the beneficial effect of low oxygen levels (5-6 % of dissolved oxygen) in improving expansion yields of mouse ESC and hESC and reducing spontaneous chromosomal abnormalities (Forsyth et al., 2006; Serra et al., 2010; Baptista et al., 2013). We demonstrated the influence of low oxygen levels on hESC by characterizing the hESC transcriptomic and metabolic profiles. These "omics" tools provided relevant findings on the physiological and metabolic changes occurring during the expansion process under fully defined and controlled conditions. These conditions favored an anaerobic glycolysis over oxidative phosphorylation, a well-known stemness feature (Agathocleous & Harris, 2013) that was less evident in the 2D culture system, also showed by Varum *et al.* and Zhang *et al.* (Varum et al., 2011; Zhang et al., 2011). Moussaieff et al. further highlighted the critical role of glycolysis to ensure chromatin acetylation in ESC, maintaining their pluripotent state (Moussaieff et al., 2015). Unexpectedly, recent studies on hiPSC expansion as cell aggregates showed a switch from glycolysis to oxidative phosphorylation without spontaneous differentiation (Abecasis et al., 2017; Kropp et al., 2016). We hypothesize that the different metabolic demands/profiles can be related to the cell origin, hESC *versus* hiPSC, since the methylome of hESC differs from hiPSC that retains an "epigenetic memory" from the somatic cells (Doi et al., 2009).

It is crucial to use complementary tools/assays for in-depth characterization of the final cell-based product as to facilitate bioprocess optimization for different culture conditions. Thus, a rational platform should integrate feasible bioprocess strategies and rapid biological assays to achieve more accurate, stringent and measurable criteria for cell products characterization.

The proposed therapeutic potential of hMSC for improving cardiac function after MI (Quevedo et al., 2009) has prompted its translation into clinical setting. Thus, in collaboration with biotechnology industry, in **Chapter 3** we implemented a scalable bioprocess approach using a single-use low shear-stress bioreactor (Vertical-Wheel™ PBS-3 Air, PBS Biotech®) for hMSC expansion amenable for translation into clinical-

grade production processes. Microcarrier-based cultures are the most reliable and explored culture approaches to expand hMSC (Jossen et al., 2018). The xeno-free synthetic microcarriers explored in **Chapter 2** were also used to expand hMSC. Here, we evaluated the impact of the bioreactor design and hydrodynamics on hMSC expansion and quality. For the first time, we were able to efficiently transfer the hMSC expansion process established in stirred-tank bioreactors towards a 2 L-scale manufacturing platform using this disposable bioreactor bioreactor. The implemented protocol allowed a high expansion yields (3×10^6 cell/mL) with homogeneous and high microcarrier colonization (up to 90 %), while maintaining the stem cell characteristics. Homogenous cell distribution per microcarrier during the attachment phase is critical to avoid formation of large hMC-microcarrier aggregates impairing efficient hMSC growth and maintenance of stem cell phenotype (Ferrari et al., 2012). Recently, Lawson T *et al*. reported the expansion of hMSC at 50-L pilot scale in single-use Mobius® 50 L bioreactor with similar cell growth profile, however using undefined media formulation and collagen-coated microcarriers (Lawson et al., 2017). Interestingly, we observed lower percentage of HLA-DR-positive cells in PBS-3 Air when compared to stirred-tank bioreactor. In 50-L pilot scale study, higher percentage of HLA-DR^+ hMSC was also detected (Lawson et al., 2017), suggesting that the bioreactor hydrodynamics may play a role on the expression of such immunomodulatory surface marker. Complementary characterization tools would provide important insights on the influence of such parameter on hMSC transcriptome, metabolome and secretome, for instance. Promising data on hMSC secretome and its potential for therapeutic applications are changing the manufacturing platforms and the way their potency is evaluated, by testing the impact of process parameters on bioactivity of secreted factors.

In **Chapter 2** and **3**, we implemented scalable platforms using synthetic microcarriers that are considered non-cell particulates with higher impact on final cell product purity. The removal of these impurities, such as plastic fragments arising

from cell culture equipment (single-use bioreactors) and materials (microcarriers), is the major bottleneck of the downstream processing. Our group and others have been working in the implementation of efficient upstream and downstream strategies for hMSC expansion and purification, using size exclusion filtration for separation of cells from microcarriers and hollow fibers for cell concentration (Cunha et al., 2015, 2017; Jossen et al., 2018). Alternatively, the use of GMP-grade biodegradable microcarriers could reduce the contaminants and DSP steps associated to their removal. Nonetheless, the scalable protocols implemented within the scope of this thesis may potentially be translated into streamlined manufacturing platforms for the expansion of human stem cells at high quantity and quality.

1.2 Cardiac therapeutic potential of CCBE1: modulatory effects on CM phenotype

In **Chapter 4**, we investigated the CCBE1 role during *in vitro* human iPSC differentiation into cardiomyocytes (CM) and endothelial cells, using CRISPR interference technology.

Despite the observations of CCBE1 expression during specific developmental stages of cardiac embryonic tissues in mouse and chicken models (Facucho-Oliveira et al., 2011; Furtado et al., 2014), its role in cardiac commitment was not yet fully disclosed. A recent CCBE1 loss-of-function study, using mouse ESC and embryoid body (EB) culture system, demonstrated that the loss of CCBE1 led to a downregulation of *MESP1* and *ISL1* expression, cardiac mesoderm and cardiac progenitor markers, respectively, at day 4 of EB differentiation (Bover et al., 2018). Despite these differences, the Nkx2-5^{+}-cardiac progenitors at day 6 were established in a seemingly normal proportion in comparison to WT cultures. In an attempt to unveil its functional role along cardiac commitment in human PSC, we combined the hiPSC technology and CRISPRi tool. Efficient CCBE1 knockdown (KD) in a hiPSC line (containing the deactivated Cas9 to repress the expression of target gene) allowed its

study along hiPSC proliferation and differentiation on CM and endothelial cells. CCBE1 KD led to a significant downregulation of cardiac troponin T2 and other cardiac myosin genes, as well as ultrastructural changes on derived CM when compared with control condition. Hence, we suggest that CCBE1 can have a modulatory effect on CM differentiation/phenotype. Further validation assays to confirm the functional role of CCBE1 on cardiac commitment and CM maturation would provide relevant information. These would include, for instance, the evaluation of CM contractility function and calcium signaling readouts. Complementary analyses of the cellular transcriptomic and proteomic profile would contribute to identify key molecules/signaling pathways modulated by CCBE1, contributing to assert whether CCBE1 could be used as cardiac therapeutic molecule. Nonetheless, it would also be interesting to evaluate its implications on cardiac matrix remodeling upon a MI, given its described affinity and interaction with extracellular matrix components (Bos et al., 2011). Due to time constraints these approaches were not followed within the scope of the present thesis but will be the focus of future work.

The supplementation of CRISPRi-CCBE1 KD cultures with recombinant CCBE1 in order to rescue the phenotype, would be imperative to validate the results reported herein. Noteworthy, the administration of growth factors to promote cardiac regeneration through increased angiogenesis and lymphangiogenesis has been in fact tested in preclinical and clinical studies. For example, targeted approaches for enhanced lymphatic regeneration in the heart have been suggested and tested in mouse models through the administration of VEGF-C (Henri et al., 2016). According to the reported literature and the work presented in **Chapter 4**, we hypothesize that CCBE1 might also be used as a therapeutic molecule for cardiac lymphatic regeneration, alone or in combination with VEGF-C.

Most of CCBE1-related studies attempting to produce the recombinant protein have claimed low productivities, hampering the study of full-length CCBE1 for

therapeutic applications. Higher productivities could only be attained with a truncated version of CCBE1, containing only the N-terminal domain (Bui et al., 2016). Therefore, we implemented an improved bioprocess for the production of full-length CCBE1 recombinant protein. The bioprocess strategy devised in **Chapter 5**, using a high-cell density at transfection (HDT), allowed a 3-fold improvement in the full-length CCBE1 when compared to the literature (Bui et al., 2016). As discussed above, for cell therapy products, the culture process parameters may also have a negative impact on product (recombinant protein) quality and potency. Here, we revealed for the first time the impact of main process parameters on CCBE1 productivity and quality. The transfection protocol and the time of harvest were shown to be critical to achieve high CCBE1 yields and guarantee CCBE1 quality (glycosylation profile). This transfection protocol was firstly employed for the production of other biopharmaceutical products (e.g. antibodies)(Backliwal et al., 2008). The lack of protein characterization assays in all the reported CCBE1-studies, has driven the application of proteomic-based tools in this thesis for CCBE1 characterization. Such tools allowed the identification of process contaminants after production and purification steps, namely host-cell proteins. Despite the presence of these contaminants in the final product, CCBE1 was able to potentiate the formation of endothelial-like vessels, showing its angiogenic potential. A recent study also demonstrated this quality attribute after CCBE1 production and enrichment step (using Strep-Tactin™ Technology) (Tian et al., 2016).

Moreover, it would be of interest to assess the therapeutic effect/potential of this protein in cardiac context, namely through its supplementation in the human CCBE1 KD *in vitro* culture system established in **Chapter 4**. More specifically, it would be relevant to address the impact of functional CCBE1 supplementation in the context of specific cardiac cell types or developmental stages, such as cardiac progenitor/stem cells, where increased CCBE1 expression was observed in wild-type hPSC CM differentiation.

2. Conclusions and Perspectives

This thesis contributed to the fields of stem cell manufacturing and cardiovascular research by i) demonstrating the importance of considering cellular physiological and metabolic hallmarks during hPSC bioprocess design and media optimization for efficient clinical-grade manufacturing platforms, and ii) suggesting a putative role of CCBE1 as a modulator of cardiomyocytes phenotype, supporting its potential as target for cardiac therapeutic approaches.

The current therapeutic approaches for cardiac regeneration and repair have been discussed but several questions remain unanswered. Should we further explore the cell-based products therapeutic potential, namely by exploring strategies for enhanced cell retention, or switch towards noncellular approaches, for example using the cell secretome, or the combination of both?

Regarding cell transplantation into injured hearts (e.g. intramyocardial injection), we still face the high incidence of ventricular arrhythmias, which may be induced by the electrophysiological heterogeneity of the transplanted cells (Mount & Davis, 2016). Over the last years, numerous preclinical studies have demonstrated that hPSC differentiated cardiac cells (e.g. cardiac progenitor cells) hold significant promise in cardiac-based therapies (Menasché et al., 2015). Nevertheless, the impact of maturation level of the transplanted cardiac cells following MI is still debatable and should be fully addressed, i.e., use of cardiac progenitors that would represent a more plastic approach, where these cells could integrate and gradually remodel the existing damaged tissue, *versus* use of fully mature CM that would be a more immediate approach, where cells could rapidly contribute to recover tissue functionality.

Therefore, this work may contribute for the implementation of knowledge-driven approaches in stem cell manufacturing and unveils that CCBE1-modulated proteins/pathways may be targeted towards novel cardiac regenerative therapies.

3. Author contribution

The author wrote the chapter.

4. References

Abecasis, B., Aguiar, T., Arnault, É., Costa, R., Gomes-Alves, P., Aspegren, A., … Alves, P. M. (2017). Expansion of 3D human induced pluripotent stem cell aggregates in bioreactors: Bioprocess intensification and scaling-up approaches. *Journal of Biotechnology*, 246, 81–93.

Agathocleous, M., & Harris, W. a. (2013). Metabolism in physiological cell proliferation and differentiation. *Trends in Cell Biology*, 23, 484–492.

Badenes, S. M., Fernandes, T. G., Rodrigues, C. A. V., Diogo, M. M., & Cabral, J. M. S. (2016). Microcarrier-based platforms for in vitro expansion and differentiation of human pluripotent stem cells in bioreactor culture systems. *Journal of Biotechnology*, 234, 71–82.

Baptista, R. P., Fluri, D. A., & Zandstra, P. W. (2013). High density continuous production of murine pluripotent cells in an acoustic perfused bioreactor at different oxygen concentrations. *Biotechnology and Bioengineering,* 110(2), 648–655.

Bos, F. L., Caunt, M., Peterson-Maduro, J., Planas-Paz, L., Kowalski, J., Karpanen, T., … Schulte-Merker, S. (2011). CCBE1 is essential for mammalian lymphatic vascular development and enhances the lymphangiogenic effect of vascular endothelial growth factor-C in vivo. *Circulation Research*, 109(5), 486–491.

Bover, O. *et al.* (2018). Loss of Ccbe1 affects cardiac-specification and proliferation in differentiating mouse embryonic stem cells. *Submitted.*

Bui, H. M., Enis, D., Robciuc, M. R., Nurmi, H. J., Cohen, J., Chen, M., … Kahn, M. L. (2016). Proteolytic activation defines distinct lymphangiogenic mechanisms for VEGFC and VEGFD. *Journal of Clinical Investigation*, 126(6), 2167–2180.

Chamuleau, S. A. J., van der Naald, M., Climent, A. M., Kraaijeveld, A. O., Wever, K. E., Duncker, D. J., … Bolli, R. (2018). Translational Research in Cardiovascular RepairTake-Home Messages. *Circulation Research*, 122(2), 310–318.

Cunha, B., Aguiar, T., Carvalho, S. B., Silva, M. M., Gomes, R. A., Carrondo, M. J. T., … Alves, P. M. (2017). Bioprocess integration for human mesenchymal stem cells: From up to downstream processing scale-up to cell proteome characterization. *Journal of Biotechnology*, 248, 87–98.

Cunha, B., Aguiar, T., Silva, M. M., Silva, R. J. S., Sousa, M. F. Q., Pineda, E., … Alves, P. M. (2015). Exploring continuous and integrated strategies for the up- and downstream processing of human mesenchymal stem cells. *Journal of Biotechnology*. 213, 97-108.

Doi, A., Park, I.-H., Wen, B., Murakami, P., Aryee, M. J., Irizarry, R., … Feinberg, A. P. (2009). Differential methylation of tissue- and cancer-specific CpG island shores distinguishes human induced pluripotent stem cells, embryonic stem cells and fibroblasts. *Nature Genetics*, 41(12), 1350–1353.

Facucho-Oliveira, J., Bento, M., & Belo, J.-A. (2011). Ccbe1 expression marks the cardiac and lymphatic progenitor lineages during early stages of mouse development. The International *Journal of Developmental Biology*, 55(10–12), 1007–1014.

Ferrari, C., Balandras, F., Guedon, E., Olmos, E., Chevalot, I., & Marc, A. (2012). Limiting cell aggregation during mesenchymal stem cell expansion on microcarriers. *Biotechnology Progress,* 28(3), 780–787.

Forsyth, N. R., Musio, A., Vezzoni, P., Simpson, A. H. R. W., Noble, B. S., & McWhir, J. (2006). Physiologic oxygen enhances human embryonic stem cell clonal recovery and reduces chromosomal abnormalities. *Cloning and Stem Cells*, 8, 16–23.

Furtado, J., Bento, M., Correia, E., Inácio, J. M., & Belo, J. A. (2014). Expression and Function of Ccbe1 in the Chick Early Cardiogenic Regions Are Required for Correct Heart Development. *PLoS ONE*, 9(12), e115481.

Hashimoto, H., Olson, E. N., & Bassel-Duby, R. (2018). Therapeutic approaches for cardiac regeneration and repair. *Nature Reviews Cardiology*.

Henri, O., Pouehe, C., Houssari, M., Galas, L., Nicol, L., Edwards-Lévy, F., … Brakenhielm, E. (2016). Selective Stimulation of Cardiac Lymphangiogenesis Reduces Myocardial Edema and Fibrosis Leading to Improved Cardiac Function Following Myocardial Infarction. *Circulation*, 133(15), 1484–1497.

Jossen, V., van den Bos, C., Eibl, R., & Eibl, D. (2018). Manufacturing human mesenchymal stem cells at clinical scale: process and regulatory challenges. *Applied Microbiology and Biotechnology*, 102, 3981–3994.

Kropp, C., Kempf, H., Halloin, C., Robles-Diaz, D., Franke, A., Scheper, T., … Olmer, R. (2016). Impact of Feeding Strategies on the Scalable Expansion of Human Pluripotent Stem Cells in Single-Use Stirred Tank Bioreactors. *STEM CELLS Translational Medicine*, 5(10), 1289–1301.

Kropp, C., Massai, D., & Zweigerdt, R. (2017). Progress and challenges in large-scale expansion of human pluripotent stem cells. *Process Biochemistry*, 59, 244–254.

Lawson, T., Kehoe, D. E., Schnitzler, A. C., Rapiejko, P. J., Der, K. A., Philbrick, K., … Rook, M. S. (2017). Process development for expansion of human mesenchymal stromal cells in a 50L single-use stirred tank bioreactor. *Biochemical Engineering Journal*, 120, 49–62.

Lipsitz, Y. Y., Timmins, N. E., & Zandstra, P. W. (2016). Quality cell therapy manufacturing by design. *Nature Biotechnology*, 34(4), 393–400.

Menasché, P., Vanneaux, V., Hagège, A., Bel, A., Cholley, B., Cacciapuoti, I., … Larghero, J. (2015). Human embryonic stem cell-derived cardiac progenitors for severe heart failure treatment: first clinical case report. *European Heart Journal*, 36(30), 2011–2017.

Mount, S., & Davis, D. R. (2016). Electrical effects of stem cell transplantation for ischaemic cardiomyopathy: friend or foe? *The Journal of Physiology*, 594(9), 2511–2524.

Moussaieff, A., Rouleau, M., Kitsberg, D., Cohen, M., Levy, G., Barasch, D., … Nahmias, Y. (2015). Glycolysis-mediated changes in acetyl-CoA and histone acetylation control the early differentiation of embryonic stem cells. *Cell Metabolism*, 21(3), 392–402.

Quevedo, H. C., Hatzistergos, K. E., Oskouei, B. N., Feigenbaum, G. S., Rodriguez, J. E., Valdes, D., … Hare, J. M. (2009). Allogeneic mesenchymal stem cells restore cardiac function in chronic ischemic cardiomyopathy via trilineage differentiating capacity. *Proceedings of the National Academy of Sciences*, 106(33), 14022–14027.

Serra, M., Brito, C., Sousa, M. F. Q., Jensen, J., Tostões, R., Clemente, J., … Alves, P. M. (2010). Improving expansion of pluripotent human embryonic stem cells in perfused bioreactors through oxygen control. *Journal of Biotechnology*, 148(4), 208–215.

Tian, G.-A., Zhu, C.-C., Zhang, X.-X., Zhu, L., Yang, X.-M., Jiang, S.-H., … Zhang, Z.-G. (2016). CCBE1 promotes GIST development through enhancing angiogenesis and mediating resistance to imatinib. *Scientific Reports*, 6, 31071.

Varum, S., Rodrigues, A. S., Moura, M. B., Momcilovic, O., Easley, C. a, Ramalho-Santos, J., … Schatten, G. (2011). Energy metabolism in human pluripotent stem cells and their differentiated counterparts. *PloS One*, 6(6), e20914.

Zhang, J., Khvorostov, I., Hong, J. S., Oktay, Y., Vergnes, L., Nuebel, E., … Teitell, M. A. (2011). UCP2 regulates energy metabolism and differentiation potential of human pluripotent stem cells. *The EMBO Journal*, 30(24), 4860–4873.

ITQB-UNL | Av. da República, 2780-157 Oeiras, Portugal
Tel (+351) 214 469 100 | Fax (+351) 214 411 277

www.itqb.unl.pt